

A High-Density 3D Microengineered Platform to Study the Role of Tumor-Stroma
Interactions on Desmoplasia and Breast Cancer Progression

by

Harpinder Saini

A Dissertation Presented in Partial Fulfillment
of the Requirements for the Degree
Doctor of Philosophy

Approved June 2019 by the
Graduate Supervisory Committee:

Mehdi Nikkhah, Chair
Robert Ros
Joshua LaBaer
Vikram Kodibagkar
Mo Ebrahimkhani

ARIZONA STATE UNIVERSITY

August 2019

ABSTRACT

Solid tumors advance from benign stage to a deadly metastatic state due to the complex interaction between cancer cells and tumor microenvironment (TME) including stromal cells and extracellular matrix (ECM). Multiple studies have demonstrated that ECM dysregulation is one of the critical hallmarks of cancer progression leading to formation of a desmoplastic microenvironment that participates in tumor progression. Cancer associated fibroblasts (CAFs) are the predominant stromal cell type that participates in desmoplasia by depositing matrix proteins and increasing ECM stiffness. Although the influence of matrix stiffness on enhanced tumorigenicity has been well studied, the biological understanding about the dynamic changes in ECM architecture and the role of cancer-stromal cell interaction on ECM remodeling is still limited.

In this dissertation, the primary goal was to develop a comprehensive cellular and molecular level understanding of ECM remodeling due to the interaction of breast tumor cells and CAFs. To that end, a novel three-dimensional (3D) high-density tumor-stroma model was fabricated in which breast tumor cells (MDA-MB-231 and MCF7) were spatially organized surrounded by CAF-embedded collagen-I hydrogel (Aim 1). Further the platform was integrated with atomic force microscopy to assess the dynamic changes in ECM composition and stiffness during active tumor invasion. The results established an essential role of crosstalk between breast tumor cells and CAFs in ECM remodeling. The studies were further extended by dissecting the mode of interaction between tumor cells and CAFs followed by characterization of the role of various tumor secreted factors

on ECM remodeling (Aim 2). The results for the first time established a critical role of paracrine signaling between breast tumor cells and CAFs in modulating biophysical properties of ECM. More in-depth analysis highlighted the role of tumor secreted cytokines, specifically PDGF-AA/BB, on CAF-induced desmoplasia. In aim 3, the platform was further utilized to test the synergistic influence of anti-fibrotic drug (tranilast) in conjugation with chemotherapeutic drug (Doxorubicin) on desmoplasia and tumor progression in the presence of CAFs. Overall this dissertation provided an in-depth understanding on the impact of breast cancer-stromal cell interaction in modulating biophysical properties of the ECM and identified the crucial role of tumor secreted cytokines including PDGF-AA/BB on desmoplasia.

DEDICATION

My Ph.D. is an achievement due to the right thinking by many people who I have been blessed with in my life.

I would first deeply thank my parents Mrs. Manjit Kaur and Mr. Bikramjit Singh for keeping faith in me and giving unconditional love and trust in taking this challenge and emerge successful in the end. Your solid support, patience and ability to adapt made me learn many virtues that helped me reach at this stage of life and will be paramount for all my future endeavors. I would also thank my sister Mrs. Harjot Saini and my brother-in-law Mr. Amardeep Singh for instilling confidence in me and providing a lovely environment whenever I came back to India. I always knew that I have a great loving family who believes in me and will be there for me at all the times. The trust that my family is always by my side helped me take over this challenge and face many hurdles that came along all my way. I have grown into a much stronger person due to love, care and support from all of you.

I am also extremely thankful to my partner-in-crime Siddharth Agarwal who never left my side and always gave me love, support and extreme confidence. Your faith in me helped me go after challenges and I hope that I can do the same for you. You are right to say that this degree is not just mine but ours!

ACKNOWLEDGMENTS

I would like to acknowledge my Ph.D. mentor and committee chair Dr. Mehdi Nikkhah for his guidance and mentorship throughout my graduate studies. I am extremely grateful to him for perceiving the potential of a Ph.D. candidate in me during my master studies and further providing with an opportunity to continue my graduate studies in his lab. Due to his excellent mentorship I have grown into a mature scientist with an enriched scientific experience. His guidance during my graduate studies helped me in being productive and work on various projects along with multiple excellent researchers.

I would also like to thank our collaborator and my committee member Dr. Robert Ros for providing me with an opportunity to work with him and use his lab resources in successfully completing this project. Along with him, I will also thank my other committee members including Dr. Joshua LaBaer, Dr. Vikram Kodibagkar and Dr. Mo Ebrahimkhani for spending time with me and providing constructive comments that helped me shape the trajectory of the project.

I would like to thank Kiarash Rahmani, Ph.D. student from Dr. Robert Ros lab who helped me in the project by performing AFM experiments. I would also thank all my former and current lab members including Ali, Danh, Jaime, Feba, Nitish, Supriya, Amrita, Eric, Alex, Yuka, Mayar, Casey, Kari, Alison for enriching my experience at ASU by providing friendship, love and support in past 6 years. I would also like to thank

my friends Swathy Sampath, Meryl Rodrigues, Rishabh Shetty for their friendship as well as moral and emotional support.

I would also thank Dr. Ghassan Mouneimne at University of Arizona for providing a constant guidance to me on various biological discussions of the project. Further, I would thank Meryl Rodrigues, Dr. Tanxi CAI and Dr. Tony Hu for assisting us in acquiring proteomics data for the project. Additionally, I would thank Crystal Willingham, Amanda Witten and Kassondra Hickey for teaching me multiple techniques including qPCR and western blot. I would also thank Dr. Barbara Smith for letting me use their lab equipment including qTower and successfully acquire data. I would also thank Dr. Nicholas Stephanopoulos and Alex Buchberger for collaborating with us on GelMA-DNA project. At the end I will acknowledge Dr. Page Baluch and Keck Bioimaging center for letting me work with confocal microscope. I also would like to extend my sincerest thanks to Laura Hawes, Tamera Cameron, Tomi St John and Jessica Jensen for providing all administration support.

TABLE OF CONTENTS

	Page
LIST OF FIGURES	ix
PREFACE	xi
Chapter	
1 Introduction	1
1.1 Breast Cancer	1
1.2 Tumor Microenvironment	2
1.3 Role of various cell types in engineering stromal matrix:	19
1.4 Engineered Models to study Tumor ECM Remodeling	22
1.5 Thesis Overview.....	34
2 The Crucial Role of Breast Tumor Stromal Interaction in ECM Remodeling and Tumorigenicity within a Microengineered 3D Platform	37
2.1 Introduction	37
2.2 Materials and Methods.....	40
2.3 Results	50
2.4 Discussion	72
2.5 Conclusion.....	76
3 Identification of Tumor Secreted Factors Participating in Desmoplasia using Liquid Chromatography Mass Spectrometry	78
3.1 Introduction:	78

Chapter	Page
3.2 Materials and Methods:.....	80
3.3 Results:	82
3.4 Discussion:	93
3.5 Conclusion:.....	97
4 The Role of Desmoplasia and Stromal Fibroblasts on Anti-Cancer Drug	
Resistance in a Microengineered Tumor Model	98
4.1 Introduction:	98
4.2 Materials and methods	101
4.3 Results	108
4.4 Discussion	122
4.5 Conclusion.....	128
5 Conclusion and Future Work	129
5.1 Significance and Contributions:	129
5.2 Project Challenges:	135
5.3 Future Directions:.....	139
REFERENCES	146
APPENDIX	
A SUPPLEMENTARY FIGURES FOR CHAPTER 2	173
B SUPPLEMENTARY FIGURES FOR CHAPTER 3	180
C SUPPLEMENTARY FIGURES FOR CHAPTER 4	186
D LIST OF SUPPLEMENTARY VIDEOS	193

	Page
E COPYRIGHTS AND PERMISSIONS	195

LIST OF FIGURES

Figure	Page
Figure 1-1: Schematic of Tumor Metastatic Cascade.....	4
Figure 1-2: Change in ECM Composition due to Cancer Initiation and Metastasis.	17
Figure 1-3: Previous Research Models to Study ECM Dysregulation in Breast Cancer..	26
Figure 2-1: Microengineering of 3D <i>In Vitro</i> Tumor-Stroma Model.	51
Figure 2-2: Invasion Assay.	54
Figure 2-3: Real Time Cell Migration Assay.	58
Figure 2-4: ECM Stiffness Assay.	62
Figure 2-5: Conditioned Media Assay.....	64
Figure 2-6: CAF Proliferation Assay.....	66
Figure 2-7:Quantification of Pro-Fibrotic Factors in Tumor Conditioned Media.....	68
Figure 2-8: Effect of PDGFR Inhibitor on CAF Based Desmoplasia.	70
Figure 3-1: Quantification of Proteins Across Various Culture Groups.....	82
Figure 3-2: Gene Ontology Results.	85
Figure 3-3: Protein-Protein Interaction Maps for Unique Proteins Detected in MCF7+CAF Group.	87
Figure 3-4:Protein-Protein Interaction Map Highlighting the Interaction Amongst Proteins Which are Known to Participate in ECM Organization.	89
Figure 3-5: Statistical Analysis on Differential Proteins Across Monoculture and Coculture Group of MCF7 Cells and CAFs.	90

Figure	Page
Figure 3-6: Statistical Analysis on Differential Proteins in Monoculture And Coculture of CAFs With MCF7/MDA-MB-231 Cells.	91
Figure 4-1: Proposed Hypothesis of Combinatorial Action of Tranilast With Doxorubicin on Tumor Progression.....	110
Figure 4-2: 2D IC-50 Assay.....	111
Figure 4-3: Characterization of Stromal Desmoplasia Under Various Drug Conditions.	114
Figure 4-4: Representative Histograms of Elastic Modulus and Stiffness Maps Under Various Drug Conditions.	116
Figure 4-5: Tumor Proliferation Assay Under Various Drug Conditions.	118
Figure 4-6: Tumor Dispersion Under Various Drug Conditions.	119
Figure 4-7: ELISA Assay for Quantifying MMP's and TIMP's.	121

PREFACE

This dissertation includes original research articles that have been published in peer reviewed journals by the first author. Chapter 2 which have described the use of 3D microengineered model to study the impact of tumor stroma interactions on ECM fibrosis is currently a manuscript in preparation. Chapter 4 which studies the influence of desmoplasia and anti-fibrotic drug tranilast in improving the efficacy of chemotherapeutic drug doxorubicin is a published article in cellular and molecular bioengineering (Saini et al., 2018).

Chapter 1

Introduction

1.1 Breast Cancer

According to recent statistics, breast cancer is the leading cause of death amongst women across the globe (Bray et al., 2018). It is estimated that in 2019 there will be 268,800 new cases of breast cancer and 41,760 number of deaths in United States alone (Howlader N, 2019). Despite multiple advancements in breast cancer diagnosis, the underlying basis of successful treatment remains the early detection of this devastating disease. Recent surveys by American Cancer Society show that while the five-year survival rate for early stage disease is ~ 99%, the advanced stage of the disease suffer from a low survival rate of ~27% ((ACS), 2017). The disparity in effectiveness of treatment at different stage of the cancer can be directly related to metastatic spread of the tumor in the body. At earlier stages, the tumor cells are localized in the native tissue and hence, the treatment options including surgery and radiation therapy are successful in restraining the cancer (Board., 2019). However, at an advanced stage the malignant cells have broken the barrier of the local tissue and invaded the surrounding region and further metastasized to distant organs (Place, Jin Huh, & Polyak, 2011). At the invasive and metastatic phase of the disease, the commonly administered treatment regime is a combination of surgery that removes all detectable tumors along with adjuvant therapy that aims to minimize the risk of relapse of the disease due to the presence of undetectable tumors (Giordano, 2003). However, due to the presence of various micro metastases at this stage the disease can relapse leading to

reduced disease-free survival (Redig & McAllister, 2013a). Additionally, multiple malignant cells incur drug resistance and therefore do not respond to the therapies leading to reduced effectiveness of the treatment (Moulder, 2010).

The lack of a successful treatment modality for invasive and metastatic stage of breast cancer is partly due to our incomplete understanding of the complex biology of disease progression (Nitish Peela et al., 2017). While the field of cancer biology initially focused on role of genetic mutations in tumor cells and their role in disease progression, a growing body of literature now demonstrate that the local tumor milieu named as “tumor microenvironment (TME)” plays a crucial role in tumorigenesis and metastasis. To that end, it is now become evident that more in-depth mechanistic studies are required to better understand the complex milieu of interaction between cancer cells and TME to understand their specific role in disease progression and design more effective targeted therapies.

1.2 Tumor Microenvironment

Breast cancer progression at various stages has been accepted to be caused by complex crosstalk between tumor and their stromal components in addition to the genetic alteration within the tumor cell (Bissell & Hines, 2011; Douglas Hanahan & Coussens, 2012). Breast cancer cells are supported by a structural framework comprising of extracellular matrix (ECM) in addition to vasculature and different non-malignant cell types including fibroblasts, immune cells, adipocytes, bone-marrow mesenchymal stromal cells and pericytes (Bussard, Mutkus, Stumpf, Gomez-Manzano, & Marini,

2016). Multiple studies have shown that stromal cells present in the TME share phenotypic and genetic similarities to cells participating in wound healing and inflammation (Balkwill, Capasso, & Hagemann, 2012; Grivennikov, Greten, & Karin, 2010). Similar to wound healing and associated inflammation, stromal cells can interact with native malignant cells by either cell-cell interaction or through secretion of growth factors, chemokines and cytokines (Balkwill et al., 2012; Grivennikov et al., 2010). In classical case of wound healing, tissue injury leads to activation of multiple processes (Stroncek JD, 2008); within few seconds of the injury fibrin clot is formed at the site of tissue injury to minimize the blood loss (Sundaram, Quah, & Sampath, 2018). Formation of fibrin attracts multiple immune cells including macrophages to clear out the dead cells and fight any infection at the site of injury. Additionally, fibroblasts cells migrate and proliferate at the site of injury and transform into myofibroblasts phenotype. These myofibroblasts initiate the deposition of collagen and various other matrix proteins to restore the scaffold of the area similar to native tissue before the injury (Sundaram et al., 2018). Epithelial cells, keratinocytes also migrate to this area and perform proliferation to repopulate the area with composition similar to pre-injury state (Sundaram et al., 2018). Once the tissue site is healed, the stimulus for the cells to proliferate, migrate and remodel decreases thereby causing the transformed cells to undergo quiescence (Sundaram et al., 2018). As opposed to wound healing, cancerous tissue does not lose the stimulus and hence the state of hyperproliferation and migration continues. Due to continued release of growth factors/cytokines by cancer cells, stromal cells maintain their

activated phenotype and participate in tumor progression. Different cell types which undergo phenotypic changes to participate in tumor progression are discussed below.

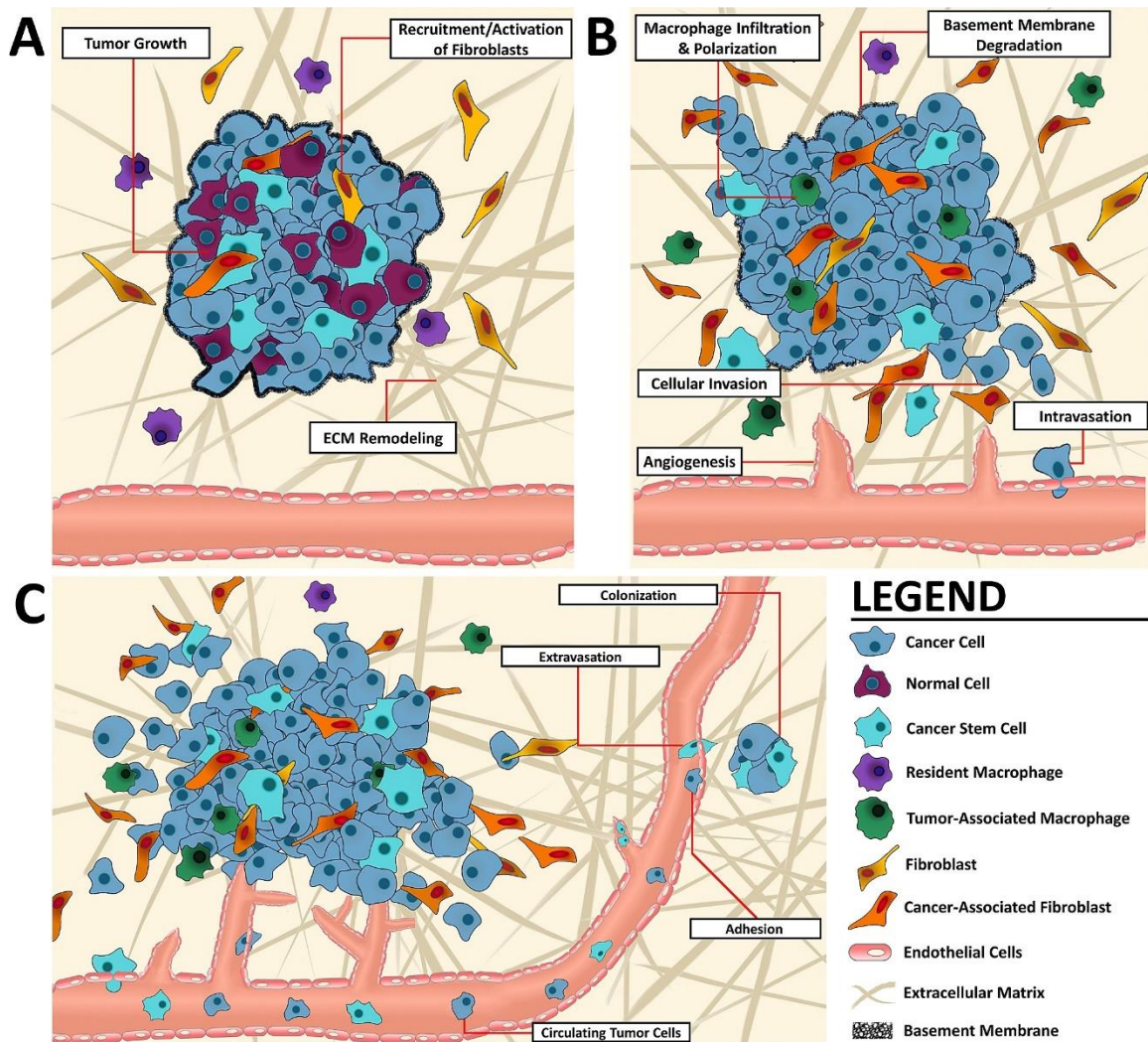


Figure 0-1: Schematic of Tumor Metastatic Cascade.

(A) Tumor growth and development results in ECM remodeling as well as differentiation of cancer stem cells and fibroblasts. (B) Subsequently, angiogenesis, cancer cell invasion, and intravasation occur. (C) Finally, surviving cancer cells and cancer stem cells circulate through the body, attach to blood vessels, and extravasate

to form secondary metastases. Adapted with permission from Biomaterials (Nitish Peela et al., 2017). For copyright please refer to Appendix D.

Cancer Associated Fibroblasts (CAFs):

Fibroblasts are the predominant stromal cell type found within the breast TME (Buchsbaum & Oh, 2016). In a normal healthy mammary tissue, fibroblasts assist in tissue homeostasis by participating in ECM production, basement membrane synthesis as well as in immune cell recruitment (Alkasalias, Moyano-Galceran, Arsenian-Henriksson, & Lehti, 2018). Additionally, normal fibroblasts (NFs) play an essential role in suppressing the growth of malignant cells by a process known as ‘neighbor suppression’ (Alkasalias et al., 2018; Klein, 2014). On the other hand, the transformation of NFs into activated CAFs like phenotype alters the tumor suppressing microenvironment to tumor promoting microenvironment and thereby participates in tumor growth, invasion and anti-cancer drug resistance as shown in Figure 1-1A (Kalluri & Zeisberg, 2006). CAFs have been implicated in multiple clinical studies as a poor prognostic marker of breast cancer. Utilizing patient tissue samples, it has been shown that high proportions of α -smooth muscle actin (α -SMA) positive CAFs correlates with tumor of high grade and reduced overall survival (Buchsbaum & Oh, 2016; SUROWIAK et al., 2007). CAFs can interact with tumor cells by cell-cell interaction (Camp et al., 2011) and paracrine signaling including soluble factor signaling (Shimoda, Mellody, & Orimo, 2010) and exosomes (X. Yang, Li, Zou, & Zhu, 2019). Utilizing this multilayered crosstalk with the tumor cells, CAFs play a crucial role in tumor initiation, tumor invasion, angiogenesis,

lymphangiogenesis, ECM remodeling, inflammation, metabolic reprogramming and anti-cancer drug resistance (Luo, Tu, Liu, & Liu, 2015). For instance, Rozenchan et.al showed in their study that CAFs alter the gene expression profiles of normal mammary epithelial cells such as MCF10A and upregulate stress responsive and pro-survival genes (Rozenchan et al., 2009). On the other hand, studies led by Soon et.al. showed that CAFs can enhance the expression of mesenchymal related markers such as vimentin in MCF10A thereby providing evidence of epithelial to mesenchymal transition (EMT) leading to tumorigenesis and tumor progression (Soon et al., 2013). In another study by Weigel et.al., CAFs were shown to express insulin like growth factor (IGF)- binding proteins which inhibit the process of anoikis in MCF10A cells further strengthening the role of CAFs in tipping the regulatory mechanisms towards cell survival as opposed to cell death (Weigel et al., 2014). Multiple chemokines such as stromal derived factor (SDF1- α), hepatocyte growth factors (HGF), transforming growth factor (TGF β 1) vascular endothelial growth factor (VEGF) and CCL12 (Tsuyada et al., 2012) are secreted by CAFs that can participate in various stages of tumor progression (Chen et al., 2012; Costanza, Umelo, Bellier, Castronovo, & Turtoi, 2017; De Francesco et al., 2013; Fiori et al., 2019; Huang, Li, Zhang, & Nan, 2010; Kojima et al., 2010; Orimo et al., 2005; Tyan et al., 2011). Similar to their normal and wound healing counterparts, CAFs play a key role in ECM remodeling by secreting a variety of matrix components including matrix metalloproteinases (MMPs), collagen, fibronectin, hyaluronic acid, lysyl oxidase, etc. (Santi, Kugeratski, & Zanivan, 2018). They also assist in collagen fiber realignment

thereby providing tracks for cancer cells to invade and migrate with minimal resistance in TME (Erdogan et al., 2017). In an interesting study by Labernadie et.al. and Miyazaki et.al., it was demonstrated that CAFs can promote collective migration of cancer cells by upregulating tight junctions such as N-cadherin at CAFs membrane and E-cadherin at cancer cell surface in squamous cell and pancreatic cancer. While these are interesting set of results that further shed light on physical interaction of CAFs with tumor cells, more investigation is needed to understand the mechanisms which promote such heterotrophic cell junction formation between these two cell types (Labernadie et al., 2017; Miyazaki et al., 2019). Responding to ECM structural realignment, CAFs can also generate high mechanical force which recently has been attributed as a positive feedback for prolonged ECM secretion as well as vasculogenesis (Lu, Weaver, & Werb, 2012; Sewell-Loftin et al., 2017). CAFs also assist tumor cells in immune cell activation and recruitment to the TME. Cohen et.al. demonstrated that fibroblasts activated by breast tumor cells express high level of chitinase 3-like 1 (Chi3L1) which further promote tumor cell migration in wound closure assays and upregulates the expression of proinflammatory and invasive factors including MMP9, CXCL1, CXCL2, IL-6 and CCL2. Knockdown of Chi3L1 in CAFs decreased macrophage infiltration in xenograft tumors and reduced their transformation to tumor promoting M2 like phenotype which is known to be tumor promoting in nature (Cohen et al., 2017). In another study by Yavuz et.al., macrophage recruitment and activation was studied in response to conditioned media collected from CAFs, NFs and cancer cells (Gok Yavuz et al., 2019). It was observed that in contrast to

NFs conditioned media, CAFs conditioned media was able to promote migration of monocytes and activate them to tumor promoting M2 phenotype confirmed by upregulated expression of CD163 and CD 206 which are predominately M2 markers (Gok Yavuz et al., 2019). Furthermore, the authors showed that CAFs educated macrophages also reduced proliferation of CD4+ T cells thereby providing a immunosuppressive environment to tumor cells (Gok Yavuz et al., 2019). Overall, CAFs are an important stromal component which modulates cancer cell and other stromal cell behavior at various stages of cancer metastasis and therefore is an important regulator of tumor progression.

Endothelial Cells:

Endothelial cells are the cell type which form the inner lining of the blood vessels that participate in transport of nutrients, gas exchange and waste in and out of the tissue while maintaining the direction of blood flow (Dudley, 2012). Tumor like normal tissues need a constant supply of nutrients to maintain themselves and perform their metabolic functions (Nishida, Yano, Nishida, Kamura, & Kojiro, 2006). When tumors grow beyond 1-2 mm³, the neoplastic cells cannot maintain their metabolic needs and hence initiate a cascade of events which leads to an angiogenic switch and formation of new blood vessels from existing vessels, a process commonly known as angiogenesis (Nishida et al., 2006; Nitish Peela et al., 2017). In a physiological state, angiogenesis involves a cascade of events where a gradient of angiogenic factors cause local degradation of the basement membrane (Douglas Hanahan & Folkman, 1996). Next, endothelial cells change their

shape and undergo hyperproliferation and invasion into the surrounding area which is primarily dictated by angiogenic factors (Douglas Hanahan & Folkman, 1996). Endothelial cells then reverse themselves into their original phenotype and form intercellular tight junctions leading to formation of new lumen that can allow passage of blood flow and maintain the direction of the flow (Douglas Hanahan & Folkman, 1996). New blood vessels are usually accompanied by a layer of pericytes and basement membrane that provides stability to the neo-vessels (Dvorak, 2015; Nitish Peela et al., 2017). Multiple studies have noted stark differences in the process of normal and tumor angiogenesis (Nishida et al., 2006). For instance, TME provides an imbalance of pro-and anti-angiogenic factors (Nishida et al., 2006). Specifically, it is noted that the TME has an abundance of pro-angiogenic factors including VEGF, bFGF, angiogenein, angiostatin, TGF- β , TNF- α , MMP9, HGF and PDGF and lower expression of anti-angiogenic factors including tissue inhibitors of matrix metalloproteinases (TIMP), thrombospondin and interferon etc. (Nishida et al., 2006). Using animal models and 3D models, it has been shown that the new vessels formed in TME are immature, thin and leaky in nature (S. Nagaraju, D. Truong, G. Mouneimne, & M. Nikkhah, 2018; Nitish Peela et al., 2017). Tumor blood vessels are generally surrounded by a reduced number of pericytes and lack a basement membrane (Dvorak, 2015; Nitish Peela et al., 2017). Additionally, the tumor endothelial cells have reduced expression of intercellular junctions that can lead to large transcellular holes. Together all these changes in tumor vasculature cause the new blood vessels to leak the plasma proteins into the TME which act as a good resource of

sequestered growth factors that leads to enhanced tumor cell migration, intravasation and macrophage recruitment to tumor sites as shown in Figure 1-1B (Nitish Peela et al., 2017).

Overexpression of multiple growth factors by cancer and other stromal cells play a crucial role in tumor angiogenesis. VEGF has been implicated to play a crucial role in tumor angiogenesis which is known to be secreted by tumor cells and CAFs (Watnick, 2012). Presence of hypoxic microenvironment due to hyperproliferation of tumor cells further enhance the expression of pro-angiogenic factors due to the activation of hypoxia inducible factor (HIF) based pathways in tumor cells (Muz, de la Puente, Azab, & Azab, 2015). Other stromal cell types including tumor associated macrophages (M2) are also known to aid in angiogenesis by assisting in immune suppression, upregulation of endothelial proliferation and secretion of multiple pro-angiogenic factors including CCL2, FGF-2, Insulin like growth factor 1 (IGF1), placental growth factor (PGF) etc (Corliss, Azimi, Munson, Peirce, & Murfee, 2016).

Immune Cells:

TME is comprised of various types of immune cells including macrophages, T-cells, NK cells and myeloid derived suppressor cells. During normal tissue homeostasis, most of the immune cells inhibit the growth of malignant cells, however, when the tumor progresses to an invasive and metastatic stage, immune cells alter their phenotype to create an immunosuppressive microenvironment. Various immune cells that participate in tumor progression are detailed below.

Macrophages are generally the resident of various organs of the body such that immune response can be elicited against any foreign body present in the organ (Williams, Yeh, & Soloff, 2016). These are specifically known as tissue resident macrophages which maintain themselves in the organ by using proliferative signaling induced by chemokine Colony stimulating factor (CSF1) (Williams et al., 2016). In TME macrophages account for a large proportion of immune cells due to the presence of various malignant tumor cells (Williams et al., 2016). At initial stages of cancer, macrophages have tumoricidal role such that it promotes anti-tumor immunity (Noy & Pollard, 2014). However, at later stages these cells adapt to a milieu of signals in TME and change its phenotype similar to that of trophic macrophages thereby participating in tissue repair, cancer cell survival, migration, intravasation and metastasis as shown in figure 1-1B (Noy & Pollard, 2014). Macrophages can usually achieve two different polarization state, M1 and M2, which are distinguished based on their ability to express two opposing functions (Hao et al., 2012). M1 phenotype of macrophages have tumoricidal and pro inflammatory abilities and release cytokines which will recruit more monocytes from circulating stream and will present antigens to adaptive immune cells such as T-cells (Hao et al., 2012). On the other hand, M2 phenotype of macrophages are specialized to suppress inflammation and thereby secrete anti-inflammatory cytokines and assist in cancer cell survival, tissue remodeling and angiogenesis (Hao et al., 2012). M1 type of macrophages are also known to be classically activated whereas M2 phenotype of macrophages are said to be alternatively activated (Sica, Schioppa, Mantovani, & Allavena, 2006; Williams et al.,

2016). M1 type of macrophages are regulated in the presence of proinflammatory stimuli such as Interferon (IFN- γ), Tumor Necrosis Factor (TNF- α), Granulocyte macrophage colony stimulating factor (GM-CSF) and release tumoricidal cytokines such as superoxide anions, nitrogen free radicals, immunogenic cytokines IL-1,2,6 and 12 (Sica et al., 2006). On the other hand, M2 state of macrophages is activated when there are anti-inflammatory cytokines such as IL-4, 13,10 and Transforming growth factor (TGF- β) and release polyamines, chemokine ligand (CCL) 17,18,22 and various other factors that make the environment immunosuppressive (Sica et al., 2006).

While M1 and M2 macrophages present opposing functions within TME, their activation state depends heavily on tumor progression stage. It has been observed that at initial stages of cancer, tissue resident macrophages or those recruited from the blood flow are usually of M1 phenotype and thus inhibit the activity of the tumor cells (Noy & Pollard, 2014). However, as the tumor cells undergo proliferation and progresses to advanced stages, tumor associated macrophages switch to M2 phenotype under hypoxic environment and various other signals derived from tumor and stromal cells (Noy & Pollard, 2014). At these advanced stages of cancer, macrophages participate in cell migration, angiogenesis and metastasis due to crosstalk between tumor and stromal cells (Bussard et al., 2016; Noy & Pollard, 2014; Williams et al., 2016). In particular, tumor associated macrophages are involved across all the steps of cancer metastasis including cell migration towards blood vessels, angiogenesis, intravasation as well as extravasation (Hao et al., 2012). Tumor associated microphages secrete chemokines such as epidermal

growth factor (EGF) which interacts with its receptor EGFR on cancer cells and allow the cells to move in chemotactic fashion towards the blood vessel that have macrophages in their proximity (Hao et al., 2012). The cancer cells in turn release colony stimulating factor (CSF1) which promotes the proliferation of macrophages and allow for their recruitment within the TME from circulating stream (Hao et al., 2012; Williams et al., 2016). In addition to release of EGF, tumor associated macrophages also release various MMPs including MMP2 and MMP9 which promote cancer metastasis by degrading ECM and promoting cancer cell migration (Hao et al., 2012). Tumor associated macrophages also secrete various proangiogenic factors such as VEGF, PDGF, bFGF etc which promote angiogenesis (Hao et al., 2012). Further, in hypoxic environment under the effect of HIF-1 α , expression of these factors is further enhanced (Hao et al., 2012).

Other type of immune cells which are found in the TME include regulatory T-cells, cytotoxic T-cells, myeloid derived suppressor cells and NK cells (Chew, Toh, & Abastado, 2012). From previous research it has been established that while NK cells and cytotoxic T-cells promote anti-tumor immunity, regulatory T cells and myeloid derived suppressor cells are pro-tumor in nature (Segovia-Mendoza & Morales-Montor, 2019). During early stages of cancer, dendritic cells and antigen presenting cells presents neoantigens to CD8⁺ T cells and hence maintain tumor suppressive microenvironment (Mittal, Gubin, Schreiber, & Smyth, 2014). However, at an equilibrium phase the anti-tumor and pro-tumor signals are balanced out which cause the tumor to stay in dormant stage (Dunn, Old, & Schreiber, 2004). Prolonged periods of equilibrium phase put a

selective pressure on tumor cells thereby causing selection of mutant aggressive cells which may mutate surface antigens to avoid immunosurveillance and move to an escape phase of immunoediting (Chew et al., 2012; Segovia-Mendoza & Morales-Montor, 2019). In this phase the regulatory T cells and myeloid derived suppressor cells gets recruited into the tissue leading to creation of an immunosuppressive microenvironment (Chew et al., 2012; Segovia-Mendoza & Morales-Montor, 2019). At this stage a more detailed investigation is required to better understand the role of multiple type of immune cells in tumor progression and development of effective immunotherapies (Segovia-Mendoza & Morales-Montor, 2019).

Besides above-mentioned stromal cell types, TME is also made up of adipocytes and mesenchymal stem cells whose role in tumor progression has recently been elucidated by different studies (Carter & Church, 2012; Choi, Cha, & Koo, 2018; Farahmand, Esmaeili, Eini, & Majidzadeh-A, 2018; Lee & Hong, 2017; Maffey et al., 2017; Nickel et al., 2018; Patel et al., 2010; Y. Y. Wang et al., 2017). For instance, Nickel. et.al. demonstrated in their study that coculture of varied breast tumor cells with adipocytes induce differential gene expression dependent on the tumor subtype. To visualize the effect of 3T3-L1 adipocytes on breast tumor cells genetic phenotype; the tumor cells and adipocytes were cultured on a transwell system such that two cell types don't intermix but interact through soluble factor signaling (Nickel et al., 2018). Using microarray system, it was identified that adipocytes upregulated estrogen (Er+) regulated genes in ER+ MCF7 and T47D cells whereas enhanced expression of inflammatory genes

in triple negative MDA-MB-231 cells. Pathway analysis further demonstrated that adipocytes conditioned soluble factors inflammatory pathway such as NF- κ B signaling (Nickel et al., 2018). Additionally, coculture of 3T3-L1 adipocytes with MDA-MB-231 cells enhanced their invasive abilities thereby suggesting a crucial role of these cells in tumor progression (Nickel et al., 2018). In an interesting study by Patel et.al. authors demonstrated a crucial role of mesenchymal stem cells (MSCs) in immunosuppressing the TME by inhibiting the proliferation and cytotoxic effects of peripheral blood mononuclear cell (PBMC) (Patel et al., 2010). Using 2D platforms authors observed that when breast cancer cells such as MCF7, T47D and MDA-MB-231 cells are co-cultured with MSCs the proliferation and migration rate of CD4+ cells was significantly reduced (Patel et al., 2010). Additionally, MSC's shielded the tumor cells from cytotoxic effects of natural killer (NK) and cytotoxic T lymphocytes (CTLs). Using ELISA and knockdown studies authors showed that MSCs derived TGF- β play a crucial role in inhibiting the cytotoxic effects of PBMCs as well as in Treg expansion (Patel et al., 2010).

In addition to various cellular components, TME also comprises of non-cellular scaffold in which different cell types are embedded. Such as complex network of fibrils, extracellular proteins and glycoproteins in known as ECM which has been discussed in detail in the following section.

Extracellular Matrix:

The extracellular matrix (ECM) in the stroma is primarily made up of fibrillar and non-fibrillar collagens in addition to various proteoglycans and glycoproteins (Lu et al.,

2012). Besides providing structural support to the tissue, it also presents various biophysical and biochemical cues to the cancer cells thereby assisting in disease progression through different signaling pathways (Xiong & Xu, 2016). Due to the presence of fibrillar collagen and various other proteins, tumor ECM provides unique physical properties in terms of its rigidity, pore size and fiber orientation in addition to providing anchorage sites (Samani, Zubovits, & Plewes, 2007). For instance, tumor cells in the presence of a rigid matrix demonstrate upregulated integrin signaling which participates in epithelial to mesenchymal transition of the cells (Kalluri & Weinberg, 2009). Additionally, if fiber thickness within the ECM is high with anisotropic fiber orientation then it can act as a migration barrier for the motility of the cancer cells (Lu et al., 2012). Tumor ECM also comprises of various growth factors immobilized on its surface which provides chemotactic gradients to the cancer cells allowing their directional movement (Lu et al., 2012). Due to the action of various proteases secreted into ECM many immobilized biomolecules also activated and initiate signal transduction such as those involved in FGF, WNT, etc. (Lu et al., 2012). Pickup et.al. demonstrated the tumor ECM plays significant role across various hallmarks of the cancer including proliferative signaling, angiogenesis, avoiding immune destruction, tumor promoting inflammation (Pickup, Mouw, & Weaver, 2014).

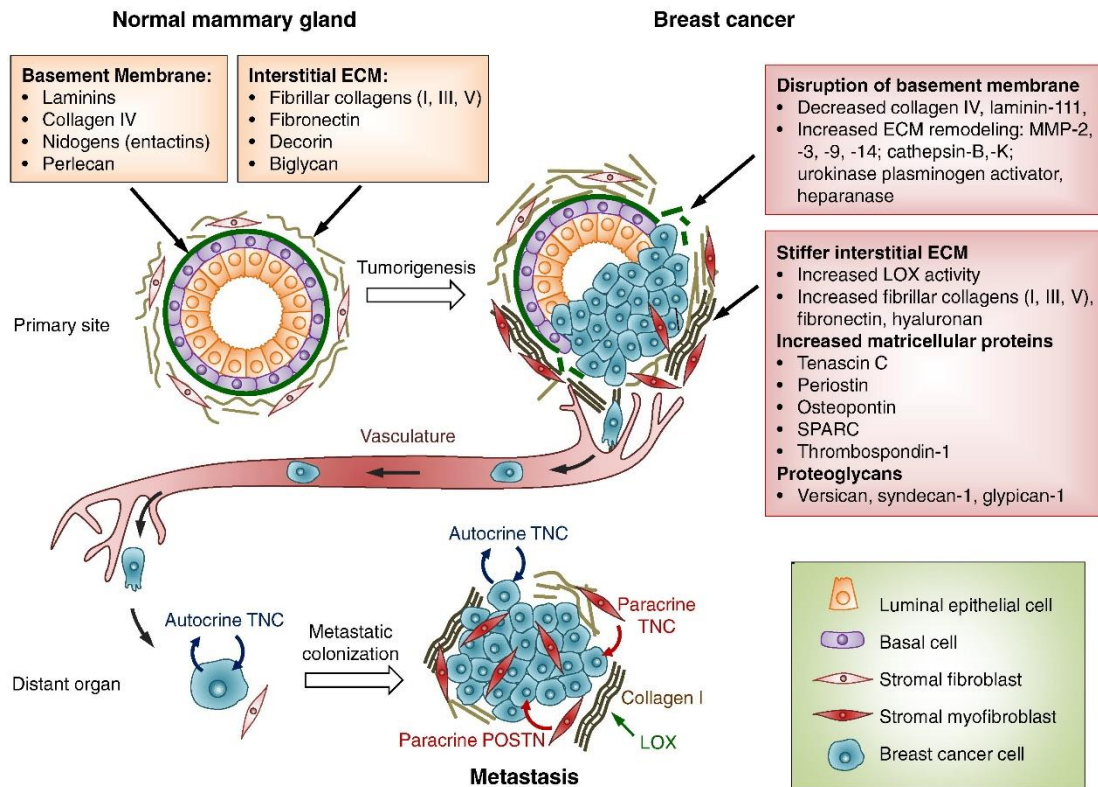


Figure 0-2: Change in ECM Composition due to Cancer Initiation and Metastasis. Adapted with full permission from Advanced Drug Delivery Reviews (Insua-Rodríguez & Oskarsson, 2016). For copyright please refer to Appendix D.

Normal mammary ECM can be broadly classified into two components namely basement membrane and interstitial matrix as shown in figure 1-2 (Mueller & Fusenig, 2004). Basement membrane is a specialized ECM which separates the epithelial and myoepithelial cell layer from the stromal cells as shown in figure 1-2 (Mueller & Fusenig, 2004). It participates in maintaining the polarity of the tissue and exhibit tumor suppressive properties (Oskarsson, 2013). On the other hand, interstitial matrix provides the connective framework to the tissue along with other cell types to maintain the tissue

homeostasis (Mueller & Fusenig, 2004). While basement membrane is made up of collagen type IV, laminin and entactins, interstitial matrix is primarily made up of fibrillar collagen including collagen type I, III, V, VI, VII, XII, fibronectin, hyaluronan and other various other glycoproteins and proteoglycans (Mueller & Fusenig, 2004). It has been observed that as cancer progresses through different stages, tumor ECM also undergoes remodeling similar to wound healing (Lu et al., 2012; Mueller & Fusenig, 2004). For instance, as carcinomas progresses to a pre-malignant phenotype, interstitial matrix show activation of fibroblasts with increased number of macrophages, higher deposition of collagen and enhanced angiogenesis while the basement membrane remains intact (Kalluri & Zeisberg, 2006; Mueller & Fusenig, 2004). On the other hand, when carcinomas become invasive in nature, the basement membrane is degraded and cancer cells come in contact with stromal components which include high amounts of collagen type 1, proteases, macrophages and myofibroblast with leaky blood vessels (Kalluri & Zeisberg, 2006; Mueller & Fusenig, 2004). To that end, tumor ECM or matrix is significantly different in its composition from physiological matrix. In general, tumor related matrix is comprised of different type of collagens including type I, III, V (Oskarsson, 2013). Furthermore, it contains large amounts of elastin, vitronectin, fibronectin, hyaluronon and laminin (Xiong & Xu, 2016). Additionally, tumor matrix is known to contain high amounts tenascin-c which otherwise is absent from normal healthy matrix (Xiong & Xu, 2016). Tumor matrix also contains large of amount of osteopontin and periostin (POSTN) that participates in cancer cell metastasis (Oskarsson, 2013;

Xiong & Xu, 2016). In addition to increase in protein content, many biophysical properties of the cancer matrix also modify. This includes, high stiffness of the tumor associated ECM due to overproduction of collagen modification enzymes including prolyl-4-hydroxylase (P4H), lysyl hydroxylase (PLOD) and lysyl oxidase (LOX) subsequently leading to enhanced collagen fiber crosslinking (Oskarsson, 2013; Xiong & Xu, 2016). The collagen fibers also become more aligned in tumor matrix such that they can assist in cancer cell migration by providing paths of least resistance (Kalluri & Zeisberg, 2006). Different type of proteases including matrix metalloproteinases (MMPs), urokinase plasminogen activator (UPA) and serine proteases are upregulated in tumor ECM such that various pathways can be activated such as FGF, PDGF, angiogenesis (Oskarsson, 2013) .

1.3 Role of various cell types in engineering stromal matrix:

Multiple studies have demonstrated that the tumor ECM components are secreted by both stromal cells as well as by cancer cells (Xiong & Xu, 2016). Major contributors of the tumor ECM synthesis include CAFs due to their abundant population amongst stromal cells (Cirri & Chiarugi, 2011; Kalluri & Zeisberg, 2006). CAFs are known to secrete collagen fibrils including collagen type I, III, V that accounts for the most abundant protein of the matrix (Cirri & Chiarugi, 2011; Kalluri & Zeisberg, 2006). Besides deposition of collagen, it also deposits large amount of fibronectin and hyaluronan such that tumor growth, and migration can be enhanced as well other stromal cell like macrophages can be recruited (Kalluri & Zeisberg, 2006). Additionally, ECM

remodeling enzymes such as MMPs including MMP 1 and 3 as well as UPA are secreted (Cirri & Chiarugi, 2011; Kalluri & Zeisberg, 2006). Other factors released by CAFs include tenascin-c which is generally absent in adult tissue but is overly expressed in cancerous matrix (Cirri & Chiarugi, 2011; Kalluri & Zeisberg, 2006; Xiong & Xu, 2016). In order to influence the stiffness of the matrix, collagen modification enzymes such as LOX are also secreted by CAFs at all stages of cancer (Cirri & Chiarugi, 2011; Kalluri & Zeisberg, 2006). Various cytokines such as insulin growth factor as well as hepatocyte growth factor that participate in tumor migration and invasion are also secreted by CAFs (Cirri & Chiarugi, 2011; Kalluri & Zeisberg, 2006).

Besides CAFs, other stromal cells including tumor associated macrophages, adipocytes and bone marrow derived mesenchymal cells also participate in tumor ECM deposition (Bussard et al., 2016; Williams et al., 2016). This type of macrophages secretes various types of MMPs including MMP 9/13 such that elastin can be generated which can in turn be useful to recruit monocytes (Bussard et al., 2016; Williams et al., 2016). It also secretes fibronectin which can be useful for establishing cancer cell adhesiveness and migration (Bussard et al., 2016; Williams et al., 2016). Other molecules secreted by macrophages include UPA, cathepsins and serine proteases (Bussard et al., 2016; Williams et al., 2016). Bone marrow derived mesenchymal cells are also known to secrete MMP 2/9 (Kessenbrock, Plaks, & Werb, 2010). Since these cells can differentiate to CAFs they can be responsible for remodeling of ECM similar to CAFs thereby conferring chemoresistance. Adipocytes also release MMP13 while endothelial cells

mainly secrete components of basement membrane (Kessenbrock et al., 2010; Lu et al., 2012). In addition to stromal cells, recent studies have demonstrated that cancer cell themselves also participate into deposition of TME matrix (Xiong & Xu, 2016). For instance, it has been observed that cancer cells deposit various matrix proteins including laminin, hyaluronan and tenascin-c and thrombospondin 1 (Xiong & Xu, 2016). While hyaluronan deposited by cancer cell promotes cell proliferation, migration, invasion, multidrug resistance and angiogenesis, tenascin-c promotes lung metastases (Xiong & Xu, 2016). Thrombospondin 1 released by cancer cells are known for their anti-angiogenic effect inhibiting the blood vessel penetration into the tumor (Xiong & Xu, 2016). Additionally, collagen modification enzymes such as PLD and LOX are also expressed by cancer cells under hypoxic conditions using HIF-1 pathway (Xiong & Xu, 2016). Cancer cells also participate in preparing metastatic niche such as that in lung metastases by deposition various components of matrix such as tenascin c-. It has been observed that cancer cell deposited tenascin-c initiates the process of cancer cell metastases which then signals more production of tenascin c by stromal cells (Xiong & Xu, 2016). Thus, both cancer and stromal cells play a significant role in tumor matrix deposition. In this regard, we can conclude that the mixture of cancer cells with stromal cells including fibroblasts, macrophages, bone marrow derived mesenchymal stem cells and adipocytes will deposit interstitial matrix of the natural cancer matrix. Additionally, stromal cells such as fibroblasts, macrophages mixed with endothelial cells secrete the basement membrane that surrounds the blood vessels. Similarly, epithelial cells mixed

with stromal cells including fibroblasts, macrophages, bone marrow derived mesenchymal cells will produce the basement membrane separating the epithelium from the stroma in normal tissue.

1.4 Engineered Models to study Tumor ECM Remodeling

Patient Biopsy based studies:

Human breast tumor biopsies also known as ‘research biopsies’ are useful platforms to visualize changes in the TME including presence of different stromal cell types, expression of various proteins and change in ECM structure (Olson, Lin, Krop, & Winer, 2011). A systematic and scientific approach of performing various assays on fresh tissue assist in determining the biophysical and biochemical changes within the TME (Olson et al., 2011). Multiple studies have taken advantage of these tissue-based assays to study the changes in ECM architecture during tumor progression (Acerbi et al., 2015; Conklin et al., 2011; Olson et al., 2011; Plodinec et al., 2012; Samani et al., 2007). For instance, Acerbi et.al. obtained fresh tissue from patients and stage matched across various tumor subtypes to visualize the changes in ECM architecture and biomechanical properties (Acerbi et al., 2015). Specifically, authors demonstrated that when tumor progresses from normal healthy tissue to invasive ductal carcinoma (IDC) collagen density increases accompanied by enhanced organization of the collagen fibers into a linearized orientation as shown in figure1-3A(Acerbi et al., 2015). It was also noted that the regions of high orientation in the stroma of invasive carcinoma had 4-fold higher stiffness than the stroma of normal healthy tissue (Acerbi et al., 2015). The change is

ECM architecture led to an upregulated integrin-based mechanosignaling which increased the phosphorylation of focal adhesion kinase and myosin light chain that are known to impact multiple downstream pathways including cell proliferation, invasion and EMT (Figure 1-3A) (Acerbi et al., 2015). Interestingly collagen fiber alignment was proposed as a prognostic signature in human breast carcinoma by Keely's group who established multiple tumor associated collagen signatures known as TACS based on collagen fiber orientation at multiple stages of breast cancer (Conklin et al., 2011). By utilizing second harmonic generation Keely's group at University of Wisconsin-Madison studied 169 breast carcinomas and established that at invasive stages of breast cancer, collagen fibers orient and align themselves perpendicular to the tumor boundary, a signature known as TACS-3 (Conklin et al., 2011). Further statistical analysis of their data established that TACS-3 can act as a prognostic signature independent of tumor subtype and is poorly correlated to disease free survival. TACS-3 was also demonstrated to be correlated to syndecan-1 receptors for collagen binding such that regions with high TACS-3 score had high expression of syndecan-1 receptors (Conklin et al., 2011). Some other groups such as Schoenenberger utilized other sophisticated techniques such as indentation type atomic force microscopy (AFM) to acquire stiffness maps of fresh breast tumor biopsies at various stages of the disease (Plodinec et al., 2012). The authors demonstrated that malignant breast tissue have a characteristic bimodal stiffness distribution as compared to healthy tissue which has a unimodal stiffness map (Figure 1-3B). Such heterogeneous distribution of stiffness in malignant tissue was correlated back

to the tissue architecture such that the softer tumor cells were observed to invade into the stiffer peripheral stromal region (Plodinec et al., 2012).

While the patient biopsy-based models provide us with clinically relevant information and establish prognostic markers, there are multiple challenges associated with these platforms. Most of the studies require a large sample size to visualize ECM changes due to the patient heterogeneity. Additionally, samples should be acquired from patients at different stages which are segregated based on tumor grade, size and subtype to establish the correlation between prognostic marker and tumor associated features including receptor status, tumor stage and molecular subtypes. Acquiring and analyzing a large sample size can be therefore be time consuming and laborious. Additionally, most of these studies are end point assays that are useful to perform correlation studies between multiple factors but can't be utilized to establish cause and effect relationship between specific biological cue and cancer cell behavior.

In vivo models:

Animal models are usually considered the gold standard in biomedical research. Due to anatomical and physiological similarities of animals with humans, these models are considered ideal for testing drugs, testing efficacy of various regenerative therapies and studying progression of multiple diseases (Barré-Sinoussi & Montagutelli, 2015). These models also provide a 3D microenvironment with presence of various other cell types, vasculature and lymphatic system making them ideal to carry long term study of diseases such as cancer progression (Barré-Sinoussi & Montagutelli, 2015). In

comparison to patient tissue biopsy models, which is an end point analysis animal models allow design of experiments with appropriate controls that can allow us to visualize the physiological changes in presence and absence of the variable in question. *In vivo* models further allow us to study the progression of the disease and identify unknown factors participating in disease progression by carrying multiple downstream studies such as RNA-sequencing and proteomics.

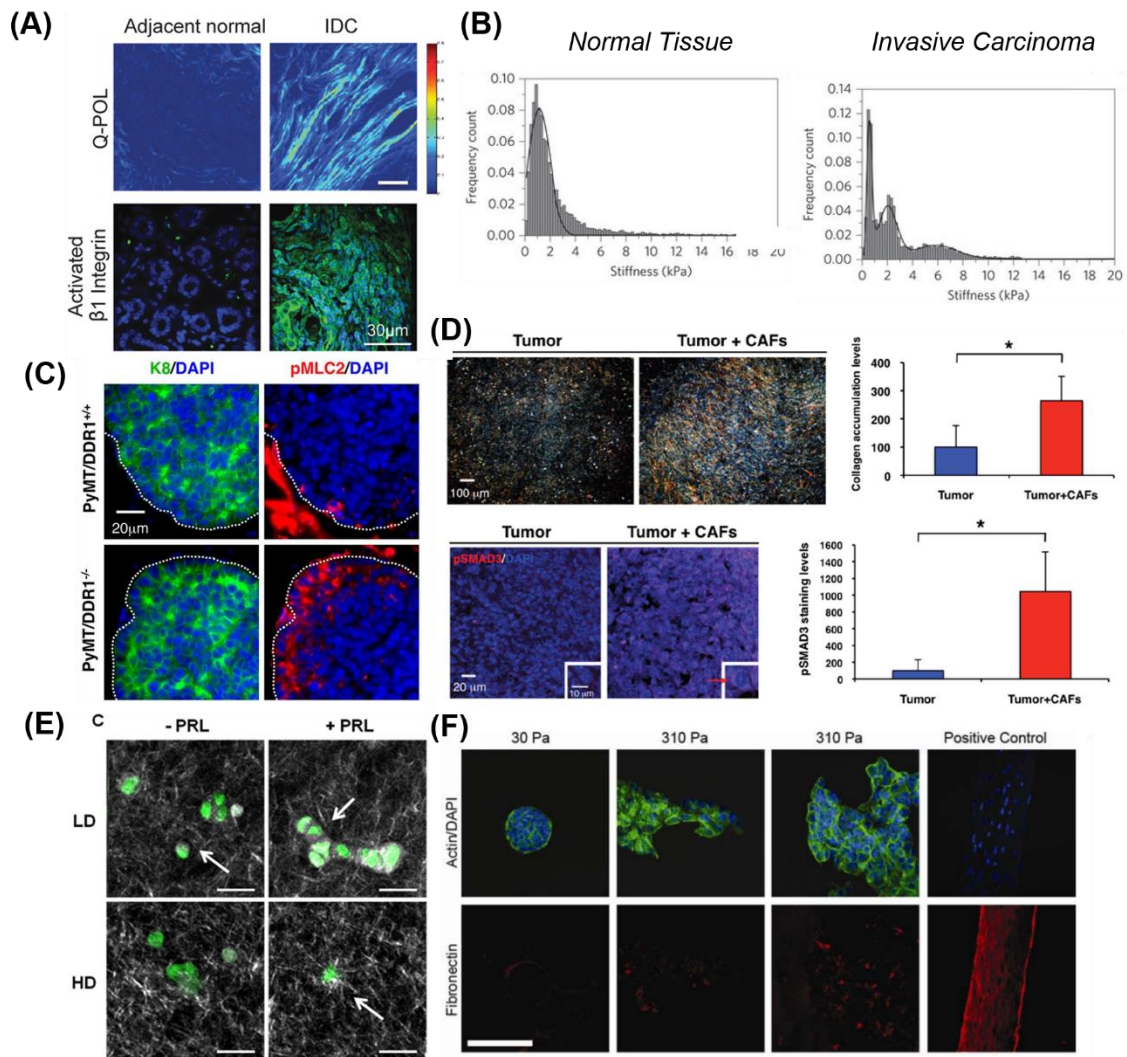


Figure 0-3: Previous Research Models to Study ECM Dysregulation in Breast Cancer.

(A) Representative birefringence maps (Q-POL) and immunofluorescent images demonstrating enhanced stromal density, matrix stiffness and fiber organization leading to upregulated mechanosignaling during tumor progression. Adapted with permission from Integrative Biology (Acerbi et al., 2015) (B) Representative histograms of stiffness

distribution showing characteristic bimodal distribution of elastic modulus for stiff invasive carcinoma as compared to unimodal distribution in normal healthy tissue. Adapted with permission from nature nanotechnology (Plodinec et al., 2012). (C) Immunofluorescent imaging showing high contractile ability (pMLC) of basal cells (K8⁺) in the absence of DDR1. Adapted with permission from genes development (K. Takai et al., 2018) (D) Representative immunofluorescent images depicting high collagen accumulation and activation of SMAD signaling pathway in tumors transplanted with CAFs. Adapted with permission from Oncotarget (Ken Takai, Le, Weaver, & Werb, 2016). (E) Representative second harmonic generation images overlaid with fluorescent images of tumor cells showing perpendicular orientation of collagen fibers to the cell membrane when incubated on high density collagen in presence of prolactin. Adapted with permission from journal of biological chemistry (Barcus, Keely, Eliceiri, & Schuler, 2013). (F) Representative immunofluorescent images for MCF10A cells demonstrating loss of acinar structure on stiff matrices as compared to soft matrices with minimal change in fibronectin expression. Adapted with permission from nature material (Chaudhuri et al., 2014). For copyright please refer to Appendix D.

Various research groups have utilized animal models to visualize desmoplasia in solid tumors such as breast cancer. One of the earliest successful xenograft models for breast cancer desmoplasia was established by Shao et.al. in 2000 (Shao, Nguyen, & Barsky, 2000). Authors utilized multiple ER⁺ (W9, W7, neo MCF7) and Er⁻ cell lines (MDA-MB-231, MDA-MB-468) and successfully created a desmoplastic xenograft

model with W9 cell line in the absence of estrogen (Shao et al., 2000). It was observed that the stroma for these desmoplastic tumors comprised of 30% stromal cells with abundance of collagen (Shao et al., 2000). Additionally, upon transfection of W9 cells with PDGF-A dominant negative mutant, the desmoplastic response was minimized suggesting that tumor cell secreted PDGF can act as an initiator of stromal desmoplasia (Shao et al., 2000). It is crucial to note here that loss of PDGF in W9 cell line did not affect the secretion of other cytokines including TGF- β , IGF or reduced the tumorigenicity of the cell line (Shao et al., 2000). This further underlines the influence of tumor cell secreted PDGF in stromal desmoplastic response. In a recent study by Valerie Weaver and Zena Werb group, authors utilized a xenograft mouse model to understand the role of discoidin domain receptor 1 (DDR1) as either pro- or anti-cancer and its possible role in fibrosis (K. Takai et al., 2018). DDR1 is a well-known collagen receptor whose role in cancer is controversial. Multiple studies have demonstrated that DDR1 at early stages of mammary ductal growth participates in epithelial cell proliferation, differentiation and migration, however, loss of DDR1 at late stages is related to increased expression of collagen in the stroma and therefore participating in mammary carcinoma fibrosis leading to cancer metastasis. By crossing a DDR1 knockout mice with MMTV-PyMT mouse, authors observed that loss of DDR1 leads to higher expression of basal markers (vimentin and keratin 14) as compared to luminal markers (E-cadherin, Keratin 8) within tumor region suggesting that the tumor formed by loss of DDR1 is basal in nature (K. Takai et al., 2018). Additionally, the tumors formed due to the loss of DDR1

were necrotic leading to an upregulation of hypoxia inducible factor (HIF- α). Results from immunofluorescence for pMLC staining and AFM further revealed high expression of contractile and stiffer tumor as compared to DDR1^{+/+} tumors (Figure 1-3C) (K. Takai et al., 2018). Enhanced stiffness lead to an upregulated contractility and integrin based signaling which is shown to participate in tumor proliferation, migration and metastasis to distant organs (K. Takai et al., 2018). Another interesting study by Cox et.al. demonstrated the role of LOX in breast tumor fibrosis and creating a tumor permissive microenvironment that can support metastatic colonization and survival at distant organs including lung and liver. In this study, authors first created successful hepatic and lung fibrotic *in vivo* models by using bleomycin (lung fibrosis) and dimethylnitrosamine (liver fibrosis) (Cox et al., 2013). In both fibrosis models, significant upregulation of α -SMA, collagen, fibronectin and LOX was observed. When the fibrotic models were treated with anti-LOX antibody, the fibrosis were reduced although levels of α -SMA remained the same (Cox et al., 2013). Next, mammary fat pads were injected with 4T1 mammary carcinomas and primary tumor growth within breast tissue remained unchanged in presence or absence of fibrotic environment within lungs or liver (Cox et al., 2013). However, after 3 weeks an enhanced metastasis of tumor cells was visualized in fibrotic organs suggesting that the fibrotic niche support metastatic colonization and survival of tumor cells (Cox et al., 2013). The metastatic load was minimized when the fibrotic organs were treated with anti-LOX antibody. Similar observations about metastatic colonization of 4T1 cells were made when they were injected through rat tail thus

augmenting the significance of fibrotic environment for tumor cell persistence and survival (Cox et al., 2013). While most of the studies focused on role of cytokines and matrix components in inducing ECM desmoplasia, limited studies have been done to study the role of stromal cell types on inducing an ECM desmoplastic reaction within breast tumor. In a study performed by Takai et.al. 4T1 tumors were implanted in a BALB/c mice and with and without CAFs (Ken Takai et al., 2016). It was observed that presence of CAFs enhanced tumor growth and increased lung metastases number. Additionally, presence of CAFs led to an enhanced expression of matrix proteins including such as collagen and an upregulated TGF- β signaling as shown in figure 1-3D (Ken Takai et al., 2016). The anti-fibrotic model thus created was then utilized by the authors to test the effect of anti-fibrotic drug pirfenidone (Approved for Idiopathic pulmonary fibrosis) on the efficacy of chemotherapeutic drug doxorubicin. Their results demonstrated that addition of pirfenidone significantly reduced the tumor growth in comparison to empty vehicle as well as doxorubicin. Additionally, lung metastases number and growth was minimized suggesting a crucial role of CAF induced desmoplasia in breast cancer progression and anti-cancer drug resistance (Ken Takai et al., 2016).

While the animal models provide an advantage over the biopsy-based models to visualize disease progression in a 3D microenvironment, these models are complex in nature and present with multiple confounding factors such as different cell types, unknown cytokines (Nitish Peela et al., 2017). Additionally, it is very difficult to perform

mechanistic studies within animal models due to physiological variability between animals and humans. This necessitates to develop 3D microengineered *in vitro* tumor models that can assist in performing a well-controlled study with appropriate controls and accurate cancer pathophysiology as well as perform real time analysis of various metrics during the course of culture (Nitish Peela et al., 2017).

In vitro models:

Most *in vitro* models have primarily focused on studying the role of ECM in various steps of breast cancer metastatic cascade. Researchers utilize various biomaterials whose stiffness can be modulated to demonstrate an upregulated proliferation and invasion abilities of tumor cells due to the difference in biomechanical properties of the matrix (Barcus et al., 2013; Cavo et al., 2016; Chaudhuri et al., 2014). For instance, Chaudhuri et.al. utilized a hydrogel composed of interpenetrating network formed by alginate and reconstituted basement membrane (Chaudhuri et al., 2014). The authors demonstrated that when normal mammary epithelial cells such as MCF10A are encapsulated on alginate-rBM based hydrogels, increase in matrix stiffness leads to a malignant transformation of the cells leading to loss of acinar structure as shown in figure 1-3F (Chaudhuri et al., 2014). Similar transformation of cells into a malignant phenotype was observed when the change in stiffness due to alginate concentration is accompanied by change in rBM concentration. These results are in contrast when the MCF10A cells are encapsulated within pure rBM hydrogels and high stiffness in these gels maintain the acinar phenotypes suggesting a crucial role of ECM stiffness and matrix composition on

tumor cell initiation and growth (Chaudhuri et al., 2014). Another study by Barcus et.al. utilized collagen matrices and observed that stiff collagen matrices switches the signaling of prolactin from physiological to pro-tumorigenic (Barcus et al., 2013). Specifically, authors utilized T47D cells and cultured them in low density and high-density gels and incubated them with prolactin. Their initial results demonstrated that when T47D cells are cultured on stiffer collagen matrix, a significant 2 fold reduction of STAT5 signaling and enhanced activation of ERK1/2 pathway was observed upon incubation with prolactin (Barcus et al., 2013). Additionally, on low density collagen prolactin leads to formation well differentiated clusters of T47D cells whereas on a stiff hydrogel prolactin disrupts the cluster formation. The change in cellular phenotype on stiff hydrogels in response to prolactin was accompanied by increase in MMP expression, tumor invasiveness and upregulated alignment of collagen fibers (Figure 1-3E) (Barcus et al., 2013).

While the aforementioned studies demonstrated the significant role of biophysical properties of the ECM in aiding tumor progression, notably, not many *in vitro* models focused on studying ECM remodeling during active invasion of tumor cells. Recently, few labs invested themselves in developing 3D *in vitro* models that can be utilized to perform *in situ* measurement of ECM rheology in pancreatic tumor stroma cultures. For instance, Jones et.al. encapsulated pancreatic tumor cells PANC-1 and pancreatic fibroblast cell line such as MRC-5 within a neutralized collagen hydrogel with fluorescent probes (Jones, Hanna, Cramer, & Celli, 2017). Using video microscopy and

particle tracking analysis the mean square distance of the probes was assessed. Interestingly the authors observed high mean square distance of probes when PANC-1 cells were cultured alone in collagen I hydrogel as compared to their coculture with fibroblasts and in ECM free hydrogels (Jones et al., 2017). They also used GSER technique to use frequency dependent rheological measurements of collagen hydrogel and demonstrated high storage modulus of coculture group over monoculture of PANC-1 cell suggesting ECM remodeling due to tumor-stroma interactions (Jones et al., 2017). While the model is one of the first few platforms to study the effect of tumor stroma interaction on ECM remodeling, there are many limitations to the study. The model can be fabricated in a 96 well plate and hence is high throughput in nature, however, the model doesn't have a physiologically relevant tumor stroma organization which has been shown to be important to model various steps of metastatic cascade (S. Nagaraju et al., 2018; Truong et al., 2016). Additionally, similar to previous studies the model did not study the biomechanical properties of ECM during active tumor invasion. Overall, there is still a critical gap in engineering *in vitro* models that can be utilized to not only study the effect of ECM on tumor progression but can also be used to perform *in situ* mechanical measurements of the matrix during dynamic cultures. While most of the models and previous studies have shed some light on role of factors such as LOX and TGF- β in CAF induced desmoplasia, there is still a critical knowledge gap on mechanistic studies about role of tumor stroma interactions on fibrosis.

1.5 Thesis Overview

While the previous models were paramount in establishing the crucial role of ECM dysregulation in cancer progression, we still do not understand the molecular mechanism of matrix remodeling due to tumor-stroma interactions. Additionally, most of the previous studies focused on end point measurement of matrix properties rather than studying the temporal changes thereby providing minimum information about alterations in ECM architecture during active tumor invasion. In this regard, it is imperative to establish an *in vitro* desmoplastic model in which multiple factors including different cell types and various growth factors can be studied with appropriate controls to dissect their individual role in stromal fibrosis. Additionally, integration of the platform with nanoindentation techniques including AFM and confocal microscopy will assist in assessing various biochemical and biophysical changes across the culture period thus enabling a comprehensive study of cancer induced desmoplasia. Building such an in-depth analysis about regulation of tumor ECM remodeling will be significant to not only advance cancer biology but also design better targeted therapies to improve the efficacy of multiple anti-cancer drugs.

In my doctoral studies, we have developed a 3D high-density breast tumor-stroma model which can be utilized to study the cellular and molecular crosstalk of tumor and stromal cells. Additionally, due to open top nature of the platform, we were able to study the change in biomechanical alterations of stromal ECM during active tumor progresses. The overall goal of the study is to visualize ECM remodeling by assessing changes in

collagen fiber deposition and matrix stiffness due to the complex crosstalk between tumor cells and stromal cells (i.e. CAFs) which can then assist in tumor progression including invasion and proliferation. As a proof of concept, this platform was utilized for breast cancer studies, while the capabilities of the platform enable it to be utilized for various other form of cancer including pancreatic cancer.

Specific Aim 1: Development of 3D tumor model to characterize matrix stiffness in presence of tumor (MDA-MB-231/MCF7) and single class of stromal cells (CAFs) : In this aim for the first time we developed a 3D high density tumor-stroma platform that can be integrated with AFM to characterize biophysical properties of the matrix during active invasion of tumor cells in the presence of CAFs. Additionally, to understand the impact of crosstalk between tumor cells of varied tumorigenicity and CAFs on matrix stiffness, we performed extensive studies on biomechanical properties of matrix for both highly invasive MDA-MB-231 cells as well as MCF7 cells.

Specific Aim 2: In depth characterization of the crosstalk between tumor cells and CAFs influencing matrix stiffness While the previous literature has shown that tumor cells depict increased tumorigenicity on enhanced matrix stiffness, not much is known about the necessary signaling molecules between tumor and stromal cells. With this in mind, we extended our studies by studying the mode of interaction between tumor and stromal cells followed by identification of tumor secreted factors that participate in CAF based desmoplasia. To identify various secretomes influencing stromal fibrosis we utilized two approaches including ELISA and label free proteomics.

Specific Aim 3: Study the influence of commercially available anti-fibrotic drug (Tranilast) on alleviating desmoplasia to improving efficacy of anti-cancer

therapeutics: In this aim we studied the influence of commercially available anti-fibrotic drug (Tranilast) on alleviating desmoplasia to improving efficacy of anti-cancer therapeutics. As stiffness has been identified by various previous studies as an important regulator of tumor progression leading to limited chemotherapeutics efficacy, we utilized a commercially available anti-fibrotic drug to reduce the stiffness of the matrix as well as study its synergistic influence on chemotherapeutic drug (doxorubicin) in the presence of single class of stromal cells (CAFs).

While specific aim 1 and specific aim 2 are detailed in chapter 2, specific aim 3 is described in chapter 4. Chapter 3 provides a detailed write up about the adopted methods and results of label free proteomics which were utilized to identify various known and unknown tumor secreted factors as outlined in specific aim 2.

Chapter 2

The Crucial Role of Breast Tumor Stromal Interaction in ECM Remodeling and Tumorigenicity within a Microengineered 3D Platform

2.1 Introduction

Metastatic breast cancer is known as one of the leading killers amongst women across United States with estimated 14% of deaths in 2017 (Siegel, Miller, & Jemal, 2017). It is now established that besides tumor cells, the surrounding mammary tissue microenvironment also plays a significant role in cancer progression from early benign stage to invasive and metastatic phases (Redig & McAllister, 2013b). The tumor stroma is predominantly composed of cancer associated fibroblasts (CAFs) besides other cell types (Balkwill et al., 2012; Kalluri & Zeisberg, 2006). Many studies have demonstrated that CAFs play multifaceted role in tumor progression as they influence various hallmarks of cancer (Kalluri, 2016). For instance, CAFs play a crucial role in epithelial to mesenchymal transition (EMT) of neoplastic cells enabling cell motility and invasion through the stroma (Yu et al., 2014). CAFs also assist in matrix remodeling by secreting proteins such as collagen I as well as proteases including matrix metalloproteinases (MMPs) (Cirri & Chiarugi, 2011). Due to overexpression of collagen and crosslinking enzymes such as lysyl oxidase (LOX), CAFs modulate the stromal stiffness leading to a significant alteration of the biophysical characteristics (Chen et al., 2012; Cirri & Chiarugi, 2011; Schedin & Keely, 2011; Yu et al., 2014).

In the past, various *in vivo* models have been utilized to develop an in depth understanding on the influence of CAFs on breast tumor growth and metastasis (Cohen et

al., 2017; Orimo et al., 2005; Ken Takai et al., 2016). These studies have been paramount in identifying molecular mechanisms through which CAFs exhibit pro-tumorigenic activity however, there are many limitations associated with these models (Nitish Peela et al., 2017). For instance, it is not trivial to assess the dynamic changes in biophysical properties of the matrix including matrix deposition, degradation as well change in stiffness. While some previous *in vivo* models have been able to assess the stiffness of the cancerous tissues by utilizing biopsies and indentation techniques such as AFM (Acerbi et al., 2015; Plodinec et al., 2012), a mechanistic study on the influence of stromal and tumor cells on change in matrix stiffness cannot be achieved due to lack of control condition and presence of confounding factors such as other cell types (Asghar et al., 2015; M. E. Katt, A. L. Placone, A. D. Wong, Z. S. Xu, & P. C. Searson, 2016; Nitish Peela et al., 2017; Shen et al., 2014). Further, such models cannot isolate the stiffness of matrix or tumor cells from that of the bulk tissues, thereby limiting their use for such an in-depth analysis (M. E. Katt et al., 2016). In this regard, various 3D tumor models have been engineered to study the influence of matrix stiffness on cancer cell migration, growth rate and drug resistance (Kraning-Rush, Carey, Lampi, & Reinhart-King, 2013; Peela et al., 2016; Nitish Peela et al., 2017; Sung et al., 2013; Truong et al., 2016). These studies modulate the stiffness of the matrix in various ways including increase in matrix density (Zaman et al., 2006), utilization of synthetic (Ehrbar et al., 2011) and use of composite hydrogel (Chaudhuri et al., 2014) as well as by crosslinking with enzymes such as glutaraldehyde (Lang et al., 2015). While these approaches have been successful

to study the influence of matrix stiffness on cancer cell migration, they do not incorporate essential stromal cells such as CAFs to study extracellular matrix (ECM) remodeling caused by dynamic interaction between tumor and stromal cells. While these models have successfully assessed the mode of interaction such as cell-cell interaction and paracrine signaling for tumor progression; similar set of assessments for ECM remodeling are still largely missing.

In this regard, we fabricated a microengineered high-density 3D tumor entity incorporated with breast cancer cells, with surrounding stroma made up of collagen I embedded with CAFs. Most importantly, our model enables us to mechanistically assess the biomechanical changes within the matrix using AFM and confocal reflection imaging. Further, we utilized RT-qPCR and ELISA to assess the change in expression of profibrotic genes and cytokines. We also characterized cancer cell invasion and migration using live cell imaging to correlate CAF based desmoplasia with tumor growth and progression. Our findings notably suggested that the crosstalk between tumor and stromal cell is necessary to cause significant changes in stiffness of the ECM while monoculture of either cell type can't modulate the biophysical properties of the matrix. Using RT-qPCR we observed high expression of matrix genes when tumor cells and CAFs are co-cultured as compared to monoculture of tumor cells. Our conditioned media (CM) results demonstrated crucial role of paracrine signaling between cancer cells and CAFs such that tumor cells secreted cytokines activate fibrotic pathways within fibroblasts. Our ELISA results suggested crucial role of tumor secreted PDGF cytokines including PDGF- AA and BB in inducing

fibrotic pathways within CAFs. By specifically blocking PDGFR based signaling using various concentrations of CP673451 drug, we further demonstrated the crucial role of PDGF pathway in CAF based desmoplasia. We also observed that CAFs increased the tumorigenicity of breast tumor cells by influencing multiple hallmarks of cancer including proliferation and invasion.

2.2 Materials and Methods

Materials: PDMS (Sylgard 184 Silicon Elastomer Kit, Dow Corning) was used to fabricate PDMS holders and stamps (Figure 2-1A). PDMS holders were surface treated using 2-aminopropyl-triethoxy-silane (APTES) and glutaraldehyde. Confocal dishes on the other hand were surface treated using Poly-D-Lysine (PDL). For surface treatment of PDMS stamps, Pluronic-F 127 was utilized.

Cells: MDA-MB-231 cells expressing red fluorescence was obtained from Dr. Ros's lab at Arizona State University. MCF7 cells expressing red fluorescence was a generous gift from Dr. Mouneimne lab at University of Arizona. Breast cancer associated fibroblasts (CAFs) used in this study were bought from ATCC. All the cells were maintained in DMEM 1X media supplemented with 10% FBS, 1% PenStrep and 1% L-Glutamine. The cells were grown in T-75 flasks within an incubator maintained at 37°C and 5% CO₂.

Antibodies: In order to characterize the cells for various markers, anti-pan-cytokeratin (1:100), vimentin (1:100) and anti- α -smooth muscle actin (α -SMA, 1:100) antibodies were utilized. Further to perform cell proliferation assay Click-iT EdU Alexa Fluor 488

Imaging Kit (Thermo Fisher) was used. To visualize cytoskeleton of cells, Alexa Fluor 488 phalloidin was used at 1:40 dilution.

Surface treatment: The PDMS holders and stamps used to micropattern the platform was designed using AutoCAD. The dimensions of the holders were 8 by 8 mm such that they can fit within a well of 24 well plate. The PDMS stamps on the hand had 300 μm posts of 75 μm diameter with 250 μm center to center distance. Each stamp had an array of 15 by 15 posts in order to fabricate high density tumor microarray. PDMS holders and stamps were casted off the silicon wafer using soft lithography techniques as explained previously (Truong et al., 2016). For surface treatment of PDMS holders, they were cleaned using scotch tape and further treated with air-based plasma for the duration of 4 minutes 30 seconds. The treated holders were immediately immersed into freshly prepared 2% APTES solution in 95% ethanol and incubated at 60 °c for 60 minutes. Next, the APTES solution was aspirated and the holders were immersed in 100% ethanol and ultrasonicated for 20 minutes at high frequency using water based ultrasonication. The ethanol solution was replaced with fresh 100% ethanol and washed 5 times consecutively with 10 minutes interval on a plate shaker to remove residual APTES. The treated holders were then incubated at 80° c for one hour. Next, the holders were incubated in 2% glutaraldehyde solution in DI water for one hour. To remove excess glutaraldehyde the treated holders were washed with DI water 5 times for 5-minute interval followed by overnight incubation at 80 °c. The confocal dishes were treated by PDL at concentration of 0.5 mg/ml for 1 hour followed by 2% glutaraldehyde treatment.

The dishes were then incubated at 80° c oven overnight. To make PDMS stamps protein resistant, they were immersed in 1% Pluronic F-127 solution in DI water overnight in 4° c.

Fabrication of 3D tumor model. Our micropatterned 3D tumor model was fabricated as explained previously by nelson et.al. with brief changes. Collagen 1 was used at the concentration of 4 mg/ml. For coculture condition, CAFs were mixed with collagen I at the cell density of 2×10^6 cells/ml. PDMS stamps were then removed from Pluronic solution and washed three times with DI water. The collagen solution prepared was then added to each stamp immediately and further inverted on top of the PDMS holders. The whole assembly was then kept for polymerization for 30 minutes at 37 °c. After polymerization of the gel, the stamps were lifted off gently and the microwells were seeded with cancer cells at a density of 7×10^6 cells/ml for 2-3 minutes. The cells from unpatterned surface were removed by washing with media as explained in previous protocols (Nelson, Inman, & Bissell, 2008). The prepared samples were kept inside the incubator for 15 minutes to allow attachment of cells to collagen wells. After 15 minutes, the samples were immersed within 500 µl of media in each well of 24 well plate.

Breast Cancer Invasion assay: In order to quantify the breast cancer invasion, samples from all groups were imaged using Zeiss Inverted microscopy and Apotome 2.0 on day 0, 2 and 4. Using phase contrast and fluorescent imaging, images were acquired of 2 x 2 tile at 2 random locations of the sample. Next, we isolated the co-ordinates of the tumor cells within each image using ImageJ and with custom-written MATLAB code performed

delaunay triangulation modelling. The area of each triangle within each delaunay plot as well as standard deviation was calculated using MATLAB. Further, we calculated average area of all triangles and quantified area disorder for each delaunay plot using following equation

$$Area\ disorder = 1 - \left(1 + \left(\frac{standard\ deviation}{average\ area}\right)\right)^{-1}$$

Migration Index was calculated using area disorder by using following formula

$$Migration\ Index = \frac{(Area\ disorder\ on\ Day\ 1 - Area\ Disorder\ on\ Day\ 3)}{Area\ disorder\ on\ Day\ 1}$$

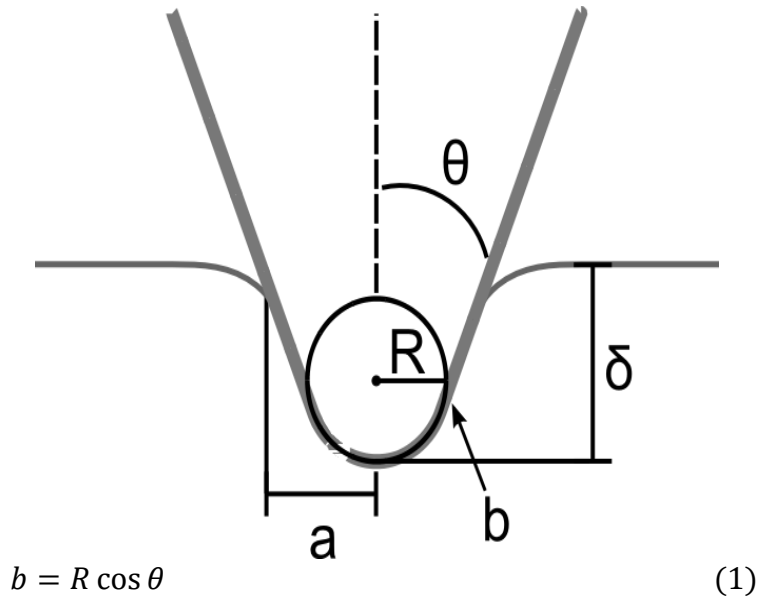
MCF7 cluster area was quantified using Image J analyze particles plugin. The average cluster area for day 2 and 4 for all the samples in each condition were normalized with respect to day 0.

Cell proliferation assay: The cell proliferation was quantified by using Click iT-Edu Imaging Kit. The assay was performed as per manufacturer's instruction. In order to quantify the cancer cell proliferation, the DsRed positive cell with EdU positive nuclei was counted in Image J using cell counter plugin. The CAF proliferation was quantified by counting the cells which were not DsRed Positive but had an EdU positive nuclei. To calculate percentage of proliferative cells, the EdU positive cancer cells or CAF cells was divided by total number of cancer cells or CAF cells respectively.

AFM

Asylum Research MFP-3D-BIO AFM was used to conduct the force-indentation measurements. Team NanoTec LRCH-750 AFM probes with sphere-cone geometry were

used. The spring constants (nominal $k \sim 0.2 \text{ N.m}^{-1}$) were determined using thermal energy dissipation method (Butt & Jaschke, 1995; Hutter & Bechhoefer, 1993). Samples were measured and imaged at 37 C in 1X Hank's Balanced Salt Solution (HBSS) containing calcium and magnesium. The samples were also buffered with 25 mM HEPES to maintain their pH during the measurements. Quasi-static measurements with cantilever approach and retraction speed $2 \mu\text{m.s}^{-1}$ were conducted to collect elastic modulus data. In $90\mu\text{m} \times 90\mu\text{m}$ area in the middle of four micro-wells a grid of 4×4 indentations was acquired by applying trigger force of 40-75 nN which resulted in 10-17 μm of indentation. The choice of trigger force was made to obtain desired indentation intervals. The first 10 μm of the force-indentation curves were fitted to a non-adhesive quasi-static contact model for a canonical indenter with a spherical tip that features continuous curvature at the transition point (Staunton, Doss, Lindsay, & Ros, 2016).



$$\delta(a \leq b) = \frac{1}{2} a \ln \left(\frac{R+a}{R-a} \right) \quad (2)$$

$$F(a \leq b) = \frac{E}{(1-\nu^2)} \left[\frac{1}{2} (a^2 + R^2) \ln \left(\frac{R+a}{R-a} \right) - aR \right] \quad (3)$$

$$\delta(a > b) = a \ln \left(\frac{R+a}{\sqrt{R^2-b^2} + \sqrt{a^2-b^2}} \right) + a \cos^{-1} \left(\frac{b}{a} \right) \cot \theta \quad (4)$$

$$F(a > b)$$

$$\begin{aligned} &= \frac{E}{(1-\nu^2)} \left[a^2 \cot \theta \cos^{-1} \left(\frac{b}{a} \right) \right. \\ &+ b \cot \theta \sqrt{a^2 - b^2} - aR + \sqrt{(R^2 - b^2)(a^2 - b^2)} + a^2 \ln \left(\frac{R+a}{\sqrt{R^2-b^2} + \sqrt{a^2-b^2}} \right) \\ &\left. - \frac{R^2}{2} \ln \left(\frac{a^2 R^2 - (b^2 - \sqrt{(R^2 - b^2)(a^2 - b^2)})^2}{b^2 (R+a)^2} \right) \right] \quad (5) \end{aligned}$$

Dynamic measurements, with the same probe approach and retraction speed, were conducted to collect viscoelastic data. In the same 90 μm ×90 μm area of each quasi-static measurement a grid of 2×2 indentations was acquired by applying trigger force of 3-7 nN which resulted in 1.5-6 μm of quasi-static indentation. At the quasi-static indentations depth (δ_0) oscillatory part of indentation ($\delta(\omega)$), with amplitude of 50 nm, at different angular frequency (ω) was applied by oscillating the z-piezo and measuring the oscillatory force respond of the sample. Later, amplitudes of force and indentation oscillation along with the phase lag between force-time and indentation-time curves were analyzed by the dynamic contact model derived from [Eq. 5] to calculate the viscoelastic

properties of sample (i.e. complex modulus). The dynamic experiment is carried out at frequencies (1, 3.16, 10, 21.54, 31.62, 46.42, 100 Hz).

$$G_{Spherecone}^*(\omega) = G'(\omega) + iG''(\omega) = \frac{1 - \nu}{4a_{0,Spherecone}} \left(\frac{F(\omega)}{\delta(\omega)} - ib_{h=0}\omega \right)$$

Where quasi-static contact radius $a_{0,Spherecone}$ is the solution of equation 6.

$$\delta_0 = a_0 \ln \left(\frac{R+a_0}{\sqrt{R^2-b^2} + \sqrt{a_0^2-b^2}} \right) + a_0 \cos^{-1} \left(\frac{b}{a_0} \right) \cot \theta \quad (6)$$

The viscoelastic features of collagen matrix can be explained by soft glassy model (Gevorkian, Allahverdyan, Gevorgyan, & Hu, 2011). Frequency sweep of the complex modulus ($G^*(\omega)$) was fitted to soft glassy model (Rother, Nöding, Mey, & Janshoff, 2014; Sollich, 1998).

Confocal reflectance microscopy

Picoquant Microtime 200 confocal laser scanning microscope was used to obtain reflectance microscopy images. Each reflectance scan was $80\mu\text{m} \times 80\mu\text{m}$, 512×512 pixels (156nm/Pixel) and took approximately 2.5 minutes. A $60\times$, 1.1 NA, 1.5 mm W.D. water immerse objective was used (Olympus LUMFL60X). Continuous blue diode laser (ex: 470 nm) was used to illuminate the sample and the reflected light was collected and went through a 30 nm pinhole, and was detected by a single-photon counting modulus (Picoquant PDM series). Intensity micrograph of the scans are constructed in the operating software (Picoquant SymphoTime).

Live Cell Tracking: To quantify cancer cell migration parameters, we performed 12 hours live cell tracking at the time period of 72 hours of the culture. The movie was acquired using Zeiss inverted microscope along with Apotome 2.0. The microscope stage was surrounded by an in-house built incubator integrated with heater and CO₂ supply to maintain optimum culture conditions. The z-stack images were acquired every 45 minutes using 10x objective across a depth of 50-60 μm . The images were analyzed using cell tracking script within MATLAB (Cell Tracker, Budapest, Hungary). Each cell was manually tracked frame by frame to record the cell coordinates. Using the software, cell velocity and persistence was calculated for each cell across all the samples. We analyzed 15 cells per movie with duplicate replicates. Each experiment was repeated three times such that 90 cells were tracked for each condition. The cell tracks were obtained using ibidi Chemotaxis and Migration Tool with an ImageJ plugin.

Conditioned media Experiments: To perform conditioned media experiments, MDA-MB-231 and MCF7 cells were cultured within our model in both monoculture and coculture condition for 4 days and media was collected on day 2 and day 4. The conditioned media was then centrifuged at 4000 RPM for 10 minutes at 4°C to remove any cell debris and further stored in -80 °C. To study the interactions between tumor and stromal cells, CAFs were cultured in monoculture condition within our 3D model for 4 days. Right after initial AFM measurement of the CAF only samples on day 0, day 2 conditioned media were added. The measurements were repeated on day 2 for the same samples followed by incubation in day 4 conditioned media and final measurement on day 4.

Western Blot: Western blot was performed according to a protocol provided by Bio-rad. Briefly, cells were lysed with a solution containing protease inhibitors. These samples were denatured in loading buffer. Proteins were separated with Gel Electrophoresis using a 10% polyacrylamide gel. The proteins were transferred to a PVDF membrane using Bio-rad Trans Blot Turbo blotting system. Membranes were blocked in 5% BSA and stained using mouse primary antibody and 800 nm tagged goat-anti-mouse secondary antibodies. These membranes were imaged using the licor Odyssey imager. For all our blots, vinculin was used as our loading control.

RT-qPCR: Cells were isolated from our 3D tissue by incubating the samples in 2mg/ml collagenase I dissolved in 1X PBS for 30 minutes inside the incubator. The samples were then mechanically digested by pipetting. The collagenase I solution was then collected and centrifuged to form a cell pellet. The cells were then mixed with 300 μ l RNA lysis buffer from Zymos to lyse the cell and collect total RNA. The RNA was purified using Zymos micro RNA prep Kit. To digest genomic DNA, isolated RNA was subjected to DNase I treatment. The quality of RNA was confirmed by using NanoDrop and reading A260/A280 and A260/A230 values. Using 1 ug as starting RNA template, cDNA was prepared by using Quantabio cDNA supermix. The qRT-PCR was performed by using Luminaris Color HiGreen qPCR Master Mix (Thermo Scientific) with appropriate controls as per manufacturer's Instructions. The qPCR plates were ran in triplicates using qTower 2.0 (Analytik Jena US). The primer sequences for various genes have been detailed in the table below.

ColI α I Forward Primer	CCTGGATGCCATCAAAGTCT
ColI α I Reverse Primer	CGCCATACTCGAACTGGAAT
ColIII α I Forward Primer	TAGGTCCATCTGGTCCTGCT
ColIII α I Forward Primer	CGAAGCCTCTGTGTCCTTTC
FN Forward Primer	GATGCTCCCACTAACCTCCA
FN Reverse Primer	CGGTCAGTCGGTATCCTGTT
LOX Forward Primer	TGCCAGTGGATTGATATTACAGATGT
LOX Reverse Primer	AGCGAATGTACAGCGTA CAA
TGF- β 1 Forward Primer	CAGAGGAGAGTGGCTGAAGG
TGF- β 1 Reverse Primer	CCAGGACTCAATCCCTGTGT
GAPDH Forward Primer	TGCACCACCAACTGCTTAGC
GAPDH Reverse Primer	GGCATGGACTGTGGTCATGAG

Quantification of cytokines within our 3D tumor model: The relative expression of cytokines was measured in our 3D samples by utilizing a custom made Quantibody array from Raybiotech. The custom-built array was built to study the expression levels of IL-4, IL-13, PDGF-AA, PDGF-BB, PDGF-AB, PDGF-CC and TGF- β within our samples. FBS containing CM was collected on day 4 from our samples and centrifuged at 4000 rpm for 10 minutes at 4 °c. The supernatant was collected and stored at -80 °c until further use. Due to the presence of serum in our CM, the media was diluted 5-fold using sample diluent. A media blank was also added to our samples to normalize the

concentration of various cytokine within our samples. The assay was performed as per the manufacturer's instruction and then shipped to Raybiotech for extracting the fluorescent values.

Statistical Analysis: All the experiments were repeated three times with triplicates samples per condition. The invasion and elastic modulus data were analyzed using two-way ANOVA with Sidak's multiple comparison test. The standards for our cytokine expression data was plotted by using Sigmoidal 4PL curve in Prism and unknown concentration of our samples was interpolated from these curves. The relative expression was compared across samples by using one-way ANOVA followed by Dunnet multiple comparison test. All other data was analyzed using paired t-test. p value less than 0.05 was considered significant for all the results. The statistical analyses and data representation were performed using GraphPad Prism v 7.0. All the data was presented as mean \pm standard deviation.

2.3 Results

Fabrication of high-density 3D breast tumor array:

In order to spatially organize cancer cells surrounded by stroma in our 3D tumor model we utilized micropatterning technique to engineer the platform. Specifically, the model was fabricated by using PDMS stamps and micromolding techniques to construct a high-density array of microwells within collagen I hydrogel similar to the previous reports (Figure 2-1A) (Nelson et al., 2008). The stromal region of the model comprised of CAFs embedded in collagen I matrix while the tumor region was engineered by seeding breast

cancer cells (MDA-MB-231, MCF7) within microwells (Figure 2-1A). The model was further integrated with AFM to assess the biophysical properties of the stroma such as matrix stiffness as shown in Figure 2-1B. As a control, the tumor cells were also cultured in monoculture condition surrounded by collagen I in the stroma. Figure 2-1 C demonstrates successful fabrication of monoculture and coculture group where cancer cells are spatially organized in microwells (DsRed) surrounded by collagen I in absence or presence of CAFs.

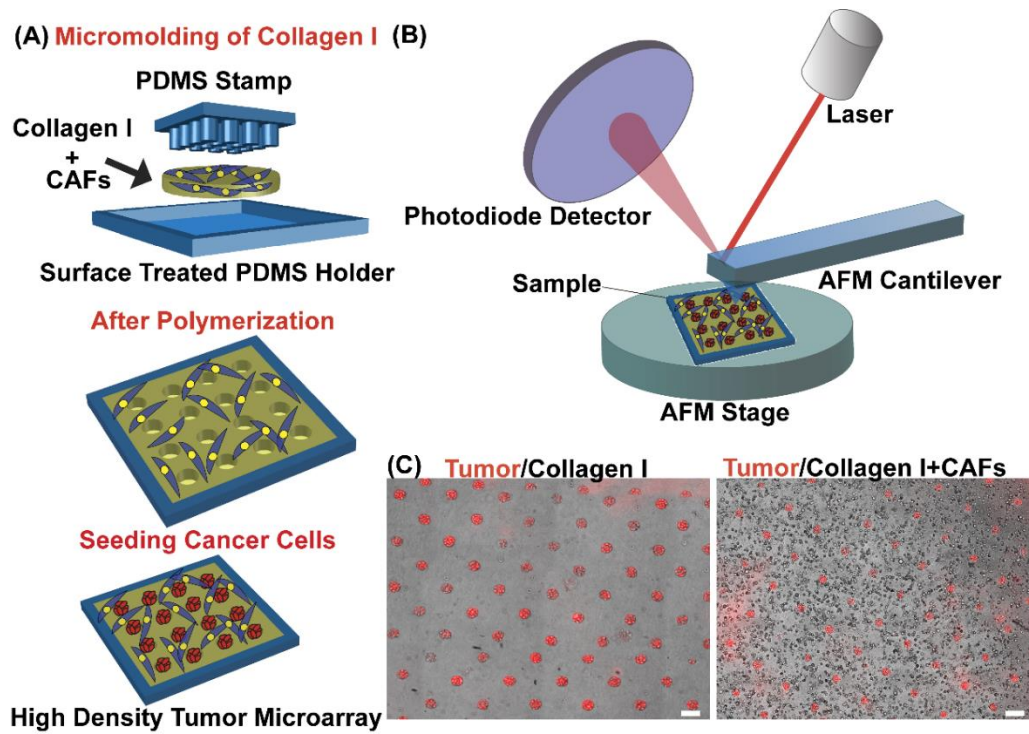


Figure 2-1: Microengineering of 3D *In Vitro* Tumor-Stroma Model.

(A) Schematic of microfabrication of 3D tumor model. (B) Schematic of AFM. (C) Representative images showing microfabricated 3D high density tumor model across monoculture and coculture group.

Prior to proceeding to further biological experiments, we characterized breast cancer cells and CAFs for expression of proteins including α -smooth muscle actin (α -SMA), vimentin and pan-cytokeratin using immunofluorescence and western blot techniques. While CAFs expressed α -SMA, MDA-MB-231 and MCF7 cells did not show positive for the protein (Supplementary Figure 1, APPENDIX A). On the other hand, vimentin a mesenchymal marker, was expressed by MDA and CAFs while pan-cytokeratin was expressed by MDA-MB-231 and MCF7 cells (Supplementary Figure 1, APPENDIX A). These data indicated that the fibroblasts used for the experiments were activated while MDA-MB-231 and MCF7 breast tumor cells depicted varied genomic make up and phenotype.

Breast cancer invasion assay

To visualize the effect of CAFs on breast tumor cells invasion, we performed an initial assessment using phase contrast and fluorescent imaging across culture period of 4 days. Our results demonstrated single cell invasion of MDA-MB-231 cells into the stroma across all experimental conditions (Figure 2-2A). While in monoculture condition, these highly invasive cancer cells aggregated near the microwells, they demonstrated cellular scattering within stroma when cultured with CAFs (DsRed, Figure 2-2A). To quantify the phenomenon of cell scattering, we further utilized mathematical and computation geometry model known as delaunay triangulation. As shown in delaunay plots in Figure 2-2B, MDA-MB-231 cells were initially located within microwells in both monoculture and coculture conditions on day 0. However, by day 4 of the culture period, tumor cells

scattered within the stroma, away from the microwells in coculture condition (Figure 2-2B). In contrast, amongst monoculture group, these cells maintained their positions and aggregated near the microwells through the duration of culture period of 4 days (Figure 2-2B). To quantify cell dispersion across monoculture and coculture group, a custom metric migration index was calculated (see Materials and Methods) using triangulation graphs. As shown in Figure 2-2D the migration index of MDA-MB-231 cells upon coculture with CAFs was significantly higher than monoculture group on day 2 and day 4. Such an analysis thus confirmed scattering of MDA-MB-231 cells in co-presence of CAFs thereby depicting enhanced invasion abilities of tumor cells in coculture condition.

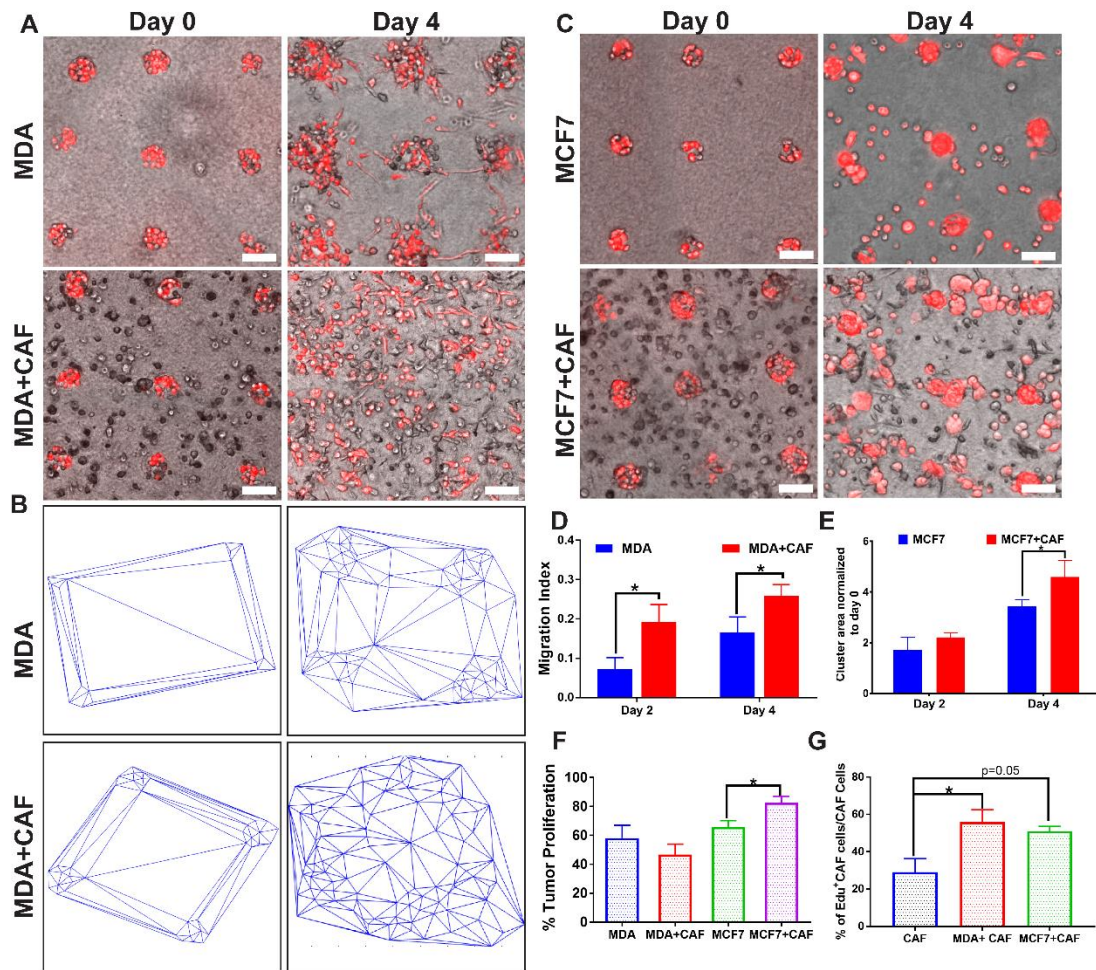


Figure 2-2: Invasion Assay.

(A) Representative phase contrast and fluorescent images across monoculture and coculture group of MDA-MB-231 cells over culture period of 4 days. (B) Representative color coded delaunay triangulation graphs across experimental groups demonstrating cellular scattering. (C) Representative phase contrast and fluorescent images across monoculture and coculture group of MCF7 cells. (D) Migration Index of MDA-MB-231 cells in monoculture and coculture conditions. (E) Quantified cluster area of tumor cells across experimental groups for day 2 and day 4 normalized to day 0. (F) Quantification of

percentage of EdU+ cancer cells between monoculture and coculture groups for MDA-MB-231 and MCF7 cells. (G) Quantification of percentage of EdU+ CAF cells between monoculture and coculture groups. All scale bar represents 100 μm . * represents p value < 0.05.

In contrast to MDA-MB-231 cells, less invasive MCF7 cells depicted colony forming tendencies within the 3D tumor model, consistent to the previous reports (Kenny et al., 2007) (Figure 2-2C, Supplementary Figure 2B, APPENDIX A). During the culture period of 4 days, MCF7 cells clustered and filled up the microwells initially seeded into across all experimental groups (Figure 2-2C). While in monoculture condition, these less invasive cells invaded in the form of single cells, they formed clusters within coculture group in the stroma (Figure 2-2C, Supplementary Figure 2B, APPENDIX A).

Quantification of normalized cluster area for day 2 and day 4 suggested that the clustering abilities of MCF7 cells enhanced in the presence of CAFs (Figure 2-2E). 3D z-stack actin images, shown in supplementary Figure 2 (APPENDIX A), further demonstrated that while MDA-MB-231 cells invaded across different planes, MCF7 cells invaded as single layer on top of the gels across all the conditions. Such a difference in invasion abilities between two tumor cells can be attributed to their genomic make up which was maintained when cocultured with CAFs (Kenny et al., 2007). Overall our results show that while MDA-MB-231 cells enhanced their invasion abilities, MCF7 cells depicted a higher tendency towards cluster formation in the presence of CAFs.

Tumor and stromal proliferation

It is widely known that tumor cells depict the phenomenon of invasion-proliferation dichotomy such that highly migratory cells lose their proliferative phenotype during invasion (Fedotov & Iomin, 2007; Hatzikirou, Basanta, Simon, Schaller, & Deutsch, 2012; Hecht et al., 2015). In this context, EdU assay was performed to isolate the influence of CAFs on cancer cell migration from proliferation to visualize the dividing tumor cells through fluorescent imaging. As shown in Supplementary Figure 3 (APPENDIX A), dividing cancer cells were marked for newly synthesized DNA (co-expressing DsRed and GFP) and demonstrated proliferation across all experimental groups. Quantification for EdU positive cancer cell (DsRed) suggested an enhanced proliferative behavior of MCF7 cells upon coculture with CAFs as compared to their monoculture group (Figure 2-2F). On the other hand, MDA-MB-231 cells did not demonstrate any significant change in their proliferation rate when cultured with CAFs (Figure 2-2F). Such a stark difference in proliferative behavior of different breast tumor cell lines combined with invasion results suggest that while CAFs enhanced MDA-MB-231 cells invasion, it primarily influenced the proliferation of MCF7 cells.

In addition to tumor cell proliferation, we also investigated CAFs proliferation across different coculture groups within our 3D tumor model. CAFs (non DsRed cells) depicted proliferation across all the experimental groups as shown in Supplementary Figure 4 (APPENDIX A). An enhanced proliferation of CAFs was observed in presence of both MDA-MB-231 and MCF7 cells (Figure 2-2G, Supplementary Figure 4, APPENDIX A). These results are in agreement to previous clinical studies where the

cancerous tissue is observed to have high number of α -SMA expressing CAFs as compared to the healthy tissue (Nakagawa et al., 2016). Thus, overall these results suggest that the crosstalk between tumor and stromal cells can profoundly influence proliferative behavior of each other.

Real time single cell tracking of tumor cells

While our invasion and proliferation assays provided comprehensive analysis of the influence of CAFs on tumor cells, in-depth mechanistic analysis including mode of migration, cell speed and persistence was performed through real time tracking of cancer cells across various experimental conditions (Figure 2-3). As shown in supplementary movie 1 and 2 (APPENDIX A), MDA-MB-231 cells migrated as single cells across monoculture and coculture conditions. The representative cell tracks further demonstrated enhanced dissemination of tumor cells in the presence of CAFs as compared to monoculture condition (Figure 2-3A). Using live cell tracking script, we quantified average cell speed and persistence and observed no significant difference for the bulk population of tumor cells between the experimental groups (Figure 2-3C, G). In contrast, when we analyzed the frequencies of various cell speeds in monoculture and coculture condition, higher percentage of MDA-MB-231 cells were observed to migrate at faster speeds ($\geq 0.2 \mu\text{m}/\text{min}$) in the presence of CAFs (Figure 2-3B) suggesting increased heterogeneity between tumor cells. Thus, after thresholding average cell speed at $0.2 \mu\text{m}/\text{min}$ from the histogram in Figure 2-3B, enhanced number of cells were observed to migrate at faster speeds ($\geq 0.2 \mu\text{m}/\text{min}$) in coculture condition as compared to

monoculture group (Figure 2-3D). Similar analysis of distribution of cell persistence between two groups was made and increased number of MDA-MB-231 cells exhibited high persistence (≥ 0.3) in coculture condition (Figure 2-3H). While the percentage of cells at high persistence were more in coculture group, this outcome was not statistically significant ($p = 0.0532$) (Figure 2-3H). Thus, our results demonstrated that when MDA-MB-231 cells are cocultured with CAFs, heterogeneity within tumor population increases with a greater number of cells acquiring enhanced migratory characteristics.

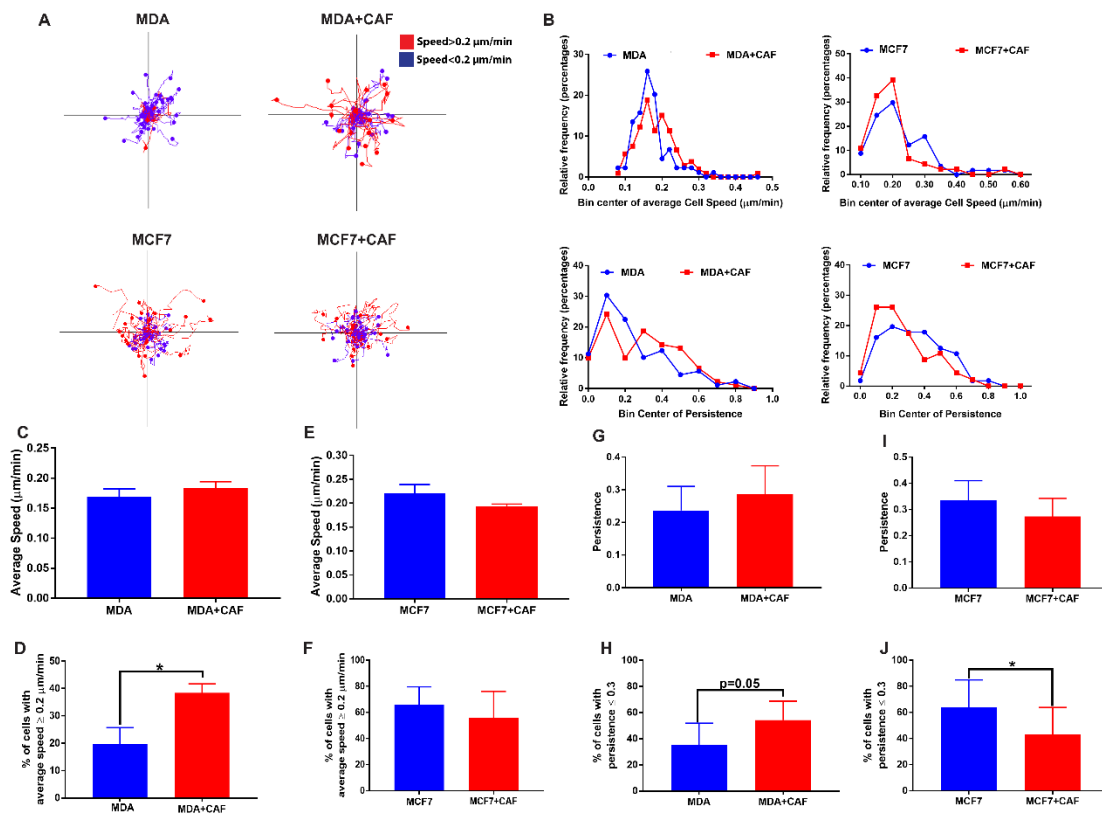


Figure 2-3: Real Time Cell Migration Assay.

(A) Representative cell tracks across monoculture and coculture group for MDA-MB-231 and MCF7 cells respectively. (B) Histogram of cell speed and persistence for MDA-MB-

231 and MCF7 cells within each group. (C) Average speed of MDA-MB-231 cells across all culture conditions. (D) Quantification of percentage of MDA-MB-231 cells with average speed greater than or equal to 0.2 $\mu\text{m}/\text{min}$ across all groups. (E) Average speed of MCF7 single cells across all culture conditions. (F) Quantification of cell speed for MCF7 cells above 0.2 $\mu\text{m}/\text{min}$ across all groups. (G) Average persistence of MDA-MB-231 cells. (H) Quantification of percentage of cells with average persistence greater than 0.3 $\mu\text{m}/\text{min}$ across all groups. (I) Average persistence of MCF7 cells. (J) Quantification of percentage of MCF7 cells with average persistence greater than 0.3 $\mu\text{m}/\text{min}$ across all groups. * represents p value < 0.05.

Similar real-time analysis was also performed for MCF7 cells as shown in Figure 2-3 and supplementary movie 3, 4 (APPENDIX A). Interestingly we observed that while MDA-MB-231 cells migrated as single cells, MCF7 cells on the other hand demonstrated a high clumping and proliferative activity during migration across all experimental groups. While MCF7 clusters were also observed to migrate within the matrix, it was difficult to quantify them due to continuous change in cluster size either due to division or clumping of more cells. Thus, we limited our analysis to single cells that neither proliferated nor clumped during 12-hour long migration (see Methods). Representative cell tracks for each condition suggest no noteworthy change in tumor cell dissemination are shown in Figure 2-3A. Further analysis demonstrated no significant differences in cell speed and persistence between monoculture and coculture group (Figure 2-3E, I). In contrast to MDA-MB-231 cells, histogram of cell speed distribution also exhibited no

significant differences between monoculture and coculture group in terms of cell speed (Figure 2-3B). However, our analysis showed a slight decrease in number of cells at high persistence in coculture group as compared to monoculture condition (Figure 2-3J, p value=0.042). Thus, overall our findings indicate that while CAFs influenced the migration of MDA-MB-231 cells by enhancing the heterogeneity of tumor cell speed and persistence, migratory characteristics of less invasive MCF7 cells were mostly unaffected in the presence of CAFs as compared to monoculture condition.

ECM remodeling characterization

A major step forward in our 3D tumor model lies within its ability to assess biophysical properties of the ECM including collagen I deposition and matrix stiffness due to stromal-tumor cross talk. To visualize biomechanical changes, specifically collagen matrix deposition and stiffness within our platform, we utilized AFM along with 3D imaging based on confocal reflectance microscopy. As shown in Figure 2-4A and B, collagen I density did not change significantly throughout the culture period of 4 days in monoculture group for both tumor cell lines. However, upon coculture with CAFs, collagen I expression gradually increased on day 2 and day 4 of the culture (Figure 2-4A, B). Such an increase in collagen deposition further influenced stiffness of the matrix, which was quantified by measurement of the elastic modulus of the matrix using AFM. As shown in Figure 2-4C, there was no significant difference in the stiffness of the matrix in monoculture and coculture condition at day 0. However, at day 4, coculture condition exhibited significantly marked difference in the matrix stiffness as indicated by higher

elastic modulus as compared to monoculture group (Figure 2-4C). Similar trend was also observed for MCF7 group where coculture condition had significantly enhanced elastic modulus at day 4 (Figure 2-4C). Furthermore, when we grouped the measurements for each experimental condition and compared across various days of the culture period, we observed that neither the monoculture of tumor cells (MDAMB-231, MCF7) nor CAFs induced any change in the matrix stiffness (Figure 2-4C). Interestingly, only during the coculture of cancer and stromal cells, significant increase in elastic modulus was observed (Figure 2-4C). Our results also show that while change in elastic modulus of ECM in coculture condition of MDA group was progressive across culture period, it was delayed for MCF7 cells till day 4 (Figure 2-4C). Thus, overall our results demonstrate that a significant crosstalk is necessary between tumor and stromal cells to alter the stiffness of the tumor matrix.

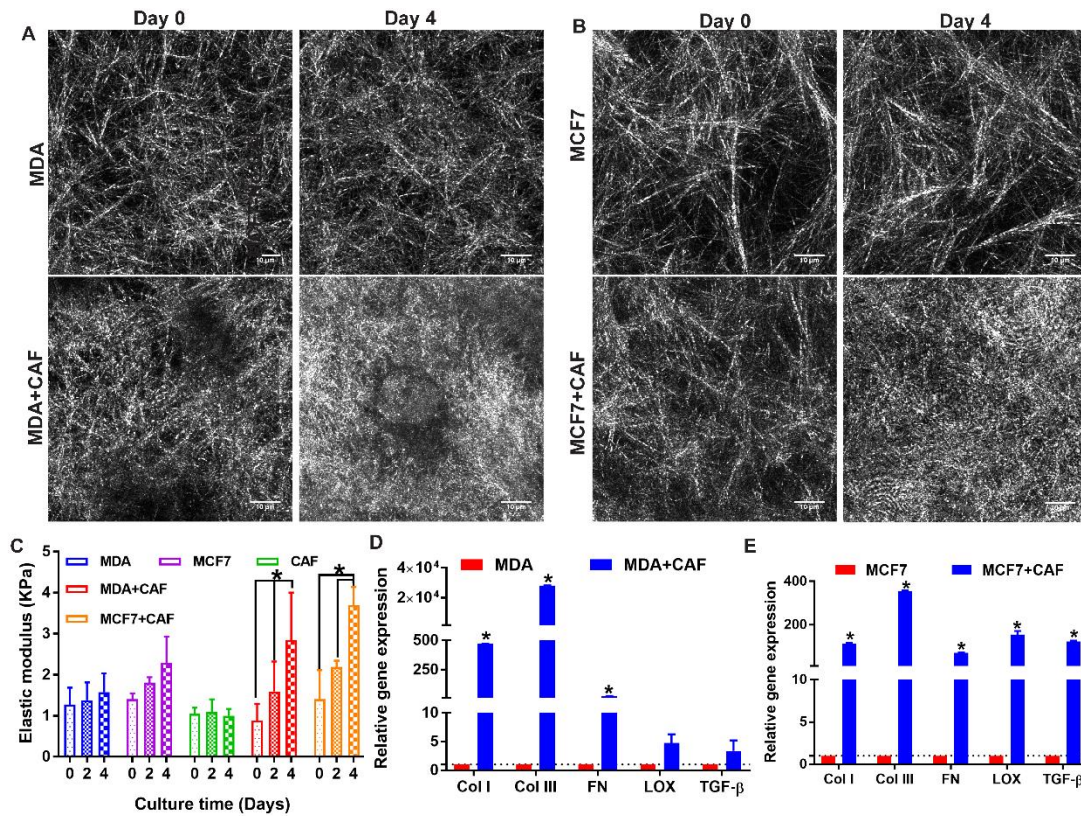


Figure 2-4: ECM Stiffness Assay.

(A), (B) Representative confocal images showing collagen deposition across various group of MDA-MB-231 and MCF7 cells over culture period of 4 days. (C) Elastic modulus of ECM across different culture conditions across 4 days demonstrating significant crosstalk between tumor and stromal cells. All scale bar represents 10 μ m. (D),(E) Quantification of RNA expression for various matrix related genes across monoculture and coculture conditions of MDA-MB-231 and MCF7 cells. * represents p value < 0.05.

To further our understanding on various biophysical changes caused by tumor-stromal crosstalk we also analyzed different parameters of dynamic modulus including storage (G') and loss modulus (G'') as well as loss tangent (loss modulus/storage

modulus) to comprehend the viscoelastic properties of the matrix (Supplementary Figure 5, APPENDIX A). Our results demonstrated a significant increase of storage modulus (G') when MDA-MB-231 cells were cocultured with CAFs as compared to monoculture group on day 4 (Supplementary Figure 5A, APPENDIX A). On the other hand, the change in loss modulus (G'') was not similar across monoculture and coculture condition (Supplementary Figure 5A, APPENDIX A). Similar change in dynamic modulus properties were also observed for MCF7 group where change in G' was more in coculture group as compared to G'' (Supplementary Figure 5C, APPENDIX A). This trend can also be inferred from loss tangent graphs where the absolute values were always less than 1 (Supplementary Figure 5B, D, APPENDIX A). Thus, our results demonstrate that while a significant change was observed in viscoelastic properties of stroma matrix, elastic properties of collagen enhanced more in presence of CAFs as compared to viscosity of the matrix.

Gene Expression Profile influencing ECM Remodeling

To further probe ECM remodeling within our coculture samples, we performed a quantitative analysis on ECM deposition by performing qRT-PCR on matrix related genes including alpha I type I collagen (Col1 α 1), alpha I type III collagen (Col3 α 1), fibronectin (FN), Lysyl oxidase (LOX) and transforming growth factor beta (TGF- β) across different experimental groups (Figure 2-4D, E). Similar to confocal imaging, our gene expression results demonstrated higher expression of matrix proteins including Col 1 α I, Col 3 α I and FN amongst coculture groups as compared to monoculture of either

tumor cell line (Figure 2-4D, E). While coculture of highly metastatic MDA-MB-231 cells with CAFs did not show upregulation of cross-linking enzyme LOX and multifunctional cytokine TGF- β , coculture of less invasive MCF7 cells with CAFs demonstrated an increased expression of these fibrosis related genes thereby suggesting a differential influence of CAFs on tumor cells of varied tumorigenicity (Figure 2-4D, E).

Assessment of tumor-CAF cross talk for ECM remodeling

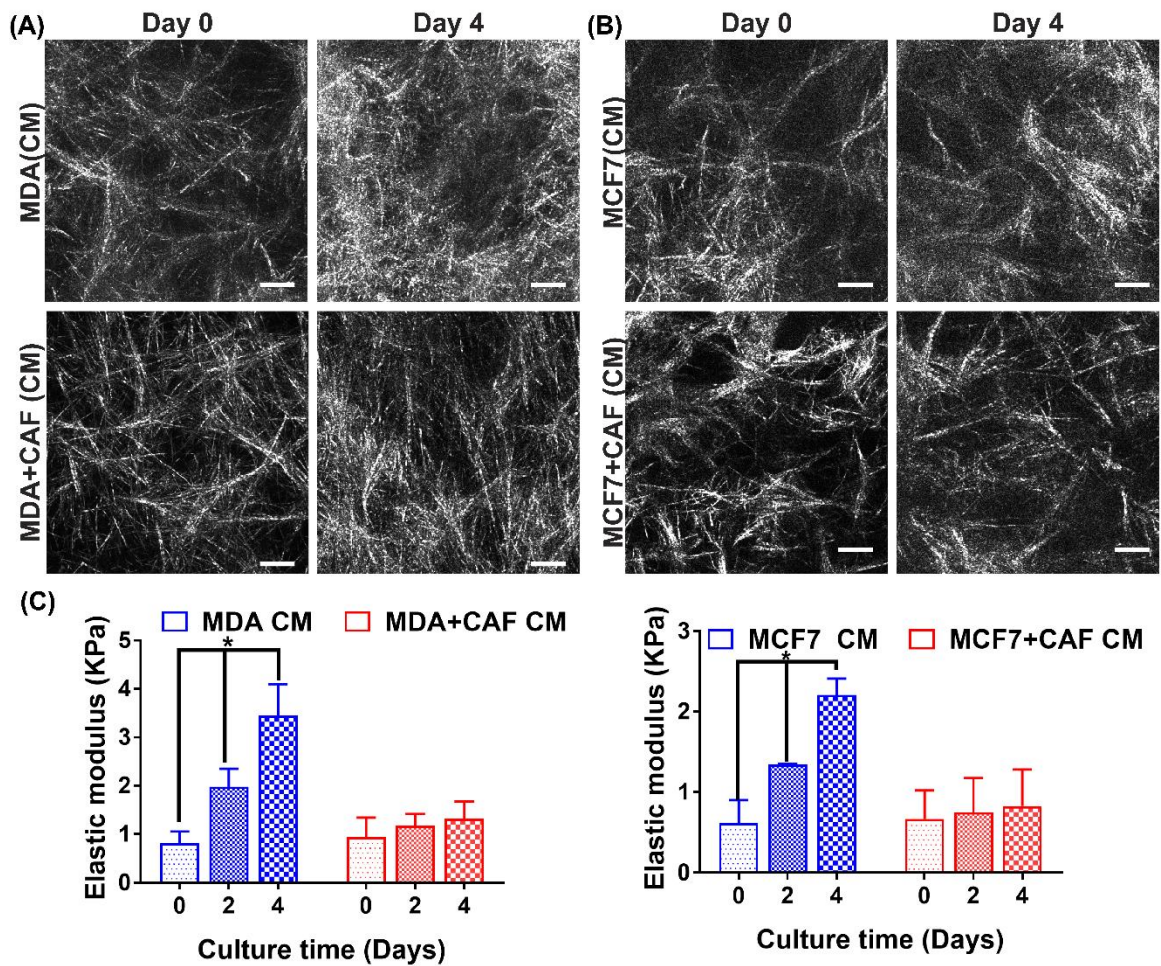


Figure 2-5: Conditioned Media Assay.

(A), (B) Representative confocal images showing deposition of collagen fibers when CAFs are incubated with CM obtained from various monoculture and coculture groups. (C) Elastic modulus of ECM for CAF only group upon incubation with CM from monoculture and coculture group of MDA-MB-231 cells. (D) Elastic modulus of CAF only group when incubated with CM from various groups of MCF7 cells. All scale bars represent 20 μm . * represents p value < 0.05.

Since our elastic modulus results demonstrate the necessity for crosstalk between tumor cells and CAFs for ECM remodeling, we next evaluated the mode of interaction between these two cell types. Specifically, we studied that whether soluble factor signaling between tumor cells and CAFs can significantly increase the matrix stiffness over the culture period. To perform these studies, we collected conditioned media (CM) from different experimental groups of MDA-MB-231 and MCF7 cells and subsequently added them on monoculture of CAFs followed by assessment of elastic modulus of the matrix. As shown in Figure 2-5A, C, collagen fiber density and matrix stiffness of CAFs only group was significantly enhanced when CM from monoculture of MDA-MB-231 cells was added to the samples on day 2 and 4 of the culture. Surprisingly, no significant change in matrix stiffness was observed when CM from coculture group of MDA-MB-231 cells was added on CAF only group across entire culture period (Figure 2-5A, C). Similar trend was also observed across MCF7 experimental conditions, where CM of monoculture of MCF7 cells enhanced the elastic modulus of the matrix while the coculture CM had no significant impact (Figure 2-5B, D). Thus, overall, we can say that

tumor cells crosstalk with CAFs in a unidirectional fashion such that tumor cells secrete biochemical cues that are sensed by CAFs to initiate ECM remodeling.

Assessment of Soluble Factor mediated CAF proliferation and Genetic Changes

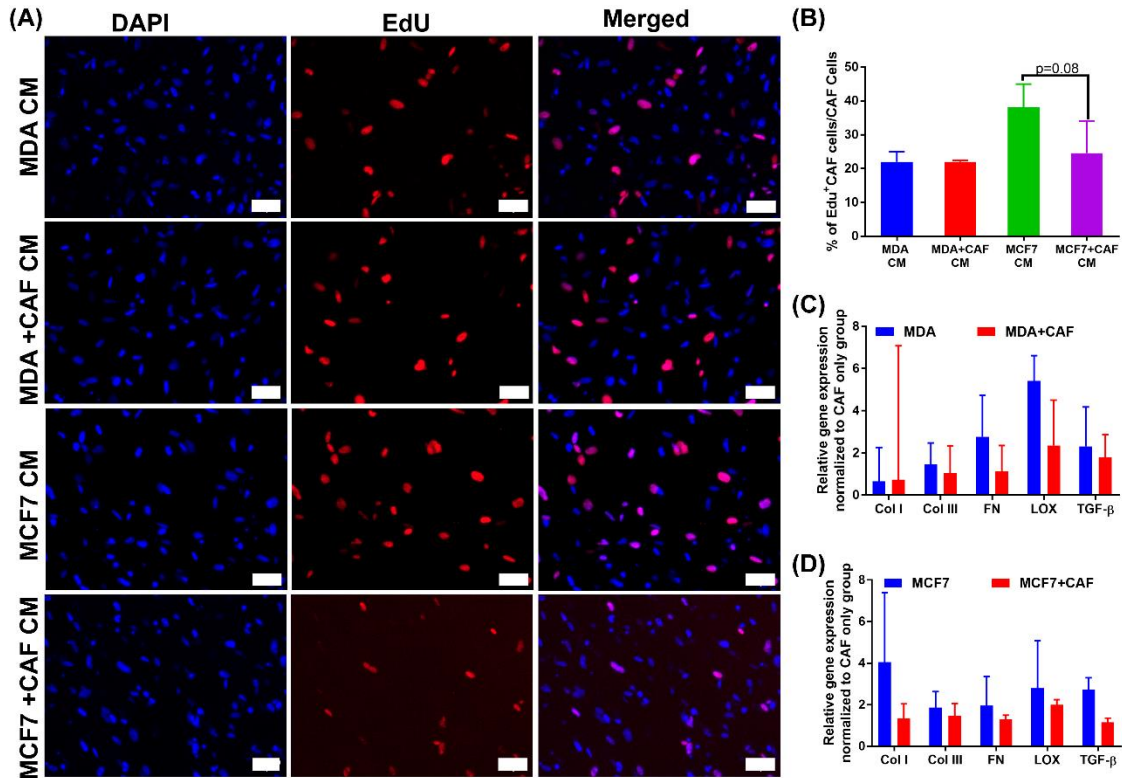


Figure 2-6: CAF Proliferation Assay.

(A) Representative immunofluorescent images showing proliferation of CAFs upon incubation with CM from various groups using Edu assay. (B) Quantification of proliferative CAFs in various CM groups. (C), (D) Quantification of matrix related gene expression in CAF only group upon incubation with various CM.

After establishing a significant role of soluble factor signaling in modulation of matrix biophysical properties by CAFs, we next wanted to evaluate changes in CAFs

phenotype and genotype under various CM experimental groups. In this regard, we first analyzed CAF proliferation upon incubation with CM obtained from different experimental groups of MDA-MB-231 and MCF7 cells. As shown in figure 2-6A, CAFs demonstrated proliferation under all the conditions. However, no significant difference was observed in proliferative behavior of CAFs when they were incubated with CM obtained either from monoculture or coculture group of MDA-MB-231 cells (Figure 2-6B). On the other hand, MCF7 monoculture CM enhanced CAF proliferation rate as compared to the MCF7 coculture CM although the difference was not statistically significant ($p=0.08$, Figure 2-6B). These results are in line with our elastic modulus results where a significant increase in matrix stiffness was evident in MCF7 monoculture CM as compared to MCF7 coculture CM. Thus, overall these results suggest a differential influence of biochemical cues released by various tumor cells on biological traits of CAFs including proliferation.

Similar reassessment was also performed for expression of matrix genes in CAFs incubated with CM obtained from various experimental groups. Our results demonstrated that CAFs did not exhibit significant change in expression of any of the matrix genes across monoculture and coculture CM for both tumor cells (Figure 2-6C, D). These results thereby suggest that soluble factor signaling did not induce any genetic changes within CAFs. Therefore, in summary our results suggest that soluble factors from MDA-MB-231 cells do not induce any change in genetic and biological traits of CAFs while

soluble factors released from MCF7 induced an upregulation of CAFs proliferation while maintaining their gene expression profiles.

Molecular Profiling of Tumor Cell Secreted Factors and Activation of Specific

Receptors in CAFs

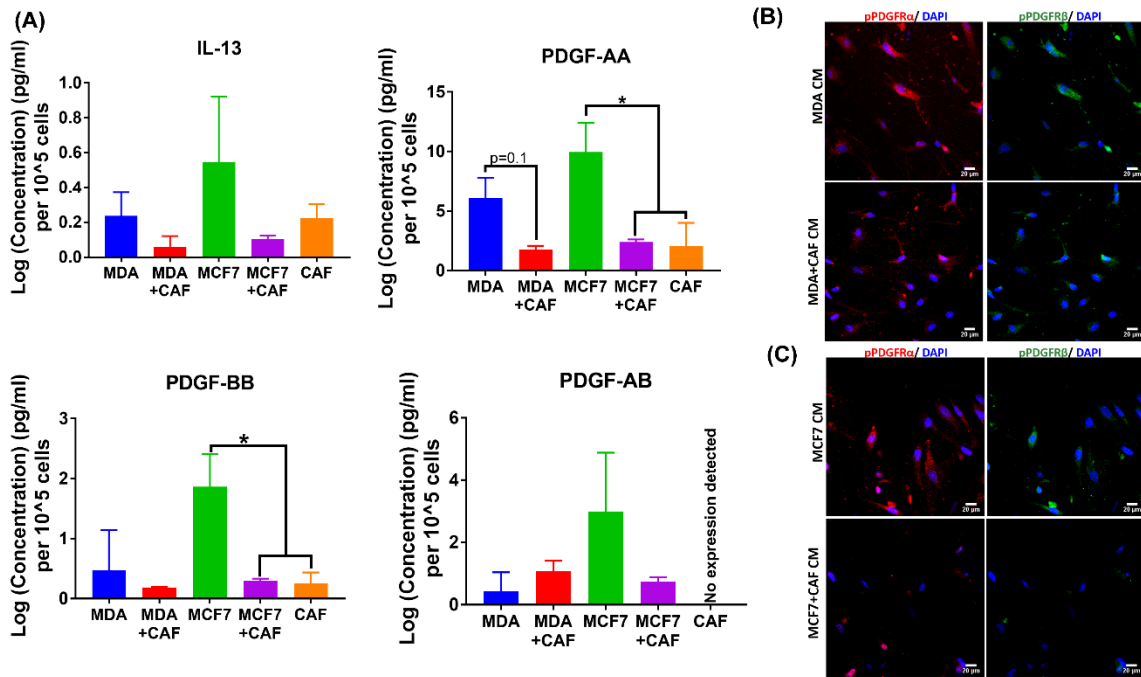


Figure 2-7:Quantification of Pro-Fibrotic Factors in Tumor Conditioned Media.

(A) Quantification of IL-13, PDGF-AA, PDGF-BB, PDGF-AB in CM obtained from various groups. (B) Representative Immunofluorescent Images showing enhanced activation of PDGFR α/β in CAFs upon incubation with CM obtained from monoculture and coculture group of MDA-MB-231 and MCF7 cells. All scale bar represents 20 μ M. * denotes $p < 0.05$.

Based on our CM results, it is clear that tumor cell secreted factors play a crucial role in upregulating the stiffness of the matrix by CAFs. To better understand this molecular

mode of interaction and the composition of tumor cell CM, we next performed ELISA to observe the presence of various known cytokines that participate in fibrosis. Specifically, we studied the expression of Interleukin 4 (IL-4), Interleukin 13 (IL-13), platelet derived growth factor AA (PDGF-AA), platelet derived growth factor AB (PDGF-AB), platelet derived growth factor BB (PDGF-BB), platelet derived growth factor CC (PDGF-CC) and transforming growth factor β (TGF- β). Based on our matrix stiffness results observed in our CM experiments, we hypothesized that the concentration of fibrotic factors would be significantly higher within our tumor (MDA-MB-231, MCF7) monoculture CM as compared to their respective coculture CM. Additionally, we also studied the expression of these cytokines by CAF monoculture CM to provide a broad understanding on expression of these factors by both tumor and stromal cells. Our results showed undetectable levels of IL-4 and PDGF-CC across all the experimental conditions. We speculate that these cytokines were not detected due to the low concentration of the analytes across all the samples. Further analysis showed expression of multiple cytokines including IL-13, PDGF-AA, PDGF-BB in all our samples (Figure 2-7A). We also observed detectable levels of PDGF-AB in various conditions, although it was found to be undetectable for CAF-CM (Figure 2-7A). Interestingly, we observed a significantly higher expression of PDGF-AA and PDGF-BB in MCF7 monoculture CM as compared to MCF7 coculture CM and CAF CM (Figure 2-7A). PDGF-AA was also observed to be highly expressed in MDA-MB-231 monoculture CM as compared to respective coculture CM and CAF CM however p value was greater than traditional value of 0.05 ($p=0.10$,

p=0.12, Figure 2-7A). Such high expression of PDGF-AA and PDGF-BB across tumor cell CM as compared to CAF-CM suggest that these ligands are primarily expressed by tumor cells. Additionally, these results are in accordance to our hypothesis where tumor monoculture CM had high expression of the fibrotic factors as compared to coculture CM thereby corroborating our elastic modulus results for all our conditioned media samples. To validate our ELISA results we next performed IF staining for phosphorylated PDGFR α/β (Figure 2-7B). Our results demonstrated that the activation of alpha and beta receptors were more prominent in CAFs incubated with MDA-MB-231/MCF7 monoculture CM as compared to their respective coculture CM (Figure 2-7B).

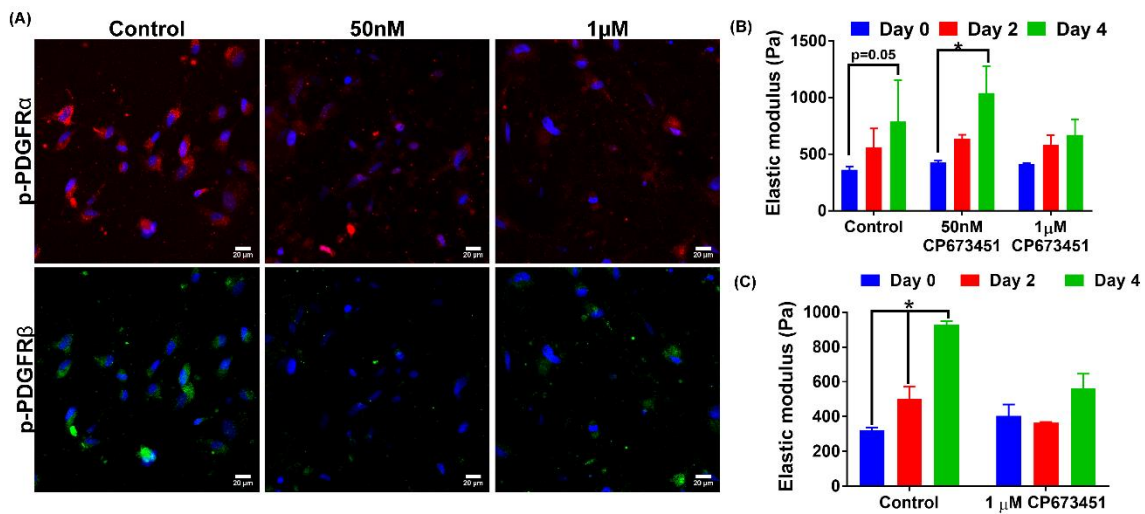


Figure 2-8: Effect of PDGFR Inhibitor on CAF Based Desmoplasia.

(A) Representative immunofluorescent images showing reduced activation of PDGFR α/β receptor after addition of drugs at different concentration in MDA-MB-231 monoculture CM. (B), (C) Elastic modulus assessment of the matrix in CAF only group upon incubation with MDA-MB-231 and MCF7 CM supplemented with different

concentration of CP673451 respectively. All scale bar represents 20 μm . * denotes p value <0.05 .

Inhibition of PDGFR pathway in CAFs to study its role in fibrosis

To investigate the role of tumor secreted PDGF AA/BB on CAF induced fibrosis, we next performed functional assessment by incubating tumor monoculture CM with concentration sweep of specific inhibitor of PDGFR (CP673451). We reassessed activation of receptors and elastic modulus of the matrix in CAF only samples across the culture period. Our results demonstrated enhanced significant reduction in activation of the receptor at 50nM and 1 μM concentration of the drug in MDA-MB-231 monoculture CM as shown in figure 2-8 A. Our quantitative analysis demonstrated that the elastic modulus of the matrix significantly increased when CAFs were incubated with tumor monoculture CM (Figure 2-8B,C). At low concentration of the drug (~50 nM), similar increase in elastic modulus of the matrix was observed. However, when the concentration of the drug was increased to 1 μM no significant change in ECM stiffness was observed at day 2 and day 4 of the culture as compared to day 0 (Figure 2-8 B). Similar observation was also made when CAF only group was incubated with MCF7 monoculture CM substituted with 1 μM concentration of the drug (Figure 2-8C). Overall, these AFM results in the presence of PDGFR inhibitor validate our ELISA findings and confirm that tumor cells secreted PDGF-AA/BB ligands are profibrotic in nature which activate desmoplastic reaction within CAFs.

2.4 Discussion

CAFs are known to participate in tumor progression by depositing various proteins, degradation of the matrix as well as by increasing the stiffness of the ECM (Kalluri & Zeisberg, 2006). While the role of matrix stiffness in tumorigenicity has been studied by various *in vivo* and *in vitro* models, not much is known about the role of tumor and stromal cell crosstalk on modulation of biophysical properties of the matrix (Chaudhuri et al., 2014; Ehrbar et al., 2011; Lang et al., 2015; Peela et al., 2016). In this study we developed a novel high-density 3D breast tumor model that can be utilized to mechanistically study the influence of tumor and stromal cells such as CAFs on alteration of biophysical properties of the matrix including collagen I deposition as well as stiffness. Due to the open top nature of the platform, we could integrate the platform with AFM to indent the matrix at nano scale to assess dynamic alteration of elastic modulus during live migration of cancer cell. Our study primarily focused on performing various functional and molecular assessments that helped in dissecting the key molecular regulators of the tumor stroma crosstalk that play a crucial role in ECM remodeling.

Our results demonstrated that when both the tumor cells MDA-MB-231, MCF7 cells and cultured alone, no significant change is observed in matrix stiffness and collagen I deposition over the entire culture period. However, when the tumor cells are cocultured with CAFs there is significant and gradual increase of the matrix stiffness for 4 days. These findings are in line with previous *in vivo* studies which have shown that transplantation of tumor cells with CAFs in mouse models lead to an enhanced fibrotic

and stiff tissue as compared to the injection of tumor cells alone (Ken Takai et al., 2016). Unlike previous *in vivo* and *in vitro* studies, we also assessed the elastic modulus when CAFs were cultured alone and observed no change in matrix stiffness across the entire culture period. We also observed that CAFs demonstrated a high proliferative index when cultured with tumor cell as compared to the monoculture condition. Similar increase in CAF population within the cancerous tissue have been observed by many previous *in vivo* and clinical studies (Acerbi et al., 2015; Ken Takai et al., 2016). Many studies have correlated high proliferation of CAFs to a more dense and fibrotic cancerous tissue (Santi et al., 2018; Ken Takai et al., 2016). Similar phenomenon was also observed within our samples where high proliferation of CAFs within coculture samples was primarily associated with enhanced elastic modulus of the matrix. Interestingly our qPCR results demonstrate that unlike tumor cells, CAFs have high expression of all matrix related genes, however still no change in matrix stiffness was observed when cultured alone. This clearly suggest that a crosstalk between tumor cells and CAFs is crucial such that tumor cells signal to CAFs to initiate and activate matrix deposition and increase in stiffness of the ECM.

While most of the previous studies primarily focused on the role of CAFs on biophysical alteration of the matrix, our study took a step forward by analyzing the mode of mechanism by which tumor cells and CAFs interact with each other to participate in ECM remodeling. Our CM results suggest that tumor cells and CAFs can interact with each other through paracrine signaling. We observe that tumor cell secreted factors are

essential to induce CAF based desmoplasia. Similar observation was made by Erik Sahai group who demonstrated that tumor secreted soluble factors participate in nuclear localization of transcription factor, Yes associated protein (YAP), to play role in normal fibroblast transformation, collagen deposition and proliferation (Calvo et al., 2013; Lampi & Reinhart-King, 2018). In this study when NF's were cultured with 4T1 cell CM, the normal fibroblast cells demonstrated significant increase in gel contraction as compared to their culture in DMEM based media (Calvo et al., 2013). Additionally, CM induced NF cells significantly supported cancer cell invasion as compared to control NF cells suggesting crucial role of tumor secreted factors in inducing CAF like phenotype (Calvo et al., 2013). In line of these observation, our results further demonstrated an interesting trend where CM obtained from tumor monoculture group significantly induced the CAF based fibrosis whereas coculture CM failed to induce any significant change in the matrix stiffness. These findings thereby suggest that tumor cells secreted pro-fibrotic cytokines can be sensed by CAFs due to the presence of their respective receptors on their membrane. We further speculate that while these pro-fibrotic factors are available within the CM obtained from tumor monoculture, they are exhausted within the coculture CM thereby causing a differential effect on CAF based tumor fibrosis. We confirmed our hypothesis of differential expression of pro-fibrotic factors using ELISA where higher expression of platelet derived growth factor (PDGF)-AA and BB was observed in both MDA-MB-231 and MCF7 monoculture CM as compared to their respective coculture CM and CAF CM. Multiple *in vivo* studies in the past have shown

that PDGF can play an essential role in fibrosis in various diseases including pulmonary fibrosis, hepatic fibrosis, lung cancer and breast cancer (Antoniades et al., 1990; Shao et al., 2000; Ying et al., 2017). While most of the cancer fibrotic models have primarily studied the effect of more studied TGF- β and CTGF based signaling, very few studies have focused on the effect of PDGF in cancer desmoplasia (Kozono et al., 2013; Papageorgis et al., 2017; Ken Takai et al., 2016). For instance, in year 2000, shao et. al. created a desmoplastic xenograft model by utilizing Er+ breast tumor W9 cells which in the absence of estrogen led to enhanced accumulation of collagen and stromal cells within the tumor microenvironment (Shao et al., 2000). Authors demonstrated that if W9 cells were transfected with a PDGF-A mutant domain the stromal fibrosis is significantly attenuated thereby demonstrating crucial role of PDGF signaling in breast carcinoma desmoplasia (Shao et al., 2000). While previous PDGF focused studies have utilized xenograft models to study its influence in fibrosis; we had limited understanding about the interplay of the cytokine due to interaction between two cell types (i.e. tumor cells and CAFs) due to the presence of various confounding factors such as other cell types. To the best of our knowledge, this is the first study in which PDGF signaling has been identified to play an essential role in desmoplasia due to the interaction between breast tumor cells and CAFs. Additionally, due to the convenience of 3D model, we were able to confirm that tumor secreted PDGF ligands interacted with their specific receptors on CAFs to induce stromal desmoplasia. Using specific inhibitor against PDGFR (CP673451), we observed a minimal increase in matrix stiffness when the tumor cell CM

was substituted with 1 μ M concentration of the drug. These functional assessment results in addition to ELISA observation thereby suggest a crucial unidirectional crosstalk between two cell types where PDGF ligands are mainly secreted by tumor cells that bind to PDGFRs on CAFs and participate in desmoplasia.

Another major finding from our study was how breast tumor cells of varied genomic make-up enhance their tumorigenicity across various hallmarks of cancer in the presence of CAFs within our model. Our findings clearly suggested that while MDA-MB-231 cells invaded more into the stroma in coculture condition as compared to monoculture group, MCF7 cells depicted higher clustering tendency. Further, our proliferation assays demonstrated that MCF7 cells had higher proliferative rate in the presence of CAFs while MDA cells proliferation rate diminished marginally. These results are in tune with the notion when cells become more invasive, they lose their proliferative tendency (Fedotov & Iomin, 2007; Hatzikirou et al., 2012). Similar conclusion can also be drawn from our live cell tracking results where CAFs influenced MDA-MB-231 cell speed and increased the heterogeneity of the tumor cell population, no discernible difference was observed for MCF -7 group in terms of cell speed. Thus, using an *in vitro* 3D tumor model, we were able to tease apart the necessary interaction between tumor and stromal cells and have successfully shown their significance in matrix remodeling as well as tumor progression.

2.5 Conclusion

In conclusion, we fabricated a 3D high density tumor stroma model to study the role of breast tumor cells and CAFs on ECM remodeling. By integrating our platform with

AFM, we clearly observed that the crosstalk between tumor cells and CAFs is necessary to induce desmoplasia. Additionally, for the first time, we provided evidence that tumor cells and CAFs interact with each other through soluble factor signaling. We also observed that tumor cells are the primary source of pro-fibrotic cytokines such that the elastic modulus of CAF embedded matrix was significantly enhanced when incubated with tumor monoculture CM as compared to coculture CM. Using ELISA, we observed that monoculture CM from MDA-MB-231 and MCF7 cells had higher expression of PDGF-AA and BB ligands as compared to their respective coculture CM. Lastly, we confirmed the role of PDGF signaling in CAF based desmoplasia by inhibiting the PDGFR activation using specific inhibitor.

Chapter 3

Identification of Tumor Secreted Factors Participating in Desmoplasia using Liquid Chromatography Mass Spectrometry

3.1 Introduction:

Intercellular signaling between various cell types is crucial in all aspects of developmental biology including tissue formation, tissue homeostasis and various pathophysiological conditions including cancer (GM., 2000b). Two cell types can communicate with each other either through physical cell-cell interaction or through secretion of cytokines including growth factors, hormones and chemokines that can act in paracrine/autocrine manner (GM., 2000b). While cell-cell interaction is shown to play a crucial role in regulating tissue architecture including apical-basal polarity of epithelial cells and modulating them in response to changes in TME, soluble factor signaling can regulate various other processes including cell proliferation, migration, differentiation, apoptosis etc (GM., 2000a, 2000b). In cancer, soluble factor signaling has been demonstrated to play a crucial role at all steps of metastatic cascade (Sever & Brugge, 2015). Most of these soluble factors including TGF- β , PDGF, FGF, IGF, EGF, HGF, pro- and anti-inflammatory signals are released by one cell type and are sensed by either same cell or other cell type due to the activation of receptors that can regulate various downstream pathways (GM., 2000b; Sever & Brugge, 2015; Witsch, Sela, & Yarden, 2010). For instance, it is well known that in cancer TGF- β is released by both cancer cells and stromal cells which upon activation can bind to multiple receptor types and

participate in either tumor suppression or tumor promotion in a context dependence manner (Massagué).

Multiple techniques are available which can be advantageous to study the expression of soluble factor signaling in different sample types including 2D cell culture, 3D tissue sample, serum and plasma. These techniques mainly include ELISA, western blot and Luminex that can be used to study the expression of soluble factors with high sensitivity and specificity (Emilia Manole, 2018; Leng et al., 2008). However, all these assays are biased in nature and can only be used to quantify the expression of limited number of pre-determined factors across different sample types. On the other hand, implementing proteomics using liquid chromatography-mass spectrometry (LC-MS) provides an advantage to visualize and quantify the expression of both known and unknown factors within a sample type (Harlan & Zhang, 2014). Multiple studies have utilized the technique of proteomics to identify crucial soluble factors whose regulation can be changed in a pathological state as compared to normal tissue (Lawrence et al., 2015; Srinivas, Verma, Zhao, & Srivastava, 2002; Yanovich et al., 2018). In this chapter we have utilized LC-MS as a technique to identify the secretome of tumor cells and CAFs in their monoculture and coculture condition within our 3D microengineered tumor stroma model. Our results suggest expression of various soluble factors that are associated with disease progression and participate in making the microenvironment tumor permissive in nature. We also discuss some of the possible factors that needs to be

optimized to fully utilize the advantage of LC-MS while working with 3D microscopic samples.

3.2 Materials and Methods:

Preparation and Collection of CM for LC-MS:

We first fabricated our 3D tumor stroma model as explained previously in chapter 2. The model was cultured for 48 hours in regular media comprising of DMEM 1X substituted with 10% FBS, 1% PenStrep and 1% L-Glutamine. After 48 hours, the samples were washed with 1X PBS 3 times followed by incubation in serum free media. At day 4, the media was collected and centrifuged at 4000 rpm at 4°C for 10 minutes before storing at -80°C until further use.

Isolation of Proteins from Conditioned Media:

The proteins in conditioned media were concentrated by utilizing methanol chloroform protein precipitation protocol followed by multiple ultracentrifugation steps ran for differential times. Briefly, add 1 volume of methanol to the protein sample and vortex followed by addition of ¼ volume of chloroform to the protein sample and mixing well by rigorous vortex. Next, ¾ volume of DI water is added so that the sample looks cloudy. The prepared solution is then centrifuged at 14000 g for 2 minutes and the supernatant is discarded carefully to avoid disruption of protein precipitate in between layers. The remaining pellet is again mixed with 1 volume of methanol and centrifuged at 14000 g for 3 minutes followed by careful removal of supernatant. The remaining solution is then air dried under vacuum and then resuspended in SDS buffer for In-gel digestion.

Removal of Serum Proteins from Conditioned Media and preparation of LC-MS samples:

The proteins were separated by running on SDS Gel Page. Using a molecular weight ladder and Coomassie blue staining, the albumin band was detected at 68 KDa. The identified band was cut, and the rest of the gel was then subjected to in-gel digestion. Briefly the gel pieces were cut and washed with 10 volumes of Millipore water. The Coomassie blue staining was removed from gel pieces using 100 mM $(\text{NH}_4)\text{HCO}_3$ / 50% Methanol. The gel was then dehydrated using 200 μl of 25 mM $(\text{NH}_4)\text{HCO}_3$ / 50% Acetonitrile followed by another incubation in 100% Acetonitrile for 30 seconds. To prepare samples for trypsin digestion, the gel pieces were rehydrated for 5 minutes at room temperature in 20 μl [10ng/ μl] Trypsin (Promega Sequence Grade Modified) in 25mM $(\text{NH}_4)\text{HCO}_3$ / 3% Acetonitrile [pH \approx 8.5]. The rehydrated gel was then incubated with a minimum amount of 25mM $(\text{NH}_4)\text{HCO}_3$ overnight at 37 $^\circ\text{C}$. Peptide were recovered 50 μl Millipore water / 1% FA by vortexing 10 minutes at room temperature (max speed). An additional extraction was performed using 80 μl of 70% ACN / 25% H_2O / 5% FA. The sample was dried in vacuum for 1-2 hours and later reconstituted in 20 μl of Millipore water / 0.1% FA by incubating for 5 minutes at room temperature with intermittent vortexing to use for LC-MS.

Acquiring LC-MS data:

The samples were run at the mass spectrometry core facility of Arizona State University at AB SCIEX 4800 MALDI TOF/TOF/ MS mass spectrometer. The results obtained

from mass spectrometry data was analyzed for peptide information and protein groups using MASCOT search engine. The results with FDR<0.05 were considered significant.

Gene ontology, Protein-Protein Interaction studies and KEGG pathway analysis on LC-MS Data:

The statistical test including one tail t-test was ran on acquired LC-MS data using Perseus. The data with FDR<0.05 was considered statistically significant. Next, gene ontology was performed on differentially expressed proteins using DAVID and Pather Online tools. The Protein-Protein Interaction Maps as well as KEGG Pathway analysis were created using STRING database.

3.3 Results:

Identification of secreted factors in CM obtained from various culture groups.

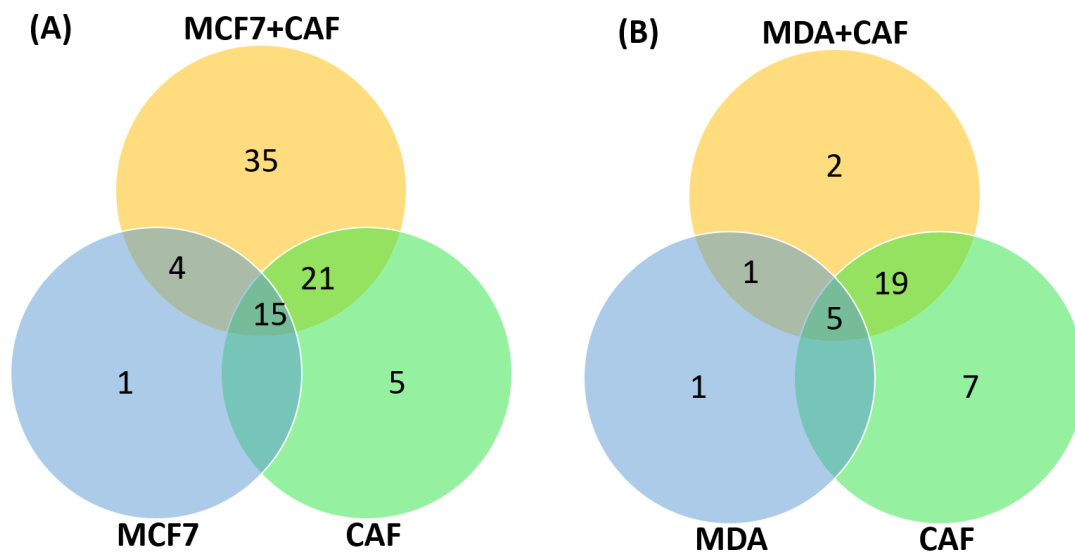


Figure 3-1: Quantification of Proteins Across Various Culture Groups.

(A), (B) Venn diagram representing number of unique and common proteins detected across various culture groups.

In order to observe the difference in expression of various soluble factors between monoculture and coculture groups of MCF7 cells, we first prepared a Venn diagram to visualize the number of proteins secreted either uniquely or commonly by each cell type including monoculture of MCF7, monoculture of CAFs and coculture of MCF7 cells with CAFs. As shown in figure 3-1A, we identified 81 proteins across monoculture and coculture groups of MCF7 cells and CAFs. Amongst these 81 identified proteins, 19 proteins were secreted by monoculture of MCF7 cells and 41 proteins were expressed by monoculture of CAFs, whereas 75 proteins were observed in MCF7+CAF coculture group. Our analysis demonstrated that 35 out of 75 proteins were expressed uniquely due to the coculture of MCF7 cells with CAFs suggesting a crucial crosstalk between two cell types modulating the biochemical milieu of the TME (Supplementary figure 1, APPENDIX B). We also observed that 5 proteins were uniquely expressed by monoculture of CAFs whereas only 1 protein was uniquely expressed by monoculture of MCF7 cells.

Similar analysis was repeated for monoculture and coculture groups of MDA-MB-231 cells with CAFs. As shown in figure 3-1B, 35 different proteins were identified for various groups of MDA-MB-231 cells and CAFs. Similar to MCF7 cells we created a venn diagram and observed that 7 out of 35 proteins were found in CM obtained from monoculture of MDA-MB-231 cells whereas 31 proteins were secreted by CAFs.

Further, 27 out of 35 proteins were found in CM obtained from coculture of MDA-MB-231 cells with CAFs. As opposed to secretome of coculture of MCF7 cells with CAFs, we observed a very low number of proteins (~2 proteins including ECM protein 1 and heat shock cognate 71 KDA protein) being uniquely expressed by coculture of MDA-MB-231 cells with CAFs. Additionally, only 1 protein (plasminogen) was uniquely expressed by monoculture of MDA-MB-231 cells whereas 7 proteins were uniquely expressed by monoculture of CAFs.

Gene ontology analysis and Protein-Protein Interaction Studies

Since we observed an enhanced ECM stiffness and collagen density within our coculture groups (MDA-MB-231+CAF and MCF7+CAF), we first evaluated the biological role of proteins which were uniquely expressed due to the coculture of tumor cells with CAFs. As noted before, coculture group of MCF7 cells with CAFs had high number of secreted proteins (35) as compared to coculture group of MDA-MB-231 cells with CAFs (2). Thus, we performed our next analysis including gene ontology and protein-protein interaction studies on list of identified factors which were uniquely expressed in secretome obtained from MCF7+CAF group.

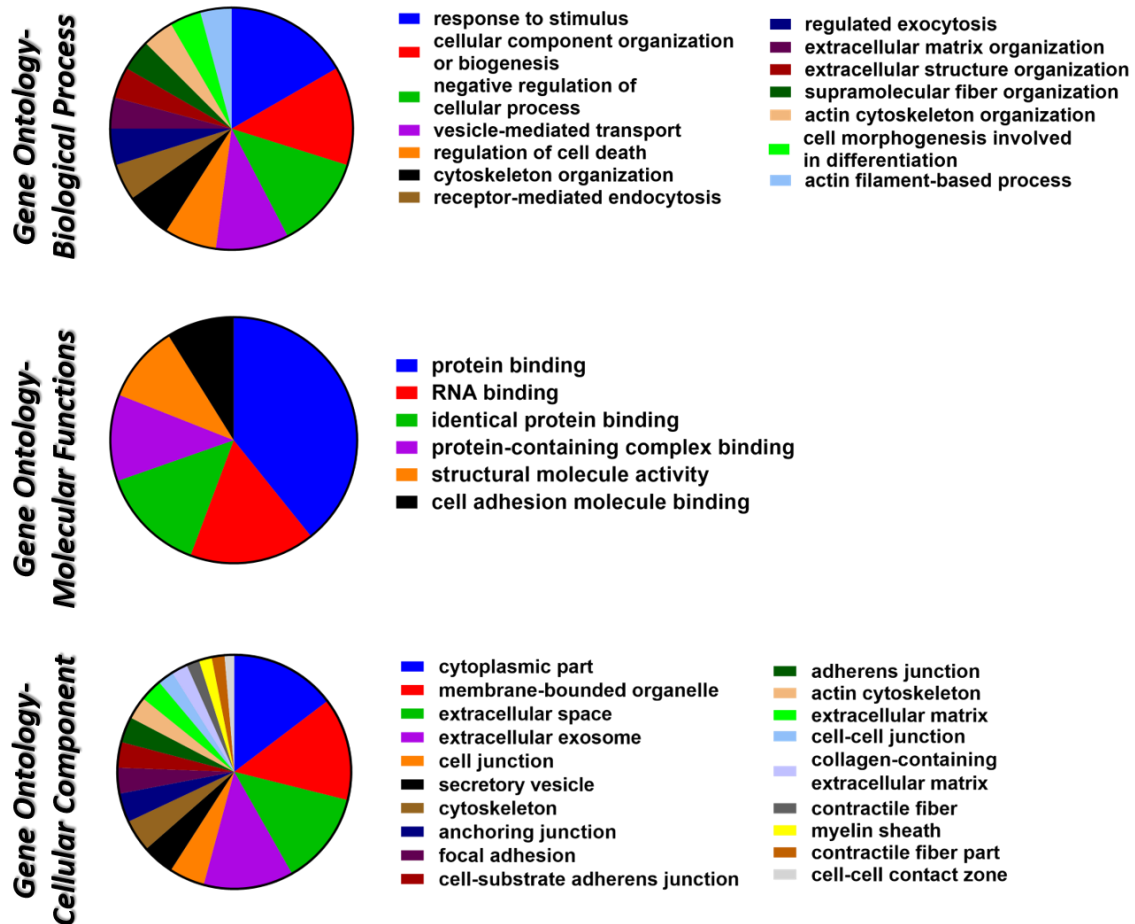


Figure 3-2: Gene Ontology Results.

Pie Chart representing Gene Ontology results for biological process, molecular function and cellular component for unique proteins detected in MCF7+CAF group.

Our analysis demonstrated that the factors secreted uniquely due to the coculture of MCF7 cells and CAFs participated in various biological functions including response to stimulus, cellular component organization, vesicle mediated transport, receptor

mediated endocytosis, ECM organization and supramolecular fiber organization (Figure 3-2). Interestingly, about 15% of the proteins were observed to play a crucial role in cell-cell adhesion whereas 12% of the proteins were found to participate in ECM organization (Supplementary table 1, APPENDIX B). We also observed that about 9% of the secreted factors are secreted in response to hypoxia and further participate in regulation of apoptotic process thereby suggesting the role of secreted factor in tumor homeostasis (Supplementary table 1, APPENDIX B). In terms of molecular function, 77% of the secreted factors were observed to be responsible for protein binding and about 21% of proteins participated in cell-cell adhesion (Supplementary table 2, APPENDIX B). When the cellular location for each of the secreted factors was studied, we visualized that about 88% of proteins are usually found in extracellular exosome and about 65% and 62% are found in cytoplasm and cytosol respectively (Supplementary table 3, APPENDIX B). An average of 30% identified proteins were found in extracellular space suggesting that the secreted factors observed into the conditioned media came from different cellular locations (Supplementary table 3, APPENDIX B).

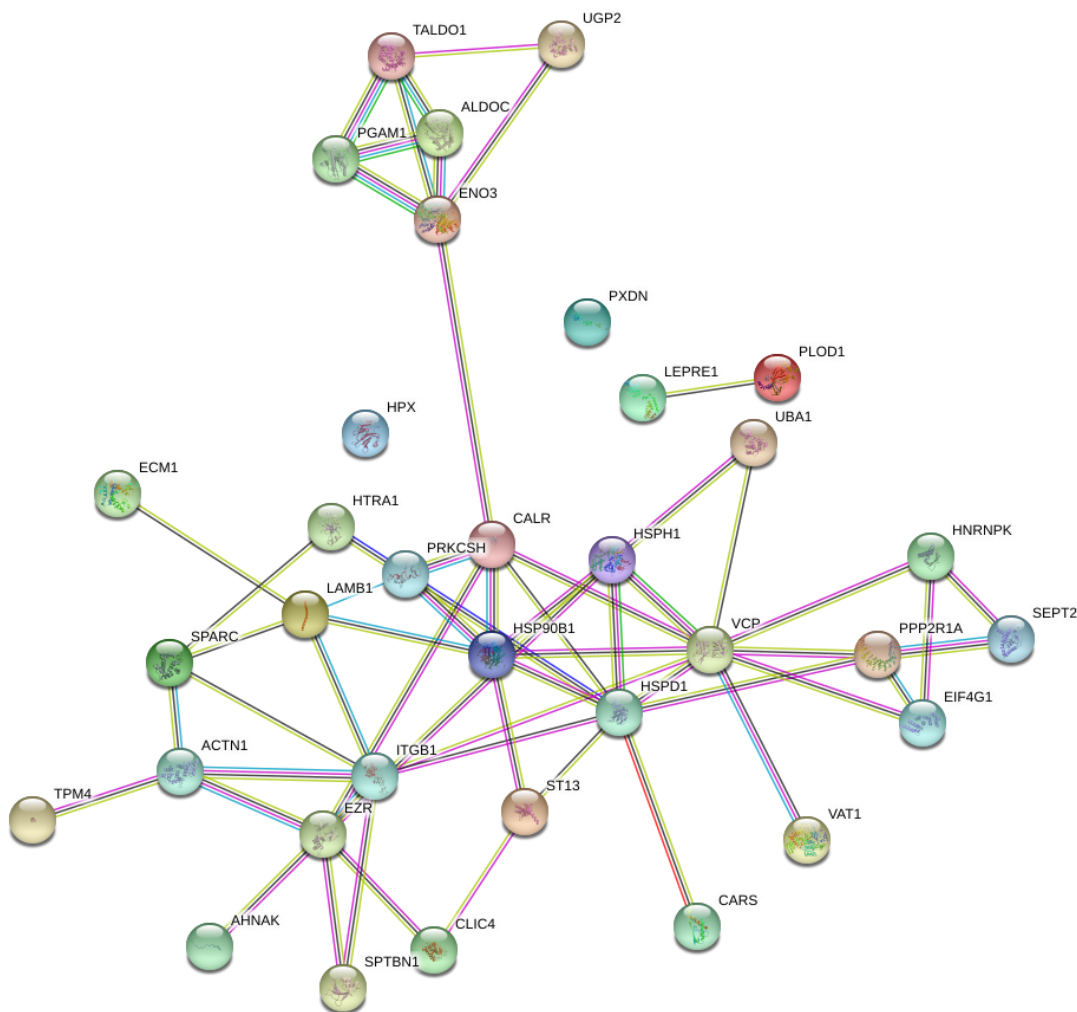


Figure 3-3: Protein-Protein Interaction Maps for Unique Proteins Detected in MCF7+CAF Group.

We next proceeded to study the molecular and physical interaction of different proteins that were identified within the secretome of coculture group of MCF7 cells with CAFs. Using STRING database for all the identified proteins we observed that the secreted factors interacted with each other with low enrichment p value (5.55×10^{-16})

suggesting a significant biological interaction between them as compared to a random set of proteins obtained from genome (Figure 3-3). The STRING database suggested that 34 proteins interacted with each other with an average node degree of 3.35. Interaction between 28 out of 35 proteins were identified as known interactions which have either been obtained from curated databases or experimentally determined (Figure 3-3). Some of the interactions between proteins were also predicted based on gene neighborhood, gene fusion and gene co-occurrence while others are expected due to protein co-expression and homology (Figure 3-3).

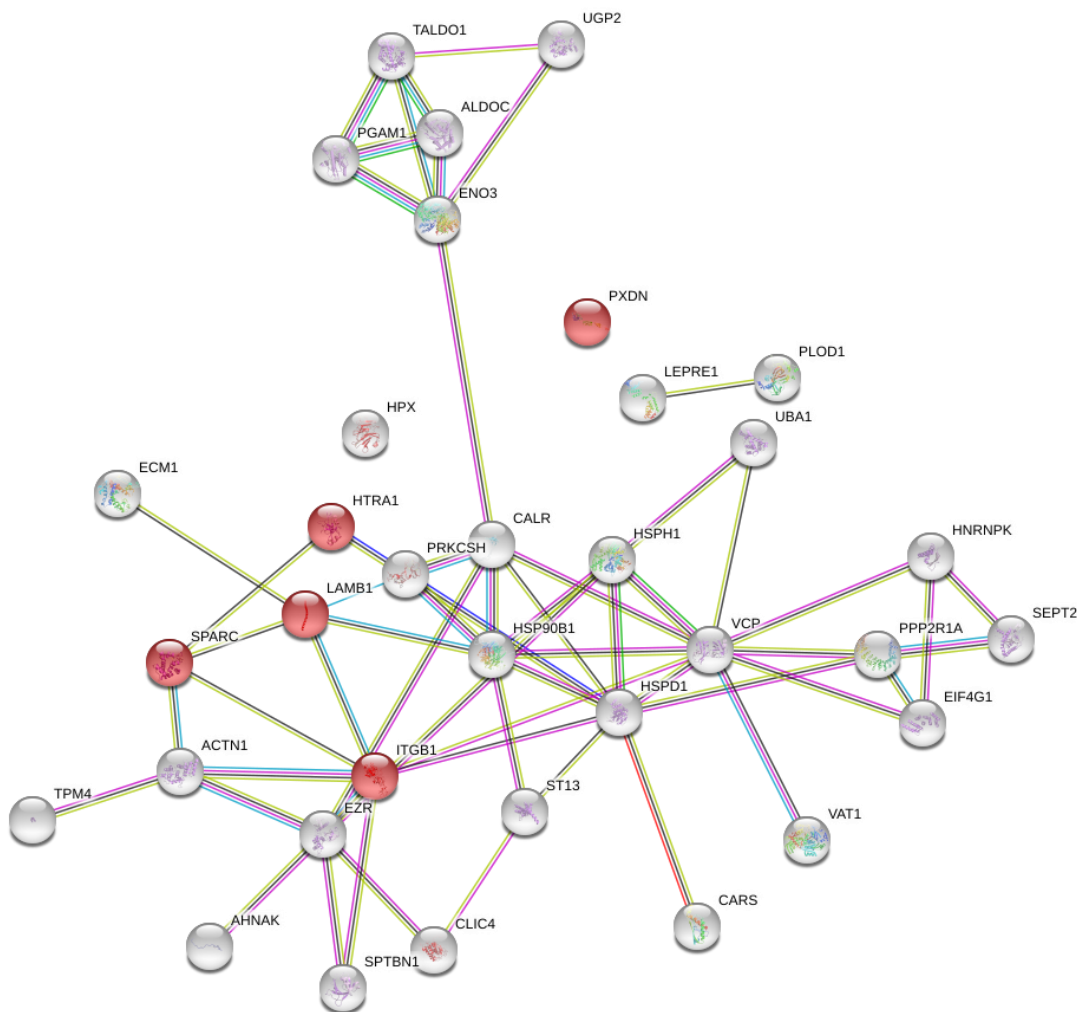


Figure 3-4: Protein-Protein Interaction Map Highlighting the Interaction Amongst Proteins Which are Known to Participate in ECM Organization.

We also visualized the protein-protein interaction between the genes that specifically participated in ECM organization and observed genes related to SPARC, laminin subunit beta 1, integrin beta 1 and Peroxidase homolog as prominent players (Figure 3-4). We next studied the KEGG pathway analysis for the identified proteins and

observed high number of proteins participating in biosynthesis of amino acids, carbon metabolism, Tight junction, Glycolysis, PI3K-AkT signaling pathways, focal adhesion amongst others (Supplementary table 4, APPENDIX B).

Identification of tumor secreted factors participating in CAF induced desmoplasia.

Since our elastic modulus results obtained from CM experiments demonstrated that secretome obtained from monoculture of tumor cells was able to induce desmoplasia as compared to coculture group CM, we hypothesized enhanced expression of fibrotic factors within tumor monoculture CM as compared to coculture CM. Keeping this in mind, we first analyzed the differential expression of factors which are secreted in both monoculture of tumor cells and coculture of tumor cells and CAFs.

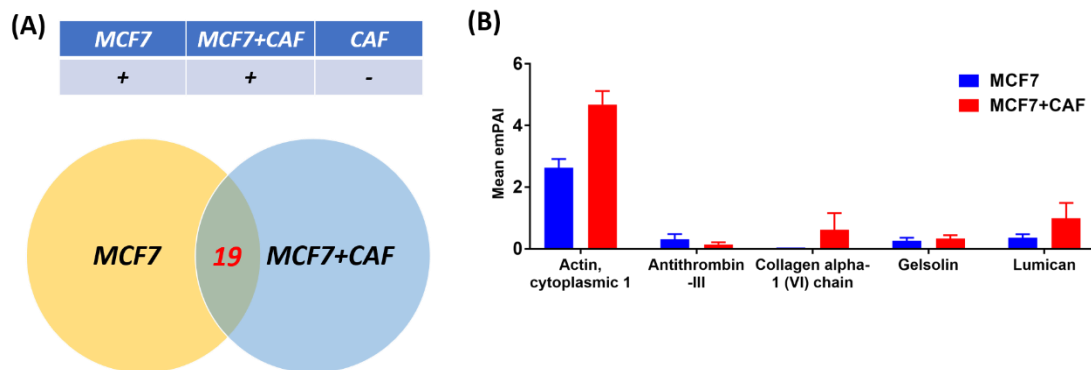


Figure 3-5: Statistical Analysis on Differential Proteins Across Monoculture and Coculture Group of MCF7 Cells and CAFs.

(A) Venn diagram showing number of common proteins within monoculture and coculture group of MCF7 cells. (B) Bar graph showing expression of differently expressed proteins across different culture groups of MCF7.

As shown in figure, 3-5A we found 19 common proteins between the secretome of monoculture of MCF7 cells and coculture of MCF7 cells with CAFs. Upon statistical analysis we observed differential expression of 5 proteins including Actin cytoplasmic 1, Antithrombin III, Collagen alpha 1 (VI) chain, gelsolin and lumican (Figure 3-5B). Except for antithrombin III, all other proteins had higher expression in coculture group CM as compared to monoculture group CM (Figure 3-5B).

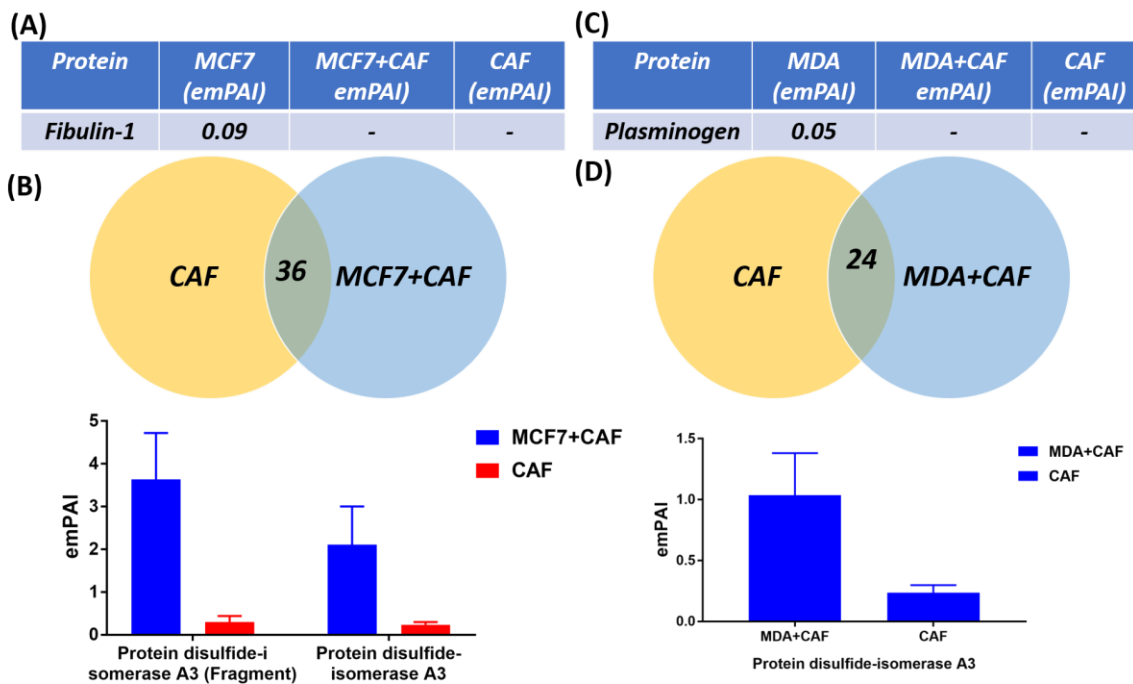


Figure 3-6: Statistical Analysis on Differential Proteins in Monoculture And Coculture of CAFs With MCF7/MDA-MB-231 Cells.

(A), (C) Table showing expression of unique protein which was detected only in monoculture of MCF7 and MDA-MB-231 cells. (B), (D) Differential expression of Protein disulfide isomerase A3 in coculture group as compared to CAF monoculture.

Additionally, we observed high expression of fibulin-1 within the secretome of MCF7 monoculture while it was completely absent from secretome of coculture of MCF7 cells with CAFs (Figure 3-6A). We also studied the differential expression of secretome obtained from CAF monoculture to the secretome of MCF7+CAF group and found 36 proteins in common. Our analysis demonstrated upregulation of only one protein known as protein disulphide isomerase A3 (Figure 3-6B). We repeated our analysis for monoculture and coculture group of MDA-MB-231 cells and CAFs. We observed 6 proteins which were expressed in secretome of both monoculture of MDA-MB-231 cells and coculture of MDA-MB-231 cells with CAFs. However, upon statistical analysis we did not find any secreted factor to be differentially expressed. We next studied the presence of unique proteins and observed expression of plasminogen in CM obtained from monoculture of MDA-MB-231 cells as compared to CM obtained from monoculture of CAFs and their coculture with MDA-MB-231 cells (Figure 3-6C). We also repeated our analysis for differential expression of proteins expressed in secretome of CAF monoculture and coculture of MDA-MB-231 cells with CAFs and observed high expression of protein disulphide isomerase A3 consistent with the results obtained from secretome of coculture group of MCF7+CAF (Figure 3-6D).

3.4 Discussion:

Multiple studies have demonstrated that ECM dysregulation is a critical hallmark of breast cancer progression. Similar to wound healing, fibroblasts cells are the major regulator of ECM remodeling and thus participates in ECM breakdown, deposition of newly synthesized and aligned fibers and increased matrix stiffness. Various studies have demonstrated that NF transform themselves into a myofibroblast like CAF phenotype and enhance their ECM secretion due to the effect of multiple tumor secreted cytokines including TGF- β . While these studies have been paramount in studying the role of known pro-fibrotic factors in transforming NF into CAF like phenotype at earlier stages of the disease, the molecular mechanism of ECM deposition by CAFs in presence of tumor cells is still not well understood. Since the stroma at invasive and metastatic state of the disease is primarily comprised of CAFs as opposed to NF's, a molecular mechanistic study is important to understand the mechanism of ECM remodeling by CAFs in the presence of tumor cells.

Many previous studies attempting to understand the molecular mechanism of ECM remodeling have been performed using patient tissue biopsies or using *in vivo* models. While these models enabled us to visualize and measure biophysical properties of ECM at different stages of the disease, these models are only end point analysis in which the cause and effect relationship of various factors can't be determined due to presence of confounding factors and lack of control groups. *In vitro* models on the other hand have primarily only focused on enhanced tumorigenicity of breast cancer cells by increasing

invasion and proliferation on stiff matrices as compared to the compliant surfaces. Additionally, most of the previous *in vitro* models lacked a stromal component and thereby remained inconclusive on the crosstalk between tumor and stromal cells (i.e. CAFs) influencing matrix stiffness. Therefore, in our study we utilized a 3D high density tumor stroma model to characterize the signaling factors that participate in ECM remodeling due to the crosstalk between tumor cells and CAFs. As noted in chapter 2, we observed a crucial role of paracrine signaling between two cell types on CAF induced desmoplasia. Further we observed that secretome obtained from tumor cell CM exhibited higher CAF based desmoplastic reaction as compared to the secretome obtained from coculture of tumor cells and CAFs. In chapter 2 we primarily focused on studying the differential expression of known profibrotic factors including IL-13, IL-6, PDGF-AA, BB, AB, CC and TGF- β in CM obtained from various culture groups by using ELISA. While this approach enabled us to better understand the role of tumor secreted PDGF, we also performed an unbiased analysis of tumor secreted factors by performing LC-MS on secretomes obtained from various culture groups.

Utilizing our 3D tumor stroma model, we assessed the expression of various soluble factors in monoculture and coculture groups of tumor cells and CAFs. Our initial results showed us high number of secreted factors (~35 proteins) being uniquely expressed due to the coculture of MCF7 cells with CAFs. While these proteins have been identified by gene ontology results to participate in multiple biological process, we observed expression of various proteins that participate in ECM organization. For

instance, we noticed high abundance of SPARC, which is also known as osteonectin usually found in bone extracts and is known to play a crucial role in proliferation, invasion and breast cancer bone metastasis. We also observed high expression of laminin beta 1 which has been clinically observed to be highly expressed in vascular membranes found in invasive and metastatic carcinomas. Prolyl -3- hydroxylase and Procollagen - lysine, 2-oxoglutarate 5-dioxygenase 1 which are known to participate in collagen fiber crosslinking were also found in detectable levels in CM obtained from coculture of tumor cells and CAFs. Thus, overall the secretome that we obtained from coculture of MCF7 cells with CAFs had secretion of multiple ECM components that can participate in ECM remodeling and creating a tumor permissive niche.

Although we were able to isolate and characterize proteins found in secretome of various culture groups, it should be noted that the number of proteins that we were able to detect in CM obtained from MCF7+CAF were low in number. In case of CM obtained from coculture of MDA-MB-231 cells and CAFs we could only detect 2 proteins. We encountered similar problem when analyzed the differential expression of pro-fibrotic factors within tumor cells and CAF monoculture CM and their coculture CM. We envision that the detection of low number of proteins within the CM from various groups can be due to various reasons which are discussed here. Firstly, our CM was collected from a 3D microengineered platform which are smaller in scale as compared to the traditional approaches of 2D cell culture and *in vivo* models. While the microscopic scale can help us successfully study various phenomena including ECM remodeling and tumor

progression, the number of cells and proteins are less in number as compared to the those obtained from macroscopic 2D cultures. Secondly, our sample type was CM obtained from culture of cells as opposed to traditional cell lysates which are known to be abundant in protein concentration. Since we wanted to visualize tumor and stroma secreted factors, we had to switch to serum free media to minimize contamination from large and abundant serum associated proteins. However, despite switching to serum free media after 48 hours culture with regular media, our CM had a large contamination of albumin even after multiple washes with 1X PBS. Hence, we had to utilize serum removal techniques to minimize the masking of low abundant proteins from serum related high abundant proteins. We utilized traditional technique of gel electrophoresis on to detect and remove the albumin band (68KDa Molecular weight). Upon detection we cut the albumin rich band from the gel and performed in gel digestion on the remaining gel. Although this method minimized the number of serum related factor in our mass spectrometry results, it is possible that multiple proteins of interest of variable size were lost due to low peptide yield associated with in gel digestion. Additionally, highly abundant proteins are commonly known to form complexes with low abundance protein and therefore depletion of them can possibly leads to a significant loss of cytokines of interest. Another factor that we envision that can possibly play a role in low number of tumor secreted cytokine is change in cellular phenotype and genotype in serum free media as opposed to regular media. Various studies have shown that removal of serum can lead to induction of stress in the cells that can alter their genotypic and phenotypic

behavior towards cell survival. We envision that switching media conditions can change cellular secretome that can possibly lead to reduced secretion of fibrotic factors. Since all our previous elastic modulus measurements were done in serum containing media, repeating the assay with serum free media can build an understanding on the role of serum in CAF based desmoplasia. Thus, overall, we can say that while use of label free proteomics is a useful technique to do an unbiased analysis of tumor cell secretome there are various optimizations that needs to be performed. The scale down of culture, role of serum and use of conditioned media are some of the important factors that we envision play a crucial role in successful LC-MS analysis.

3.5 Conclusion:

In summary we observed a significant number of proteins being secreted due to the coculture of MCF7 cells with CAFs and observed abundant expression of various ECM related proteins. We observed that most of the ECM related factors secreted in coculture CM has been previously related to enhanced tumorigenicity and hence can be crucial to create a tumor permissive niche. Due to low number of proteins being detected our LC-MS analysis was not conclusive and require various optimizations. Amongst various factors, including sample preparation, role of serum, and scale of culture can be some crucial factors which needs to be optimized to integrate label free proteomics with our 3D tumor stroma model.

Chapter 4
**The Role of Desmoplasia and Stromal Fibroblasts on Anti-Cancer Drug Resistance
in a Microengineered Tumor Model**

4.1 Introduction:

Breast cancer is known as the second most leading cause of death amongst women across the globe (Siegel et al., 2017). While the early stage of the disease can be treated with high success rates, the invasive and metastatic phase of the disease still suffer from poor therapeutic outcomes (Siegel et al., 2017). It is now widely accepted that the TME plays a crucial role in the disease progression as well as in inherent resistance to anti-cancer therapeutics during the metastatic cascade (Place et al., 2011; Tredan, Galmarini, Patel, & Tannock, 2007). Due to the complexity of the TME, chemotherapeutic drugs do not primarily perfuse through the parenchyma of the tissue in lethal amounts, primarily because of the high interstitial fluid stress, gradients of growth factors and hypoxia (Netti, Berk, Swartz, Grodzinsky, & Jain, 2000; Tredan et al., 2007). Additionally, the signaling crosstalk between the stromal and cancer cells induce resistance by upregulating pro-survival mechanisms such as reduced cell death, enhanced proliferation and invasion etc (Farmer et al., 2009; D. Hanahan & Weinberg, 2011; Sentebrane et al., 2017). In this regard, specific therapeutics are being developed to target the interactions between tumor and the surrounding stroma (Tredan et al., 2007). The stromal targeting drugs along with classical chemotherapeutics are now being considered as enhanced combinatorial treatment strategies compared to monotherapy regimes (Tredan et al., 2007).

Amongst various stromal cells found within breast TME, cancer associated fibroblasts (CAFs) are dominant in number (Kalluri, 2016). Previous studies have demonstrated that CAFs play a significant role in inducing the microenvironment conducive for the progression of the disease (Dumont et al., 2013; Kalluri, 2016; Tredan et al., 2007; Tripathi, Billet, & Bhowmick, 2012). For instance, CAFs deposit abundant and aligned ECM proteins such as collagen, fibronectin, lysyl oxidase within local TME as compared to their normal counterparts (i.e. mammary fibroblasts) (Dumont et al., 2013; Tripathi et al., 2012). High expression of ECM proteins leads to the formation of a desmoplastic stroma with elevated biophysical properties (i.e. stiffness), which subsequently promote tumor cell invasion, proliferation, and also reduces the functional efficacy of drugs due to the upregulation of integrin and focal adhesion kinase (FAK) (Gjorevski, Piotrowski, Varner, & Nelson, 2015; Han et al., 2016; Hirata et al., 2015; Jeong, Lee, Shin, Chung, & Kuh, 2016; Netti et al., 2000; Stanisavljevic et al., 2015).

Due to the significant role of ECM proteins and matrix properties (i.e. stiffness), in inherent drug resistance, many studies in the past have utilized anti-fibrotic drugs that directly target the desmoplastic stroma (Darakhshan & Ghanbari, 2013; Papageorgis et al., 2017; Seniutkin et al., 2018; Suklabaidya et al., 2016; Ken Takai et al., 2016; Zhang et al., 2016). Most of the previous *in vitro* studies in this regard have utilized two-dimensional (2D) monolayer of cancer cells, either alone or in coculture with stromal cells, to study the influence of these drugs on tumor growth and invasion (Chuang & Khorram, 2017; Darakhshan & Ghanbari, 2013; Izumi et al., 2009; Mediavilla-Varela,

Boateng, Noyes, & Antonia, 2016; Okazaki et al., 2014; Saito et al., 2018; Sato et al., 2010; Subramaniam, Ace, Prud'homme, & Jothy, 2011). These studies have provided valuable insight on cytotoxicity level of drugs and the biochemical pathways being influenced during the therapy (Chuang & Khorram, 2017; Darakhshan & Ghanbari, 2013; Nikkhah et al., 2011; Strobl, Nikkhah, & Agah, 2010). However, due to 2D nature of these platforms, the dynamic alterations in the biophysical properties of the matrix (i.e. stiffness) in the presence of anti-fibrotic drugs cannot be retrieved (Nitish Peela et al., 2017). Additionally, the lack of a third dimension in 2D models does not enable recapitulation of the native characteristics of the TME, ultimately leading to notable differences in pharmacodynamic outcomes (Peela, Barrientos, Truong, Mouneimne, & Nikkhah, 2017). *In vivo* animal models, on the other hand, provide crucial insights on the role of the drugs in alleviation of stress, interstitial fluid pressure as well as deposition of stromal matrix proteins (Papageorgis et al., 2017; Sakai et al., 2016; Ken Takai et al., 2016; Zhang et al., 2016). However, due to the physiological differences between animal models and humans, clinical translation of the drug target has been limited (Mak, Evaniew, & Ghert, 2014; Nitish Peela et al., 2017). Additionally, the inherent complexities of *in vivo* models, does not enable quantitative assessment of the alterations of ECM matrix during tumor progression in presence of a single class of stromal cells (i.e. CAFs) (Moriah E. Katt, Amanda L. Placone, Andrew D. Wong, Zinnia S. Xu, & Peter C. Searson, 2016; Peela et al., 2016; Plodinec et al., 2012). In this regard, microengineered 3D tumor models, integrated with novel biomaterials, provide enormous

potential to mimic the complexities of TME with precise control on various factors including the spatial organization of cancer and stromal cells, matrix composition and so forth (Supriya. Nagaraju, Danh. Truong, Ghassan. Mouneimne, & Mehdi. Nikkhah, 2018; Nitish Peela et al., 2017; Truong et al., 2016). Microengineered tumor models also enable better visualization of the dynamic changes within cell cytoskeleton and stromal matrix for enabling specific mechanistic studies (Nikkhah, Strobl, & Agah, 2008; Nitish Peela et al., 2017).

In this study we developed a 3D microengineered platform incorporating high density of tumor cell-embedded microwells, surrounded by stromal cells such as CAFs. Due to the open top nature of the platform, we probed the matrix with AFM to assess the alterations of the ECM stiffness over the experimental period. Further, we studied the impact of combinatorial action of anti-fibrotic drug tranilast and doxorubicin on ECM remodeling, tumor growth and cancer cell invasion in the sole presence of CAFs. We focused our study on breast cancer in this work, however, due to highly versatile nature of the proposed platform, the model can be adapted to various other types of desmoplastic cancer.

4.2 Materials and methods

Materials

Poly dimethyl siloxane (PDMS Sylgard 184 Silicon Elastomer Kit, Dow Corning) was utilized to fabricate PDMS holders and stamps to engineer our 3D micropatterned breast tumor model. 2-aminopropyl-triethoxy-silane (APTES), Poly-D-Lysine (PDL) and

glutaraldehyde was utilized to surface treat our substrates (PDMS holders, glass bottom confocal dishes). PDMS stamps were treated with Pluronic F-127 to render them protein resistant. Tranilast was bought from TCI America and stock was prepared at the concentration of 100 mM in DMSO. Doxorubicin (alfa aesar) was diluted in DI water with stock solution of 1 mM

Cell Culture

In our study we utilized 3 different breast tumor cell lines namely MDA-MB-231, MCF7 and MCF10A. MDA-MB-231 and MCF10A cells were transduced to express tdTomato fluorescence and was provided by McCarty lab (Oregon Health & Science University). MCF7 cells on the other hand were obtained from Mouneimne lab at University of Arizona Cancer Center and expressed mCherry fluorescence. CAFs, which were isolated from human mammary gland tissue peripheral to invasive ductal carcinoma, were purchased as an immortalized cell line from ATCC (HTB-125). MDA-MB-231, MCF7 and CAFs were cultured in DMEM 1X media supplemented with 10% FBS, 1% PenStrep and 1% L-glutamine. MCF10A cells were maintained in a DMEM: F12 supplemented with 1% Lglutamine, epidermal growth factor, cholera toxin, hydrocortisone, insulin and 5% horse serum. For all experiments, the cell lines were cultured within T-75 flasks and maintained at 37°C and 5% CO₂ with subsequent change of media every two days. The passage number used for various experiments for different cell lines are as listed below for consistency for the experiments: MDA-MB-231 (17-22), MCF7 (5-9), MCF10A (10-13), CAFs (54-62).

IC 50 assay

Alamar blue assay (Thermo Fisher) was utilized to study the metabolic activity of cells and *IC 50* analysis within 96 well plates after exposure to individual treatments for 48 hours. To calculate *IC 50* on 2D surface, the cells were trypsinized and plated within well plates at the cell density of 3×10^4 and 5×10^4 for MDA-MB-231 and CAFs respectively and were allowed to adhere to the well plate overnight. For studying *IC 50* values of drug in 3D hydrogel, the cells at above mentioned cell densities were encapsulated within 4mg/ml of collagen I and 30 μ l of the cell embedded gel was pipetted in 96 well plate. Tranilast and doxorubicin at various doses was prepared from stock in cell culture media and added to cells for 48 hours. The media was removed, and cells were washed with 1X PBS three times. Alamar blue was prepared at the dilution of 1:10 in cell culture media and added to cells for 3 hours at 37 °C similar to our previous work. The plates were read using a plate reader as per manufacturer's instruction.

Development of the 3D tumor model

The 3D tumor model was fabricated using micromolding techniques (Nelson et al., 2008). Specifically to develop the model, we primarily fabricated PDMS stamps and holders using soft lithography techniques. While the holders were utilized as a substrate to immobilize collagen I hydrogel, stamps were engineered to micromold the gel and create a high-density array of microwells. Both PDMS platforms were prepared by mixing SYLGARD Silicone Elastomer Base and the SYLGARD Silicone Elastomer curing agent in the ratio 10:1. The mixture was then vacuumed until no air bubbles

remained. The mixture was poured on a silanized silicon wafer and degassed for 30 minutes after which it was incubated overnight at 80 °C. PDMS holders were first threated with air-based plasma for 4 minutes and then immediately immersed in 2% of 2-(aminopropyl) triethoxysilane (APTES) prepared in 95% ethanol. The holders were incubated in APTES for 1 hour at 60 °C. To remove unbound APTES, the holders were transferred to 100% ethanol solution, and sonicated using a water-based ultrasonic bath for 20 minutes. The holders were washed with 100% ethanol in five 10 minutes intervals followed by 1-hour incubation at 80 °C. To allow covalent immobilization of collagen I, the PDMS holders were then incubated in 2% glutaraldehyde (GA) at room temperature for 1 hour. GA was removed by five consecutive 5-minute washes with DI water and then incubated overnight at 80°C. PDMS stamps were made protein-repellant through incubation with a 1% Pluronic F-127 solution.

To fabricate the tumor model, rat tail collagen I was used at the concentration of 4 mg/ml. CAFs were mixed with collagen I at the optimized cell density of 2×10^6 cells/ml (Figure 4-1A). PDMS stamps were removed from pluronic solution and washed three times with DI water. The collagen solution was then added to each stamp immediately and further inverted on top of the surface treated PDMS holders (Figure 4-1A). The whole assembly was then kept for polymerization for 30 minutes at 37 °C (Figure 4-1A). After polymerization of the gel, the stamp was lifted off gently and the microwells were seeded with cancer cells at a density of 7×10^6 cells/ml for 2-3 minutes (Figure 4-1A). The cells from unpatterned surface were removed by washing with media. The prepared samples

were kept inside the incubator for 15 minutes to allow attachment of cells to collagen wells. After 15 minutes, the samples were immersed within 500 μ l of media in each well of 24 well plate overnight. On day 1, freshly prepared media with drug was added to the samples for 48 hours. The experimental groups include control (i.e. MDA+CAF without drug), DMSO (0.62%), Tranilast (620 μ M), Doxorubicin (280nM) and Tranilast +Doxorubicin.

Cell proliferation assay

Tumor cell proliferation was quantified by using Click iT-Alexa Fluor -488- Edu Imaging Kit (Thermo Fisher) as per manufacturer's instruction. To quantify cancer cell proliferation, the DsRed positive cell (MDA-MB-231) with EdU positive and DAPI stained nuclei was counted in Image J using cell counter plugin. To further calculate the percentage of proliferative cancer cells, the EdU positive cancer cells was divided by total number of DsRed positive tumor cells. Additionally, we also performed the assay on non-invasive MCF7 and normal mammary epithelial MCF10A cells for control and tranilast+doxorubicin experimental group across two experiments.

Cancer cell invasion assay

To visualize invasion of tumor cells across all groups, prepared samples were imaged using fluorescence and phase contrast microscopy (ZEISS) on day 1, before addition of drug as well as on day 3 of the culture. Tile images were acquired from 2 random locations of the sample. Using ImageJ, we thresholded each image and utilized particle analyzer plugin to extract co-ordinates of each cell within an image. Next, we used a

custom-written MATLAB code to perform delaunay triangulation modelling similar to previous reports (Nawrocki Raby et al., 2001). The area of each triangle within delaunay plot was calculated using MATLAB. We calculated average area of all triangles and quantified area disorder for each delaunay plot using following equation:

$$Area\ disorder = 1 - \left[1 + \left(\frac{standard\ deviation}{average\ area} \right) \right]^{-1}$$

The invasion index was calculated based on following equation:

$$Invasion\ Index = \frac{(Area\ disorder\ on\ Day\ 1 - Area\ Disorder\ on\ Day\ 3)}{Area\ disorder\ on\ Day\ 1}$$

Immunostaining

To visualize the deposition of collagen I and fibronectin within the matrix of the micropatterned mode, primary monoclonal mouse antibodies against collagen I and fibronectin were used (Santa Cruz Biotechnology) at dilution of 1:200 and 1:100 respectively. To fluorescently stain the fibers, Alexa Fluor 488 secondary antibodies (Life Technologies) were used at the dilution of 1:400 and 1:200 respectively. The fluorescently labelled fibers were visualized using confocal reflectance microscopy (Leica Microsystems, SP8) available at KECK bioimaging center at ASU.

Atomic Force Microscope (AFM) based mechanical characterization

The measurement for elastic modulus (i.e. stiffness) of the matrix were made on day 1 before addition of drug followed by day 3 of the culture. The matrix stiffness was measured by indenting MDA-MB-231 free areas within the platform and convoluting elastic moduli of ECM and CAFs since fibroblasts have been shown to match the

stiffness of the substrate (Solon, Levental, Sengupta, Georges, & Janmey, 2007). Force indentation curves were recorded with a commercial atomic force microscope (MFP-3D-BIO AFM, Asylum Research, Santa Barbara CA, USA) using sphere-conical probes ($K_{\text{nominal}}=0.2$ N/m, LRCH, Team Nanotec, Germany) with a half cone angle of 18.8 degrees and sphere radius of 850 nm. Force-indentation curves were collected in 4×4 grids as force maps in an area of $90 \mu\text{m} \times 90 \mu\text{m}$ located in the center between four wells at 37°C and with indentation speed of $2 \mu\text{m} \cdot \text{s}^{-1}$. The trigger force was selected to 60-80 nN resulting in indentation depths of at least $10 \mu\text{m}$. The spring constant of each cantilever was determined before the experiment by the thermal noise method (Butt & Jaschke, 1995; Hutter & Bechhoefer, 1993). Three force maps per sample per day were collected. The first $10 \mu\text{m}$ indentation of each force distance curve was fitted to a non-adhesive elastic contact model for a conical indenter with a spherical tip (Staunton et al., 2016). Data analysis was done using MATLAB. The poisson ration of collagen was assumed to be $\nu_{\text{collagen}}=0.5$.

Quantification of expression of proteases within our 3D microengineered platform

The quantification for expression of various proteases and their inhibitors was done by utilizing a commercially available RayBiotech human MMP1 antibody array (QAH-MMP-1-1) for quantification of the expression of MMP1,2,3, 8,9,10,13 and TIMP-1,2 and 4. To perform the assay, the samples were prepared and cultured in 10% serum containing media for 24 hours and then washed three times with 1X DPBS to remove serum. The samples were then incubated in various drug conditions prepared in serum

free media. The conditioned media was collected after 48 hours and centrifuged at 14000 rpm for 10 minutes to remove cell debris. The supernatant was collected and stored at -80 °c until further use. To perform the antibody array all the samples were run as per manufacturer instructions. To get a comprehensive analysis, all conditions were repeated in triplicate technical and biological replicate.

Statistical Analysis

Unless otherwise stated, all the assays were repeated three times with three technical replicates per condition. The IC 50 results were analyzed using sigmoidal curves in GraphPad. The elastic modulus data was analyzed using two-way ANOVA with Sidak's multiple comparison test. All other data was analyzed using repeated one-way ANOVA with Tukey multiple comparison test. Due to unavailability of samples for some groups in few experiments, the statistical analysis was reported for EdU and Tunnel assay using ordinary one-way ANOVA. p value less than 0.05 was considered significant for all the results. The statistical analyses and data representation was performed using GraphPad Prism v 7.0. All the data was presented as mean \pm standard deviation.

4.3 Results

Microengineering of the 3D breast tumor model

The 3D breast tumor model was fabricated by utilizing micromolding technique to create a high-density array of microwells within collagen I hydrogel as shown in Figure 4-1A. The stromal region was fabricated by encapsulating CAFs within collagen I hydrogel while the tumor region was engineered by seeding tumor cells (MDA-MB-231) within

the microwells (Figure 4-1A). As shown in Figure 4-1B, the tumor and stromal regions were accurately organized to mimic the native spatial organization of TME and thus study the invasive behavior of tumor cells as well as change in biophysical properties of the ECM. The experimental groups were designed to study the influence of tranilast and doxorubicin on alterations of matrix properties and tumor progression either individually or in combination. The control condition included the coculture of cMDA-MB-231 cells and CAFs without the addition of any drug. The time period for the current study was kept constant for 3 days since CAFs exerted high traction force on collagen I which caused folding of hydrogel and disruption of the model for extended period of culture.

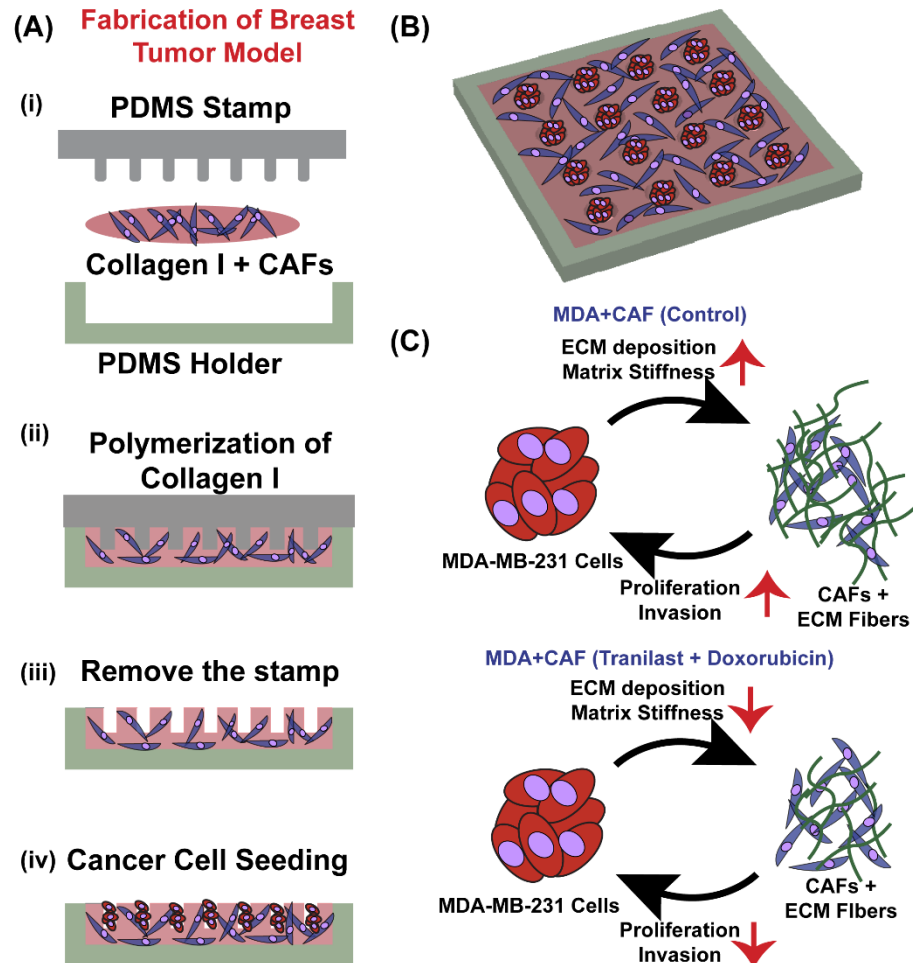


Figure 4-1: Proposed Hypothesis of Combinatorial Action of Tranilast With Doxorubicin on Tumor Progression.

(A) Schematic of the main fabrication steps of 3D microengineered high-density tumor model. (B) 3D view of the micropatterned breast tumor model. (C) Representative illustration of the proposed hypothesis of the study demonstrating the role of desmoplasia on tumor survival, growth and cancer cell invasion. Addition of antifibrotic drug tranilast

along with doxorubicin downregulate ECM remodeling thereby reducing overall tumor progression.

We hypothesized that within the control condition (i.e. no drug), the presence of tumor and stromal cells lead to remodeling of the matrix and elevated stiffness by deposition of proteins such as collagen I and fibronectin (Figure 4-1C). The increase in the elastic modulus of the matrix eventually lead to enhanced tumor growth, invasive activity of MDA-MB-231 cells as well as resistance to cell death (Figure 4-1C). On the other hand, addition of tranilast will reduce the fibrosis of the matrix due to its known inhibition of collagen synthesis and ECM turnover, leading to impaired desmoplasia (Figure 4-1C) (Papageorgis et al., 2017). Reduced fibrosis of the matrix will downregulate the biomechanical signaling of the ECM, thereby enhancing the efficacy of doxorubicin and condensing tumor growth and invasion (Figure 4-1C).

Characterization of IC 50 concentrations

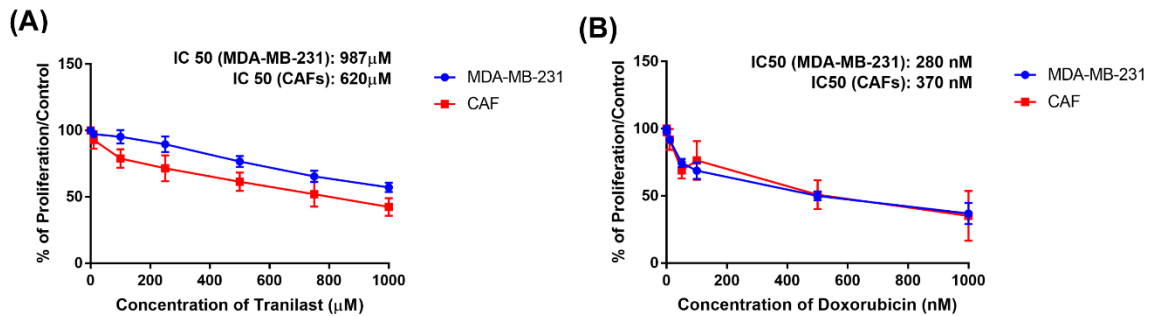


Figure 4-2: 2D IC-50 Assay.

(A) Metabolic activity of MDA-MB-231 and CAFs in response to different doses of Tranilast in a 96 well plate. (B) Doxorubicin induced metabolic activity of MDA-MB-231 cells and CAFs with different concentrations.

Prior to proceeding with our tumor model, we characterized the IC 50 values for each of the drugs (tranilast, doxorubicin) on both cell lines (MDA-MB-231, CAFs) using 2D cell culture and alamar blue assay. Based on the metabolic activity of cells across various concentration of drugs, relative IC-50 values were calculated using standard mathematical models. Our results demonstrated lower IC 50 value of tranilast for CAFs (620 μ M) as compared to MDA-MB-231 cells (987 μ M, Figure 4-2A). Similar results have been also observed by previous studies, on pancreatic tumor and stellate cells seeded on 2D surfaces in presence of anti-fibrotic drug, pirfenidone, depicting enhanced influence of the drug on fibroblasts as compared to the tumor cells (Kozono et al., 2013). On the other hand, doxorubicin had lower IC 50 value for MDA-MB-231 cells (280 nM) as compared to CAFs (370 nM) as shown in Figure 4-2B. Previous studies in the literature have reported the IC 50 of doxorubicin for MDA-MB-231 cells in the range of 0.5 nM to 5 μ M (Abu, Akhtar, Ho, Yeap, & Alitheen, 2013; Lovitt, Shelper, & Avery, 2018; Pilco-Ferreto & Calaf, 2016; Rahman et al., 2016; L. Smith et al., 2006; Tassone et al., 2003; Wu et al., 2013). Consistently, our IC 50 value is within this previously reported range. Such a wide range of IC 50 for MDA-MB-231 cells can be due to multiple factors including passage number, culture conditions as well heterogeneity of the cell population. We also performed similar IC 50 assay within 3D collagen I hydrogel. As

shown in supplementary Figure 1A-B (APPENDIX C), both MDA-MB-231 and CAFs demonstrated IC 50 values for tranilast and doxorubicin higher than those observed in 2D assay. In order to experimentally achieve 50% inhibition in cell metabolic activity, we therefore expanded the range of concentration of doxorubicin to as high as 10 μ M. Our results demonstrated IC 50 values for MDA-MB-231 and CAFs for Doxorubicin to be 2073 nM and 2108 nM respectively within 3D collagen I hydrogel (Supplementary Figure 1C, APPENDIX C). Higher IC 50 values for the drug within 3D hydrogel assay can be possibly attributed to reduced diffusion of the drug, difference in cell phenotype and genetic make-up within 3D systems as compared to 2D systems (Netti et al., 2000; N. Peela et al., 2017; Nitish Peela et al., 2017). Similar analysis for tranilast could not be achieved as the drug remained insoluble at higher concentrations in cell culture media. Such insolubility of the tranilast can be explained due to its super hydrophobic nature, as also demonstrated by previous studies (Onoue et al., 2012). Since our main goal was to study the effect of combination of two drugs on desmoplasia, tumor growth and invasion, we proceeded with IC 50 values obtained within our 2D assay. Therefore, based on our preliminary studies, we fixed the concentration of tranilast to be 620 μ M and doxorubicin to be 280 nM for our future experiments. We also added blank DMSO vehicle (0.62%) as another control group.

Characterization of desmoplasia

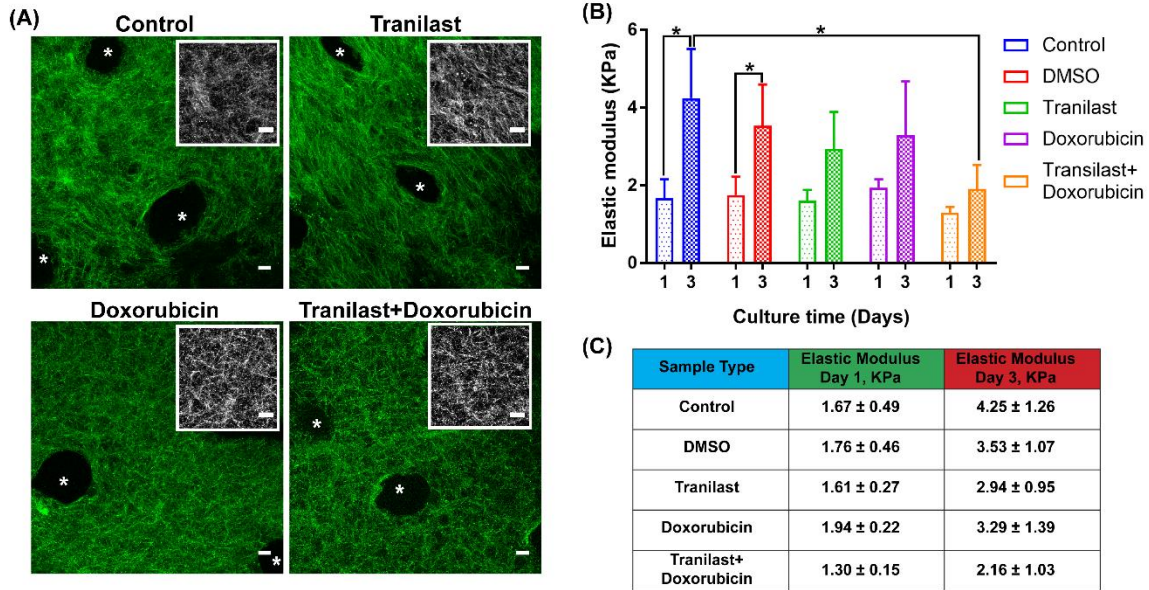


Figure 4-3: Characterization of Stromal Desmoplasia Under Various Drug Conditions.

(A) Representative immunofluorescent images of collagen I within 3D matrix across all the groups. Inset represent a magnified view of fiber density across all the conditions. (B) Elastic modulus of matrix across all the groups on day 1 before addition of drug and day 3 after addition of drugs. (C) Table of average elastic modulus values across various drug conditions on day 1 and day 3 of culture. All values are written as mean \pm standard deviation. * represent the microwells molded in collagen. Scale bar represent 20 μ m. (* represents p value < 0.05).

A major advantage of our 3D platform is the ability to measure the changes in biomechanical properties of the matrix during active invasion of cancer cells in the presence of the drugs as compared to traditional 2D *in vitro* as well as *in vivo* models. To

visualize the changes in matrix protein deposition, we immunostained the samples for collagen I and fibronectin on day 3 of culture. Additionally, we measured the changes in stiffness of the matrix using AFM on day 1 before addition of drugs and on day 3 after 48 hours of drug treatment. As show in Figure 4-3A, the stromal matrix of the control group demonstrated a high density of collagen I fibers as compared to the samples exposed to combinatorial drugs. Similar observation was made with respect to fibronectin assembly within stromal matrix (Supplementary figure 2, Arrows, APPENDIX C). Additionally, both collagen and fibronectin fibers were more punctuated in the presence of both drugs (Figure 4-3A, Supplementary Figure 2, APPENDIX C). Such differences were also reflected in matrix stiffness across all culture groups (Figure 4-3B, C, Supplementary Figure 3, APPENDIX C). Specifically, our results showed that, while both control and DMSO treated groups depicted significant increase in elastic modulus on day 3 ($E_{control,day3} = 4.25 \pm 1.26 \text{ kPa}$ and $E_{DMSO,day3} = 3.53 \pm 1.07 \text{ kPa}$) as compared to day 1 ($E_{control,day1} = 1.67 \pm 0.49 \text{ kPa}$, $E_{DMSO,day1} = 1.76 \pm 0.46 \text{ kPa}$), tranilast, doxorubicin and tranilast+doxorubicin treated groups did not exhibit any significant change in the matrix stiffness (Figure 4-3B, C Supplementary Figure 3, APPENDIX C). Additionally, the elastic modulus for the tranilast+doxorubicin group on day 3 of culture was significantly lower than the control and DMSO group. ($E_{control,day3} = 4.25 \pm 1.26 \text{ kPa}$, $E_{DMSO,day3} = 3.53 \pm 1.07 \text{ kPa}$, $E_{Tranilast+Doxorubicin,day3} = 2.16 \pm 1.03 \text{ kPa}$, Figure 3C). These findings suggest enhanced anti-fibrotic activity when the two drugs were added together to the model.

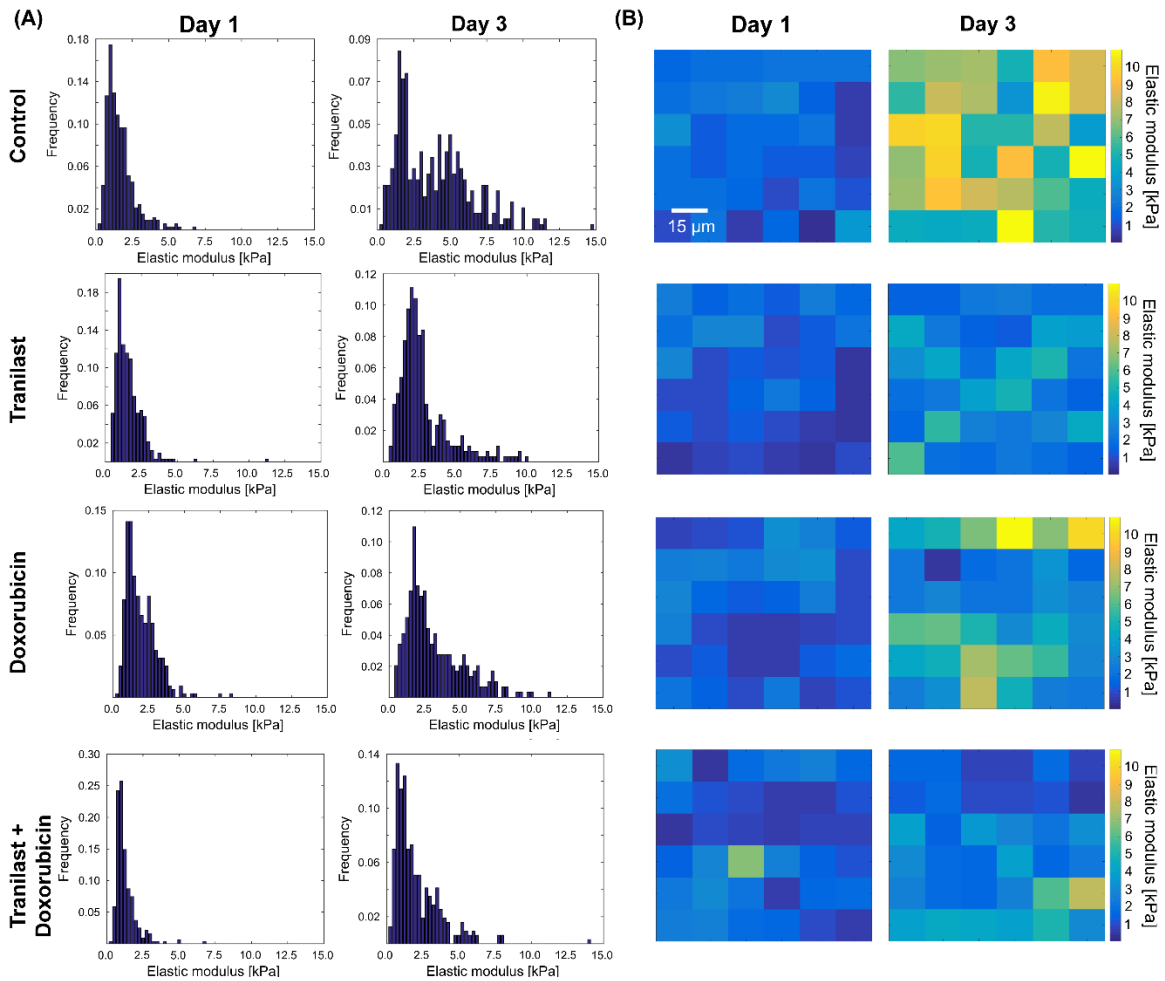


Figure 4-4: Representative Histograms of Elastic Modulus and Stiffness Maps Under Various Drug Conditions.

(A) Representative histograms showing distribution of elastic modulus of the stromal matrix across various groups. (B) Representative color maps curves of stiffness across all the experimental conditions.

Figure 4-4A, B show histograms and 2D color-maps of the indented matrix on days 1 and 3. Stiffness histograms on day 1 demonstrated similar unimodal distributions,

consistent to the data shown by Plodinec *et al.* for normal tissues (healthy human and MMTV-PyMT mice biopsies) (Plodinec et al., 2012). For the untreated control group of our 3D tumor model we found multi-peaks in the stiffness histogram on day 3. Bimodal stiffness with broad distribution as seen for control group has been associated with cancer biopsies indicating a biomechanical heterogeneity in diseased tissue (Plodinec et al., 2012). Narrower matrix stiffness distributions on day 3 for treated groups within our model suggested lower level of interplay among CAFs and tumor cells. Therefore, the control group on day 3 demonstrated significant desmoplasia. Notably, the combinatorial addition of tranilast and doxorubicin drugs impaired these biophysical alterations.

Tumor growth

Since the stiffness of the matrix was significantly modulated by the combinatorial action of two drugs, we next hypothesized that the proliferative behavior of tumor cells will also be altered upon exposure to varied drug treatments. To assess tumor growth, we utilized Alexa Fluor 488 EdU assay to fluorescently label replicating MDA-MB-231, MCF7 and MCF10A cells and further visualized them using fluorescent microscopy (co-expressing DsRed and GFP). As shown in Figure 4-5A, MDA-MB-231 cells proliferated the most within the control group. While monotherapy with tranilast and doxorubicin reduced the tumor growth however, the reduction was not statistically significant (Figure 4-5A, B). Further, quantification for EdU positive cells demonstrated a significant decrease in proliferative behavior of tumor cells (MDA-MB-231) due to the combinatorial action of tranilast and doxorubicin (Figure 4-5B).

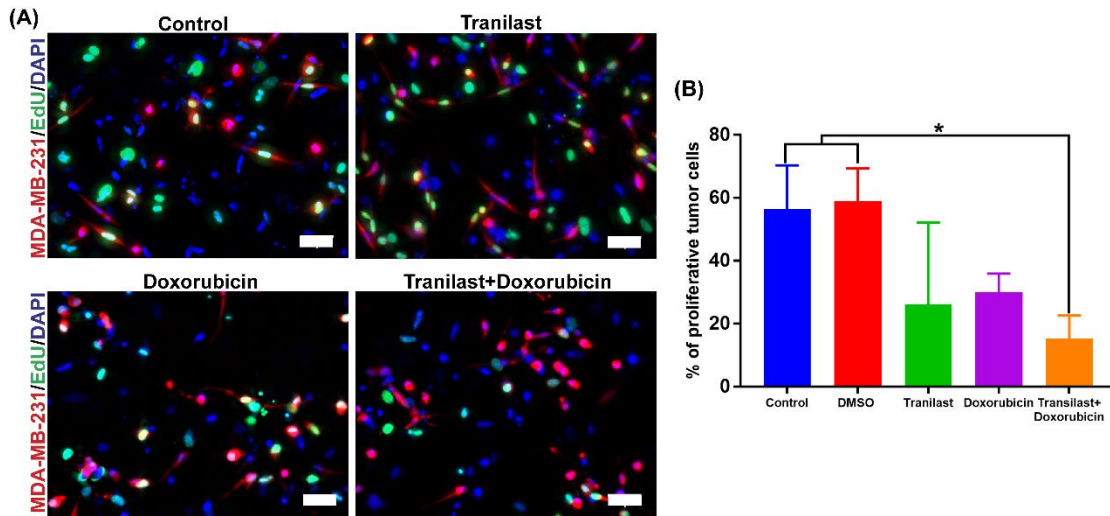


Figure 4-5: Tumor Proliferation Assay Under Various Drug Conditions.

(A) Representative immunofluorescent images of EdU assay depicting tumor cell proliferation across all experimental groups. (B) Quantification of proliferation of MDA-MB-231 cells within all conditions. Scale bar represents 50 μm . (* represents p value < 0.05).

Similar trend was observed when non-invasive MCF7 cells and normal mammary epithelial cells (MCF10A) were cultured with CAFs in presence and absence of drugs. Specifically, in the control group both MCF7 and MCF10A cells demonstrated high replicative ability (~ 90%, Supplementary Figure 4A, B, APPENDIX C). However, when tranilast and doxorubicin was added together, the proliferation rate for both cell types reduced significantly (MCF7= $35 \pm 5.4\%$, MCF10A = $30 \pm 18 \%$, Supplementary Figure 4A, B, APPENDIX C). Thus, overall our results demonstrate reduced proliferative ability of invasive and non-invasive (MDA-MB-231, MCF7) tumor cells as well as

normal mammary epithelial cells when the two drugs act in synergy in presence of CAFs as compared to untreated condition.

Cancer cell invasion

Based on our hypothesis, we further speculated a limited ability of cancer cells to invade the surrounding stroma in combinatorial treatment of drugs. To visualize the dispersion of tumor cells within the 3D matrix, we utilized phase contrast and fluorescent imaging along with delaunay triangulation.

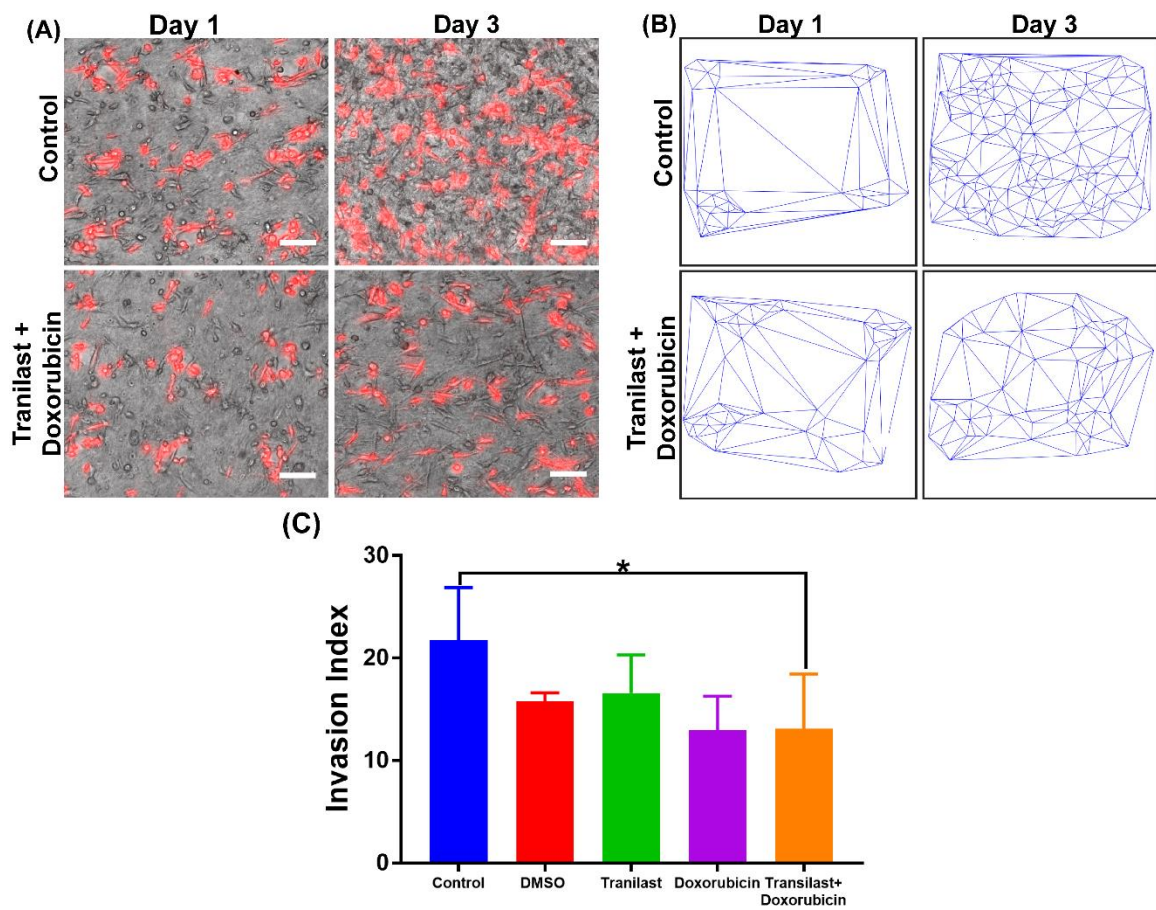


Figure 4-6: Tumor Dispersion Under Various Drug Conditions.

(A) Representative phase contrast and fluorescent images of tumor cell dispersion in control and tranilast + doxorubicin group on day 1 (before addition of drug) and day 3 (after addition of drug). (B) Representative triangulation graphs depicting tumor cell invasion into the stroma. (C) Quantification of invasion index of MDA-MB-231 cells. Scale bar represent 100 μm . (* represents p value < 0.05).

As shown in Figure 4-6A and Supplementary figure 5A (APPENDIX C), tumor cells demonstrated enhanced invasive capacity across all the groups on day 3 as compared to day 1 of the culture. Similar analysis was drawn from triangulation graphs (Figure 5-6B and Supplementary figure 5B, APPENDIX C), where tumor cells appeared more scattered within the stroma on day 3 as compared to day 1 of the culture. Quantification of area disorder demonstrated invasion of tumor cells into matrix for all groups (Supplementary Figure 5C, APPENDIX C). However, quantification of invasion index across all the conditions, indicated a significant decrease in invasion of tumor cells in combinatorial treatment of tranilast and doxorubicin as compared to control. These results are in fact similar to previous *in vivo* studies where metastasis was observed to be minimalistic only when tumors were subjected to combinatorial therapy of anti-fibrotic drug and doxorubicin (Ken Takai et al., 2016).

Assessment of proteases and their tissue inhibitors expression

To complement our matrix remodeling and stiffness results, we performed a comprehensive analysis of expression of various matrix remodeling factors including matrix metalloproteinases (MMPs) and tissue inhibitor of metalloproteinases (TIMPs).

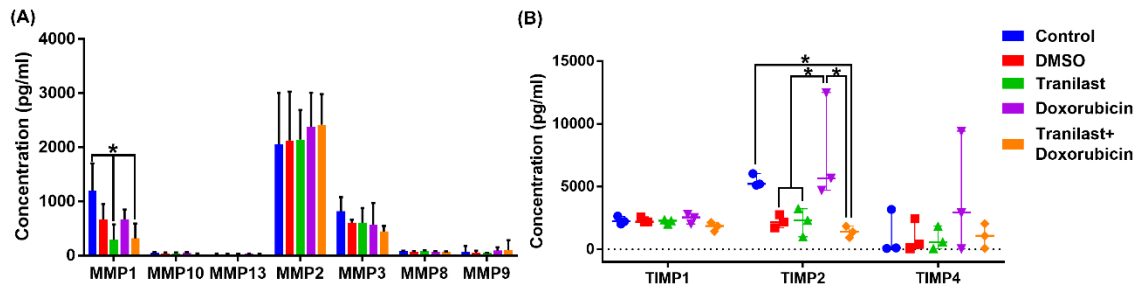


Figure 4-7: ELISA Assay for Quantifying MMP's and TIMP's.

(A) Quantification of various proteases of MMP array for all culture conditions. (B) Quantification of concentration of different TIMPs across all culture conditions. (* represents p value < 0.05).

Our results demonstrated that MMP1 a known interstitial collagenase had highest concentration within the control group (1197 ± 508.789 pg/ml) which was not significantly different from DMSO (668.93 ± 282.191 pg/ml) and doxorubicin group (673.98 ± 177.03 pg/ml), thereby suggesting enhanced ECM remodeling within these groups. However, upon addition of tranilast, concentration of MMP1 significantly decreased both in tranilast (291.3 ± 284.142 pg/ml) and tranilast + doxorubicin groups (316.926 ± 276.208 pg/ml, Figure 5-7A). Besides, MMP1 we also observed significant difference in expression of TIMP2 across different culture conditions. As shown in Figure 5-7B, the expression of TIMP2 within the control group (5449.974 ± 504.055 pg/ml) was significantly higher than tranilast + doxorubicin group (1389.667 ± 455.242 pg/ml). Furthermore, the doxorubicin group (7625.03 ± 4234.258 pg/ml) had significantly higher expression of TIMP2 as compared to DMSO (2222.955 ± 526.215

pg/ml), tranilast (2173.451 ± 1127.598 pg/ml) and tranilast + doxorubicin group. Besides MMP1 and TIMP2, we did not observe any significant difference for other proteases across all culture conditions.

4.4 Discussion

In this study we utilized a 3D microengineered breast tumor model to study the influence of anti-fibrotic drug tranilast in combination with doxorubicin on desmoplasia, tumor growth and cancer cell invasion. Many previous studies have suggested that tumor cells activate stromal cells such as fibroblasts surrounding them to alter the microenvironment and make it more conducive for tumor progression (Kalluri, 2016; Tripathi et al., 2012). Fibroblasts in particular are known to get activated in presence of tumor cells and adopt a myofibroblast like phenotype (CAFs) similar to a wound healing process (Kalluri, 2016; Tripathi et al., 2012). Such a change in phenotype of fibroblasts leads to remodeling of the matrix and hence induction of fibrosis within the surrounding microenvironment (Kalluri, 2016; Tripathi et al., 2012). Therefore, to initially construct an *in vivo* like TME, the proposed model was compartmentalized into tumor and stromal regions by seeding MDA-MB-231 cells within microwells that were surrounded by collagen-based stroma encapsulating CAFs. Such a spatial organization of tumor- stromal region was purposefully chosen to mimic the native breast TME. The choice of collagen I hydrogel, to establish the model was motivated by the abundance of this ECM protein within native TME (Fang, Yuan, Peng, & Li, 2014). Our proposed platform enabled dissection of the

role of CAFs as the most dominant cell within the mammary carcinoma, on desmoplasia and tumor progression.

To disrupt the desmoplastic response of CAFs within breast TME, we studied the action of tranilast, a clinically approved drug in Japan and South Korea for treatment of fibrotic diseases such as keloids (Darakhshan & Pour, 2015). While in previous 2D *in vitro* studies, this drug has been shown to be paramount in influencing tumor cell viability as well as growth (Chuang & Khorram, 2017; Darakhshan & Pour, 2015; Izumi et al., 2009; Sato et al., 2010; Subramaniam et al., 2011), not much has been studied about its efficacy on the dynamic change in biophysical properties of the ECM (i.e. stiffness) during active invasion. Additionally, a quantitative study on the impact of tranilast on matrix stiffness and tumor progression has been missing in the sole presence of CAFs. Therefore, our study was motivated by these critical knowledge gaps in the literature.

A major finding of our study was the limited increase in elastic modulus of the matrix in combination treatment of tranilast and doxorubicin as compared to control after 48 hours of exposure (Figure 5-3B). Immunostaining of collagen I and fibronectin, further confirmed reduced density and assembly of these matrix protein fibers within combinatorial drug treatment, which are known to be regulators of ECM stiffness (Dumont et al., 2013; Kalluri, 2016; Tripathi et al., 2012). Such an observation can be attributed to various factors including reduced proliferation of CAFs due to the action of tranilast (Suzawa, Kikuchi, Arai, & Koda, 1992), downregulation of biochemical

pathways and limited viability of tumor and stromal cells in the presence of doxorubicin (Pilco-Ferreto & Calaf, 2016). While the mode of action of tranilast is still not clear, many previous studies have shown that this specific anti-fibrotic drug downregulates the proliferation of fibroblasts of various lineage including dermal, corneal and CAFs (Ohshio, Hanaoka, Kontani, & Teramoto, 2014) consistent with our alamar blue results (Figure 5-2A, B). Additionally, it has been shown by previous *in vivo* studies that tranilast can downregulate the expression of growth factors such as CTGF, TGF β which play a crucial role in ECM protein synthesis and deposition, therefore limiting the increase in the stiffness of the matrix (Branton & Kopp, 1999; Papageorgis et al., 2017; Subramaniam et al., 2011). Furthermore, due to the known cytotoxic effect of doxorubicin on cancer cells, the impaired crosstalk between MDA-MB-231 and CAFs can influence the autocrine/paracrine signaling and hence lead to reduced fibrosis (Kalluri, 2016; Place et al., 2011; Truong et al., 2016; W. Wang et al., 2009). Such specific action of these drugs also explains the insignificant change of stiffness within monotherapy groups, while the synergistic influence of these drugs can significantly reduce desmoplasia (Figure 5-3B).

To further develop a comprehensive understanding on remodeling abilities of cells under various drug conditions, we also performed an antibody array analysis on various MMP and TIMP expression. Our results demonstrated reduced expression of proteases such as MMP1 within tranilast and tranilast + doxorubicin group suggesting limited remodeling ability of tumor and stromal cells due to the action of this drug. Many

previous studies have demonstrated similar reduced expression of various other proteases including MMP2 and MMP9 under the influence of tranilast (Darakhshan, Bidmeshkipour, Khazaei, Rabzia, & Ghanbari, 2013; Harigai et al., 2018; Subramaniam, Chakrabarti, Prud'homme, & Jothy, 2010). For instance, Darakhshan *et al.* showed that when MCF7 and MDA-MB-231 cells were treated with tranilast, MMP9 mRNA expression was significantly reduced as compared to untreated cells (Darakhshan et al., 2013). While most of these studies have been primarily 2D monoculture of tumor cells (Darakhshan et al., 2013; Harigai et al., 2018; Subramaniam et al., 2010), similar assessment of MMP analysis for 3D coculture of tumor and stromal cells has not been attempted in the past. Such discrepancy in cell culture conditions can be a possible explanation for differences in our findings from those of previous studies. Our results also demonstrated reduced expression of TIMP2 within tranilast + doxorubicin group as compared to control and doxorubicin. Since TIMP2 is known to play a significant role in inhibiting the action of various proteases (Têtu et al., 2006), crosstalk between tumor cells and CAFs in control condition can possibly lower the expression of TIMPs to favor ECM remodeling, an observation made in Figure 5-3 and supplementary Figure 2 (APPENDIX C). However, in doxorubicin condition such a crosstalk between tumor cells and CAFs is altered due to limited number of tumor cells (i.e. less proliferative), thereby maintaining the expression and activity of TIMP2. On the other hand, in combinatorial group limited viability of tumor and stromal cells can minimize the overall expression of different proteins thus minimizing the concentration of TIMP2.

Another finding of our study was reduced tumor growth and invasive behavior of MDA-MB-231 cells within the combinatorial treatment group as compared to untreated condition. Our results also demonstrated similar trend for non-invasive MCF7 and normal mammary MCF10A cells such that combinatorial action of tranilast and doxorubicin reduced their replicative ability significantly. We envision that these findings can be primarily correlated to our elastic modulus results where the combinatorial action of tranilast and doxorubicin treatment significantly reduced the stiffness as compared to control. Various studies have established that stiffness of the ECM can provide biomechanical cues by controlling the activity of integrins as well as FAKs, which in turn can influence proliferation and migratory behavior of the cells (Dumont et al., 2013; Hirata et al., 2015; Kalluri, 2016; Stanisavljevic et al., 2015). For instance, Schrader *et al.* utilized polyacrylamide gels (PAA) of variable stiffness and demonstrated tight regulation of proliferation of hepatocellular carcinoma cells by substrate stiffness due to upregulation of integrin $\beta 1$ and FAK signaling in stiff matrices (Schrader et al., 2011). Moreover, they demonstrated that the inhibition of integrin $\beta 1$ and FAK signaling, significantly reduced the proliferative ability of the cells (Schrader et al., 2011). Besides decrease in elastic modulus, presence of doxorubicin in the combinatorial treatment can further target proliferating cells, leading to overall reduction of growth of cancer and normal mammary cells within our 3D microengineered platform. In another study by Rosa *et al.*, MCF10A cells demonstrated enhanced migratory and wound closure activity upon seeding on PAA gels of high stiffness (Ng, Besser, Danuser, & Brugge, 2012).

These findings were consistent even when tumor cell proliferation was inhibited with mitomycin-C (Ng et al., 2012). Further inhibition of myosin contractility reduced the cell speed on stiff matrices, suggesting the role of integrin mediated myosin contractility on tumor cell invasion (Ng et al., 2012).

Several previous *in vivo* studies have demonstrated a significant decrease in tumor growth with monotherapy of doxorubicin as compared to combinatorial action with tranilast (Papageorgis et al., 2017; Ken Takai et al., 2016). We did not observe a significant reduction in tumor growth and stiffness in sole presence of doxorubicin or tranilast. Such differences in results can be attributed to various factors such as interstitial stress, leaky vasculature, and the presence of other cell types (i.e. immune cells) within *in vivo* models (Papageorgis et al., 2017; Ken Takai et al., 2016). In this regard, a previous study by Stylianopoulos *et. al.*, demonstrated that the administration of antifibrotic drugs such as tranilast and pirfenidone significantly reduce the interstitial stress that further enable penetration of doxorubicin into tumor parenchyma, thereby influencing the tumor growth (Papageorgis et al., 2017). Since our platform lacked tumor vasculature, doxorubicin did not encounter any limitation in terms of penetration within the matrix. It is also important to note that the aforementioned *in vivo* studies were performed for longer duration (i.e. 20-30 days) with continuous addition of tranilast as compared to our platform (Papageorgis et al., 2017). Nevertheless, our platform provides a unique ability to dissect the role of a single class of stromal cells on drug resistance. Additionally, we were able to visualize matrix remodeling as well as quantitatively assess the

biomechanical changes during the course of experiment within our microengineered tumor model. In future, we aim to conduct further mechanistic and gene expression studies on cancer cells in the presence of different drug combination.

4.5 Conclusion

In conclusion, we demonstrated the use of our 3D microengineered tumor stroma platform to assess the influence of anti-fibrotic drug (tranilast) on efficacy of chemotherapeutics such as doxorubicin in the sole presence of CAFs. We observed that while the matrix stiffness was significantly increased within our control group leading to a bimodal distribution of stiffness, such alteration in matrix properties were minimized due to the combinatorial action of tranilast and doxorubicin. Further, the synergistic influence of the two drugs diminished tumor growth and invasion thereby demonstrating an improved therapeutic regime than the monotherapy of each drug. We also performed molecular studies by assessing the expression of various MMPs and TIMPs and observed significantly lower expression of MMP1 and TIMP2 within the combinatorial group. In the future, we aim to conduct more mechanistic studies by assessing the genetic changes in tumor cells and CAFs under different drug conditions for genes related to ECM, proliferation and invasion.

Chapter 5

Conclusion and Future Work

This chapter summarizes the major findings of each specific aim as well as the project challenges and future directions.

5.1 Significance and Contributions:

Specific Aim 1:

In specific aim 1, we fabricated a 3D high density tumor stroma model using micromolding techniques. The platform was built such that it had a high-density array of tumor seeded microwells surrounded by stroma comprised of collagen I and CAFs. To perform *in situ* measurements of matrix biomechanical properties during active tumor invasion we integrated our platform with AFM and confocal reflectance microscopy. We incorporated breast tumor cells of varied tumorigenicity (MDA-MB-231 Triple negative and more invasive, MCF7 Er/PR+ and less invasive) and studied their molecular interaction with CAFs that induce desmoplasia. We also utilized the platform to study tumor progression in response to CAFs by performing invasion assays including delaunay triangulation and real time cell migration as well as study tumor growth. Our results demonstrated enhanced ECM remodeling with upregulated matrix stiffness and increased deposition of collagen fibers when MDA-MB-231 cells were cocultured with CAFs as opposed to monoculture of either cell type. Similar desmoplastic reaction was observed due to the coculture of MCF7 cells with CAFs suggesting the crucial role of tumor stroma interaction in modulating the biomechanical properties of the matrix. Using

phase contrast and fluorescent microscopy, we observed an enhanced dispersion of MDA-MB-231 cells in presence of CAFs, while MCF7 cells depicted high clustering tendency. We also observed a significant increase in cell speed and persistence in the population of MDA-MB-231 cells upon coculture with CAFs while no significant change in migration metrics were detected for MCF7 cells. Proliferation assays such as EdU demonstrated an enhanced replicative ability of MCF7 cells in the presence of CAFs as compared to their monoculture group. Thus, overall both tumor cells upon coculture with CAFs induced CAF based desmoplasia with enhanced matrix stiffness and collagen deposition. While MDA-MB-231 cells adopted a more invasive phenotype in presence of CAFs, MCF7 cells became more proliferative.

In this aim, for the first time, we utilized an *in vitro* 3D microengineered model to study the dynamic change in breast cancer matrix properties during active tumor cell invasion in the presence of CAFs. As opposed to traditional *in vivo* and tumor biopsy models commonly used to study ECM remodeling, we designed the experiments with appropriate controls and minimal confounding variables and demonstrated the crucial role of tumor-stroma interaction in ECM remodeling. Although our current study focused primarily on breast cancer, various other desmoplastic tumors including prostate cancer and non-small lung cancer can be studied on this platform.

Specific Aim 2:

While in aim 1 we focused on developing a physiologically relevant 3D *in vitro* tumor-stroma platform for breast cancer desmoplastic reaction, in aim 2 we utilized the platform

to perform mechanistic studies to better understand the mode of interaction between tumor cells and CAFs, which leads to desmoplasia. In particular, we assessed the role of soluble factor signaling between tumor cells and CAFs on ECM remodeling. Our results demonstrated crucial role of tumor secreted factors on inducing CAF based desmoplastic reaction. Additionally, soluble factors obtained from monoculture of tumor cells upregulated ECM remodeling while the soluble factors from coculture group of tumor cells and CAFs did not induce any significant change in matrix properties. We took two different approaches to characterize various pro-fibrotic factors secreted by tumor cells. In an unbiased approach we utilized LC-MS to identify the tumor secretome and assess their role in breast cancer fibrosis. Although we observed upregulated secretion of tumor associated ECM components within our coculture group, the number of proteins identified were small in number to perform a conclusive analysis. On the other hand, we utilized an informed biased approach where we identified multiple pro-fibrotic factors from various other fibrotic diseases and observed a crucial role of PDGF-AA/BB in CAF based desmoplasia. We also inhibited the activation of PDGFR using a concentration sweep of specific inhibitor (CP 673451) and observed minimal fibrosis in the presence of CAFs.

In this aim, for the first time, we were able to clearly establish the role of tumor secreted factors on induction of CAFs based desmoplasia. Due to a well-designed study with appropriate controls we demonstrated that tumor cell secretes profibrotic factors which are sensed by CAFs due to the presence of specific receptors that activates fibrosis

related pathways. To the best of our knowledge, this is the first *in vitro* 3D tumor stroma model which established the crucial role of PDGF AA/BB in breast cancer fibrosis. Thus, overall, we demonstrated the ability of our platform in performing mechanistic study to classify the mode of interaction between tumor and stromal cells and identify key molecular targets participating in CAF based fibrosis.

Specific Aim 3:

In this aim, we utilized our established platform to validate our model and study the effect of an approved anti-fibrotic drug, tranilast, on stromal desmoplasia and efficacy of anti-cancer drug doxorubicin in the presence of CAFs. We identified the IC-50 value of tranilast and doxorubicin on MDA-MB-231 cells and CAFs in 2D and 3D conditions. We demonstrated that while tranilast in monotherapy was not able to reduce ECM stiffness, the combinatorial action of tranilast and doxorubicin minimized CAF induced desmoplasia by disrupting collagen fiber assembly and fibronectin deposition. We also demonstrated that secretion of matrix metalloproteinases (MMPs) such as MMP1 and TIMP 2 were significantly affected due to the synergistic influence of tranilast and doxorubicin. The combinatorial action of the tranilast and doxorubicin also significantly reduced tumor invasion and growth.

Although tranilast has been shown to be effective anti-fibrotic drug in multiple *in vivo* studies, our study was the first 3D *in vitro* study to analyze the effect of tranilast on desmoplasia in the sole presence of CAFs. Our results related to effectiveness of combinatorial therapy in minimizing tumor growth and invasion were corroborated to

previous *in vivo* data. We also took a step forward by provided an insight on the influence of tranilast and doxorubicin on expression of MMP's and TIMP's in addition to collagen and fibronectin expression, an analysis missing from previous *in vivo* and *in vitro* studies. Thus, overall, we utilized our desmoplasia based model to test an anti-fibrotic based therapy to allow better availability of chemotherapeutic drug and minimize mechanotransduction based signals for tumor progression.

Contributions:

Below is the list of contributions of this work in peer reviewed journal articles and conference oral and poster presentations.

Journal Articles:

- **H. Saini**, K. Rahmani, M. Allam, C. Silva, J.Veldhuizen, D. Truong, G. Mouneimne, T. Hu, R. Ros, M. Nikkhah*, “The Role of Breast Tumor Stromal Interactions in ECM Dysregulation within a 3D Microengineered Model”, *Manuscript in Preparation*, July 2019.
- A. Buchberger, **H. Saini**, K. Rahmani, N. Stephanopoulos, R. Ros, M. Nikkhah*, “Reverse Tunable Gelatin based DNA Hydrogel to Modulate Matrix Stiffness for Cancer studies”, *Manuscript in Preparation*, July 2019.
- **H. Saini**, K. Rahmani, C. Silva, M. Allam, R. Ros, M. Nikkhah*, “The Role of Desmoplasia and Stromal Fibroblasts on Anti-Cancer Drug Resistance in a Microengineered Tumor Model”, *Cellular and Molecular Bioengineering (CMBE)*, 11: 419-433 (2018), [[Young Investigator Award Issue](#)].

- N. Peela#, D. Truong#, **H. Saini**#, H. Chu, S. Mashaghi, S. L. Ham, S. Singth, H. Tavana, B. Mossadegh, M. Nikkhah*, “Advanced Biomaterials and Microengineering Technologies to Recapitulate the Stepwise Process of Cancer Metastasis”, *Biomaterials*, 133: 176-207 (2017). [[Among the Most Downloaded Biomaterials Articles, # Equal Contribution](#)].
- D. Truong, A. Kratz, J.G. Park, E.S. Barrientos, **H. Saini**, T. Nguyen, B.A. Pockaj, G. Mouneimne, J. LaBaer, M. Nikkhah, (2019). “Human Organotypic Microfluidic Model to Investigate the Interplay Between Patient-derived Fibroblasts and Breast Cancer Cells”, *Cancer Research*, 2019 (online version)

Conference Oral and Poster Presentations:

- **H Saini**, K Rahmani, C Silva, M Allam, G Mouneimne, R Ros, M Nikkhah* -‘The Role of Desmoplasia and Stromal Fibroblasts on Anti-Cancer Drug Resistance in a Microengineered Tumor Model’, Biomedical Engineering Society, Young Investigator Award Issue, Oral Presentation, October 2018.
- **H Saini**, K Rahmani, M Rodrigues, T Cai, M Allam, C Silva, D Truong, T Hu, R Ros, M Nikkhah*, ‘Identification of Molecular Signaling Cues between Cancer Cells and Stromal Fibroblasts Enhancing ECM Deregulation in a 3D Microengineered Platform’ Biomedical Engineering Society, Poster Presentation, October 2018.

- **H Saini**, K Rahmani, C Silva, R Ros, M Nikkhah*, ‘Elucidation of the Role of Stromal Fibroblasts on Anti-Cancer Drug Resistance within a Microengineered Tumor Model’, Molecular and Cellular Tissue Engineering, Poster Presentation, March 2018.
- **H Saini**, K Rahmani, D Truong, E Assefa, R Ros, M Nikkhah*, ‘A High-Density Tumor Model to Assess Breast Cancer Dispersion and ECM Remodeling under the Influence of Stromal Cells’, Biomedical Engineering Society, Oral Presentation, October 2017.
- **H Saini**, K Rahmani, C Silva, M Allam, R Ros, M Nikkhah*, ‘Investigating the Role of Stromal Cells on Breast Cancer Invasion using Three Dimensional (3D) High density Tumor Microarray Model’, Molecular and Cellular Tissue Engineering, Poster Presentation, March 2017.
- **H Saini**, K Gomaz, K Rahmani, R Ros, M Nikkhah* ‘Three Dimensional (3D) High Density Tumor Microarray to Study the Influence of Stromal Cells on Cancer Invasion’, Biomedical Engineering Society, Poster Presentation, October 2016.

5.2 Project Challenges:

During the course of this dissertation we faced multiple challenges that we overcame to successfully complete the project. Amongst our very first challenge was fabrication of our microengineered 3D *in vitro* tumor stroma model. During year 1 and 2 of the dissertation we worked exclusively on fabricating the model and optimizing

various parameters including dimension of the pattern, distance between two adjacent microwells and tumor cell density. We learnt from various experiments, that in order to form a high-density tumor cell seeded microwells, the diameter and depth of each microwell were the most crucial factors. When the platform was fabricated with relatively large diameter ($\sim 300 \mu\text{m}$) microwells, the tumor cells could not be retained within the pattern upon washing due to their easy dislodging. We identified that it was crucial that the cells get physically restrained by dimension of the pattern to avoid dislodging of cells with multiple washing. Upon optimization with different diameter of the microwells we identified that the best patterning of tumor cells was achieved at the diameter size of $75 \mu\text{m}$. We also varied the distance between the patterns to create a high-density tumor microarray and observed that the large distance between two adjacent microwells caused difficulties in removing tumor cells from stroma which in turn can lead to dislodging of cells from the patterns due to multiple washes. From a series of optimization experiments, it became clear that a center to center distance of about $250 \mu\text{m}$ between two microwells was ideal to create a pattern of tumor seeded microwells. We also ran optimizations on tumor cell density and observed that a high cell density ensure complete filling of the microwells enabling fabrication of accurate tumor stroma architecture (Nelson et al., 2008).

Another critical challenge that we faced during the project was to quantify the dispersion of MDA-MB-231 cells into the stroma in the absence and presence of CAFs. Unlike most other microengineered platforms such as microfluidic models, the initial

tumor boundary could not be easily recognized as the culture period increased due to the remodeling of the microwells by CAFs (S. Nagaraju et al., 2018; Truong et al., 2016; D. D. Truong et al., 2019). While tumor migration in many *in vitro* models is measured in terms of the distance travelled from initial tumor boundary to final tumor boundary, this metric could not be applied to our platform. Hence, we took inspiration from metrics which are used to measure tumor cell invasiveness by using mathematical model known as Delaunay Triangulation (Nawrocki Raby et al., 2001). In this regard, we utilized ImageJ and our custom written MATLAB code using in built function of Delaunay triangulation to measure area disorder and migration index on various days of the culture as explained in chapter 2 and 4. Since MCF7 cells mostly clustered, such an analysis was difficult to perform for these cells and hence we measured tumor clustering tendency using ImageJ.

One of our major challenge was during proteomic studies on our collected CM to identify various tumor secreted factors participating in CAF based desmoplasia. For this analysis we resorted to serum free media for easy identification of low abundant tumor secreted factors in absence of large proteins found within serum. However, even after multiple washes of samples with 1X PBS to remove any trace serum, we observed significant amount of albumin and other serum related proteins within our CM which made it difficult to visualize tumor and CAF based secretomes. As explained in chapter 3, we used traditional gel electrophoresis and in gel digestion techniques to remove albumin from our media (Shevchenko, Tomas, Havli, Olsen, & Mann, 2006). However, due to

the use of this technique we lost various low abundant proteins either due to complex formation with large serum proteins or due to poor yield of various peptides from the gel (Millioni et al., 2011; Speicher, Kolbas, Harper, & Speicher, 2000). It is also crucial to note here that our samples were microengineered 3D samples which have lower cell number as compared to traditional 2D samples. Despite combining conditioned media from various replicates (8 per condition) we did not detect a large number of proteins. Additionally, since our sample type was cell conditioned media as compared to cellular lysate, the amount of proteins was found to be low. Due to various technical challenges that came up regarding use of LC-MS with our platform, it became evident that a series of further optimizations will be required to use traditional discovery-based proteomics with microengineered platforms. For starting, different serum depletion approaches need to be utilized to retain low abundant proteins. For instance, multiple columns including MARS column are available which have high specificity and sensitivity to serum related proteins and can remove minimize the presence of various contaminants (M. P. W. Smith et al., 2011). Additionally, the depletion techniques of high abundant serum proteins can be conjugated with enrichment techniques for low abundant proteins to recover a significantly large number of proteins (Millioni et al., 2011). Although in this project we resorted to use traditional ELISA technique to identify tumor secreted pro-fibrotic factors, the integration of LC-MS with our 3D microengineered model will be a subject of future research for our group.

5.3 Future Directions:

Modeling cancer fibrosis under in vivo like hypoxic microenvironment

Cancer is a disease in which malignant cells maintain their proliferative phenotype and grow in size (D. Hanahan & Weinberg, 2011). When tumors grow beyond the size 1-2 mm, the core of the tumor becomes necrotic leading to secretion of various pro-angiogenic factors that leads to formation of new blood vessels to regulate the supply of nutrients and gas exchange to the cancer cells (Gilkes, Semenza, & Wirtz, 2014). The resultant new blood vessels have multiple structural abnormalities that leads to the formation of torturous vascular architecture and leaky blood supply. The tumor associated vessels do not provide adequate blood supply to various regions of the tumor and hence leads to development of hypoxic areas. Hypoxia although initially restricts tumor growth but later on activates multiple cell survival pathways which leads to tumor progression (Gilkes et al., 2014).

While the effect of hypoxia on tumor angiogenesis, cell invasion, EMT are well studied, recent reports have argued that hypoxia may also have a significant impact on stromal fibrosis. In an interesting study by Gikes et.al. it was demonstrated that under hypoxic conditions breast tumor cells including MDA-MB-231, MCF7 and MCF10A shows an elevated expression of collagen crosslinking enzymes including prolyl 4-hydroxylase 1 and 2 (P4H1, P4H2) (Gilkes et al., 2013). Since hypoxia inducible factors including HIF-1 α and HIF-2 α are significantly upregulated under hypoxia conditions,

the authors studied the mRNA expression of P4H1 and P4H2 after silencing H1F-1 α and H1F-2 α (Gilkes et al., 2013). Authors demonstrated that the loss of H1F-1 α but H1F-2 α leads to a significant reduction in P4H1 and P4H2 mRNA expression. Authors further confirmed the *in vitro* results by injecting sh1/2 α MDA-MB-231 clones into mouse mammary fat pad and observed reduced expression of P4H1 and P4H2 with condensed deposition of collagen fibers (Gilkes et al., 2013). Additionally, using MDA-MB-231 clones with shRNA against P4H1 and P4H2 authors demonstrated that loss of these two factors can minimize tumor growth and lung metastatic burden (Gilkes et al., 2013). Many other reports have suggested that H1F factors can also regulate expression of other ECM related enzymes including LOX and MMP's by elevating their expression levels by transformed tumor and stromal cells (Gilkes et al., 2014; Muñoz-Nájjar, Neurath, Vumbaca, & Claffey, 2006; Wong et al., 2011).

Microengineered models such as ours enable accurate characterization of stromal fibrosis by studying dynamic changes in ECM architecture and perform mechanistic molecular studies on various pro-fibrotic factors as opposed to conventional animal models. While the preliminary studies about the role of hypoxia in ECM dysregulation has been performed using animal models, there is still a lack of in-depth studies that focus on the mechanism of hypoxia on ECM turnover due to tumor stroma interactions. Additionally, more focused studies need to be performed to understand the synergistic influence of hypoxia and stromal fibrosis on drug resistance since these factors are two critical bottlenecks in anti-cancer drug resistance. As opposed to conventional animal

models, microengineered 3D platforms, similar to ours, will aid in better assessment of the expression of pro-fibrotic factors under various conditions. Additionally, due to minimal confounding variables, our 3D model will help in dissecting the individual and synergistic role of fibrosis and hypoxia on drug resistance. Therefore, we envision that by culturing our platform under hypoxic conditions and by using advanced biotechnology techniques such as gene knockdown strategies we can study the crucial role of hypoxia on cancer desmoplasia. Additionally, we can also study the synergistic influence of ECM fibrosis and hypoxia on the efficacy of chemotherapeutic drugs. Such an understanding will therefore help in designing more targeted adjunct therapies that can be given to patients along with conventional chemotherapy and radiation therapy to improve their effectiveness.

Role of fibrosis in activation of other stromal cell within the TME

It has been well studied that various other stromal cells besides CAFs transform themselves and participate in tumor progression (Bussard et al., 2016). For instance, endothelial cells show an enhanced proliferation and migration towards necrotic cores to form new blood vessels and supply nutrients for maintaining tumor metabolism (Dudley, 2012). Macrophages on the other hand change their phenotype from tumor inhibiting M1 to tumor promoting M2 state and secrete anti-inflammatory cytokines and matrix components to promote tumor invasion (Noy & Pollard, 2014). Regulatory T-cells participate in cancer by immunosuppressing the tumor specific immunity thereby tipping the tumor cells towards survival and proliferation (Balkwill et al., 2012; Segovia-

Mendoza & Morales-Montor, 2019). Tumor cells are generally known to secrete elevated levels of various growth factors including VEGF, IGF, TGF- β and PDGF that can assist in transformation of these stromal cells to an alternate tumor promoting phenotype (Balkwill et al., 2012). Besides tumor cells, some reports have suggested that CAFs can also transform different cell types to participate in tumor progression (Gascard & Tlsty, 2016). While multiple studies have elucidated the role of tumor cells in activation of stromal cells and in turn their influence on tumor progression, not much is known about how biophysical properties of ECM can activate and transform these cell types to create a tumor permissive niche.

Some recent reports have elucidated that biophysical properties of ECM can activate and switch the phenotype of stromal cells. For instance, it has been shown by various research groups that stiff matrices as compared to soft matrices promote secretion of anti-inflammatory cytokines which are usually associated with tumor inhibiting M1 phenotype (Hsieh et al., 2019; Okamoto et al., 2018; Previtiera & Sengupta, 2016). However, from clinical research biopsies we know that advanced stages of tumor are correlated with enhanced stiffness as well as tumor promoting M2 phenotype of macrophages. Such contradicting results thereby raise the question that whether the interaction of tumor cells and ECM stiffness modulate the secretome that can alternate the activation of these immune cells. Such analysis can easily be performed on our 3D tumor stroma model by utilizing different tunable biomaterials whose stiffness can be

modulated to study the synergistic role of tumor cells and stiffness on phenotype of different stromal cells including macrophages, adipocytes and T-cells.

Characterization of stromal desmoplasia due to interaction of tumor cells and CAFs isolated from patients

Most of the studies in cancer research utilize cancer and stromal cell lines due to their easy availability and culture requirements (Hynds, Vladimirou, & Janes, 2018). While most of these cell lines have been established from patient derived cells, it has now been accepted that these cell lines adapt a different phenotype and genotype with increase in passage number as compared to their early cultures (H. Yang, Sun, Liu, & Mao, 2018). Furthermore, cell lines provide a simplistic view of the biological question since they don't represent the patient to patient heterogeneity. Some researchers argue that widespread use of cancer cell lines to screen drugs can be another crucial factor in clinical failure of various drugs (H. Yang et al., 2018). In this regard, cancer research community is slowly moving towards use of patient derived cells. Multiple protocols have been established using which different cell types including fibroblast cells and monocytes can be isolated with high success from patient derived tissues (Menck et al., 2014; Orimo et al., 2005; D. Truong et al., 2019; D. D. Truong et al., 2019). For instance, one of the recent studies in our lab utilized patient derived CAFs to study their role in cancer progression including proliferation and invasion within an organotypic microfluidic model (D. D. Truong et al., 2019). Tissue biopsies were obtained from three different patients with difference in their hormone and Her2 receptor status. Upon

characterization of isolated CAFs from different patients we observed morphological heterogeneity with difference in α -SMA expression across the population of CAFs (D. D. Truong et al., 2019). Additionally, when co-cultured with tumor cells, 2 out of 3 CAF populations enhanced the migration of tumor cells as compared to the monoculture condition. The study also assessed the transcriptomic signature of SUM-159 cells in the presence and absence of CAFs and observed significant role of GPNMB in tumor cell invasion (D. D. Truong et al., 2019). Another interesting study by Rudnick et.al. demonstrated that fibroblast cells isolated from either reduction mammoplasty tissue or breast cancer tissues are heterogenous in their activity in tumor promotion (Rudnick et al., 2011). Authors utilized tissues obtained from invasive lobular, ductal carcinoma as well as from various reduction mammoplasty disease free tissues. Despite their origin, it was observed that fibroblasts cells which were able to secrete high levels of prostaglandin (PEG2) act as tumor promoting by expanding the population of cancer stem cells thereby supporting MCF7 tumor growth (Rudnick et al., 2011). Such studies thus demonstrate the crucial role of patient derived cells in understanding the heterogeneity in biological behavior of tumor cells and their subsequent role in tumor expansion.

While most of the studies primarily focused on the role of patient derived cells on tumor progression, not many studies focus on role of these isolated cells from different tumor subtype of cancer on stromal ECM desmoplasia. By isolating patient cells from tumor of various hormone receptor subtypes, similar to our previous study (D. D. Truong et al., 2019), we can study the difference in ECM biochemical and biophysical properties

deposited by the CAFs. By utilizing novel techniques such as second harmonic generation and AFM we can further visualize the changes in ECM fiber organization and deposition during tumor invasion. Similar to our ELISA assessments in Chapter 2, expression of various factors can be studied in presence of different CAF population to provide better understanding on expression patterns of tumor secreted growth factors. Additionally, we can study the change in transcriptomic profile of CAFs upon coculture with tumor cells to visualize the regulation of genes participating in desmoplasia, inflammation and immune suppression. Besides enabling cancer biology, these isolated cells can further be useful to test clinically approved anti-fibrotic drugs such as tranilast used in Chapter 4 to study their influence in disrupting desmoplasia in presence of fibroblasts obtained from various patients.

REFERENCES

(ACS), A. c. s. (2017). *Breast cancer facts and figures 2017-2018*. Retrieved from Atlanta:

Abu, N., Akhtar, M. N., Ho, W. Y., Yeap, S. K., & Alitheen, N. B. (2013). 3-Bromo-1-hydroxy-9,10-anthraquinone (BHAQ) inhibits growth and migration of the human breast cancer cell lines MCF-7 and MDA-MB231. *Molecules*, *18*(9), 10367-10377. doi:10.3390/molecules180910367

Acerbi, I., Cassereau, L., Dean, I., Shi, Q., Au, A., Park, C., . . . Weaver, V. M. (2015). Human breast cancer invasion and aggression correlates with ECM stiffening and immune cell infiltration. *Integr Biol (Camb)*, *7*(10), 1120-1134. doi:10.1039/c5ib00040h

Alkasalias, T., Moyano-Galceran, L., Arsenian-Henriksson, M., & Lehti, K. (2018). Fibroblasts in the Tumor Microenvironment: Shield or Spear? *International Journal of Molecular Sciences*, *19*(5), 1532.

Antoniades, H. N., Bravo, M. A., Avila, R. E., Galanopoulos, T., Neville-Golden, J., Maxwell, M., & Selman, M. (1990). Platelet-derived growth factor in idiopathic pulmonary fibrosis. *The Journal of Clinical Investigation*, *86*(4), 1055-1064. doi:10.1172/JCI114808

Asghar, W., El Assal, R., Shafiee, H., Pitteri, S., Paulmurugan, R., & Demirci, U. (2015). Engineering cancer microenvironments for in vitro 3-D tumor models. *Mater Today (Kidlington)*, *18*(10), 539-553. doi:10.1016/j.mattod.2015.05.002

Balkwill, F. R., Capasso, M., & Hagemann, T. (2012). The tumor microenvironment at a glance. *J Cell Sci*, *125*(Pt 23), 5591-5596. doi:10.1242/jcs.116392

Barcus, C. E., Keely, P. J., Eliceiri, K. W., & Schuler, L. A. (2013). Stiff Collagen Matrices Increase Tumorigenic Prolactin Signaling in Breast Cancer Cells. *Journal of Biological Chemistry*, *288*(18), 12722-12732. doi:10.1074/jbc.M112.447631

- Barré-Sinoussi, F., & Montagutelli, X. (2015). Animal models are essential to biological research: issues and perspectives. *Future Science OA*, 1(4), null. doi:10.4155/fso.15.63
- Bissell, M. J., & Hines, W. C. (2011). Why don't we get more cancer? A proposed role of the microenvironment in restraining cancer progression. *Nat Med*, 17(3), 320-329. doi:10.1038/nm.2328
- Board., P. A. T. E. (2019). Breast Cancer Treatment (PDQ®).Health Professional Version. . In *PDQ Cancer Information Summaries* Bethesda (MD): National Cancer Institute (US).
- Branton, M. H., & Kopp, J. B. (1999). TGF- β and fibrosis. *Microbes and Infection*, 1(15), 1349-1365. doi:https://doi.org/10.1016/S1286-4579(99)00250-6
- Bray, F., Ferlay, J., Soerjomataram, I., Siegel, R. L., Torre, L. A., & Jemal, A. (2018). Global cancer statistics 2018: GLOBOCAN estimates of incidence and mortality worldwide for 36 cancers in 185 countries. *CA: A Cancer Journal for Clinicians*, 68(6), 394-424. doi:10.3322/caac.21492
- Buchsbaum, R. J., & Oh, S. Y. (2016). Breast Cancer-Associated Fibroblasts: Where We Are and Where We Need to Go. *Cancers*, 8(2), 19.
- Bussard, K. M., Mutkus, L., Stumpf, K., Gomez-Manzano, C., & Marini, F. C. (2016). Tumor-associated stromal cells as key contributors to the tumor microenvironment. *Breast Cancer Research*, 18(1), 84. doi:10.1186/s13058-016-0740-2
- Butt, H. J., & Jaschke, M. (1995). Calculation of thermal noise in atomic force microscopy. *Nanotechnology*, 6(1), 1.
- Calvo, F., Ege, N., Grande-Garcia, A., Hooper, S., Jenkins, R. P., Chaudhry, S. I., . . . Sahai, E. (2013). Mechanotransduction and YAP-dependent matrix remodelling is

- required for the generation and maintenance of cancer-associated fibroblasts. *Nature Cell Biology*, 15, 637. doi:10.1038/ncb2756
- <https://www.nature.com/articles/ncb2756#supplementary-information>
- Camp, J. T., Elloumi, F., Roman-Perez, E., Rein, J., Stewart, D. A., Harrell, J. C., . . . Troester, M. A. (2011). Interactions with Fibroblasts Are Distinct in Basal-Like and Luminal Breast Cancers. *Molecular Cancer Research*, 9(1), 3-13. doi:10.1158/1541-7786.Mcr-10-0372
- Carter, J. C., & Church, F. C. (2012). Mature breast adipocytes promote breast cancer cell motility. *Experimental and Molecular Pathology*, 92(3), 312-317. doi:<https://doi.org/10.1016/j.yexmp.2012.03.005>
- Cavo, M., Fato, M., Peñuela, L., Beltrame, F., Raiteri, R., & Scaglione, S. (2016). Microenvironment complexity and matrix stiffness regulate breast cancer cell activity in a 3D in vitro model. *Scientific Reports*, 6, 35367. doi:10.1038/srep35367
- Chaudhuri, O., Koshy, S. T., Branco da Cunha, C., Shin, J. W., Verbeke, C. S., Allison, K. H., & Mooney, D. J. (2014). Extracellular matrix stiffness and composition jointly regulate the induction of malignant phenotypes in mammary epithelium. *Nat Mater*, 13(10), 970-978. doi:10.1038/nmat4009
- Chen, P., Mo, Q., Wang, B., Weng, D., Wu, P., & Chen, G. (2012). Breast cancer associated fibroblasts promote MCF-7 invasion in vitro by secretion of HGF. *Journal of Huazhong University of Science and Technology [Medical Sciences]*, 32(1), 92-96. doi:10.1007/s11596-012-0016-8
- Chew, V., Toh, H. C., & Abastado, J.-P. (2012). Immune Microenvironment in Tumor Progression: Characteristics and Challenges for Therapy. *Journal of Oncology*, 2012, 10. doi:10.1155/2012/608406

- Choi, J., Cha, Y. J., & Koo, J. S. (2018). Adipocyte biology in breast cancer: From silent bystander to active facilitator. *Progress in Lipid Research*, 69, 11-20. doi:<https://doi.org/10.1016/j.plipres.2017.11.002>
- Chuang, T. D., & Khorram, O. (2017). Tranilast Inhibits Genes Functionally Involved in Cell Proliferation, Fibrosis, and Epigenetic Regulation and Epigenetically Induces miR-29c Expression in Leiomyoma Cells. *Reprod Sci*, 24(9), 1253-1263. doi:10.1177/1933719116682878
- Cirri, P., & Chiarugi, P. (2011). Cancer associated fibroblasts: the dark side of the coin. *American Journal of Cancer Research*, 1(4), 482-497.
- Cohen, N., Shani, O., Raz, Y., Sharon, Y., Hoffman, D., Abramovitz, L., & Erez, N. (2017). Fibroblasts drive an immunosuppressive and growth-promoting microenvironment in breast cancer via secretion of Chitinase 3-like 1. *Oncogene*, 36(31), 4457-4468. doi:10.1038/onc.2017.65
- Conklin, M. W., Eickhoff, J. C., Riching, K. M., Pehlke, C. A., Eliceiri, K. W., Provenzano, P. P., . . . Keely, P. J. (2011). Aligned Collagen Is a Prognostic Signature for Survival in Human Breast Carcinoma. *The American Journal of Pathology*, 178(3), 1221-1232. doi:10.1016/j.ajpath.2010.11.076
- Corliss, B. A., Azimi, M. S., Munson, J. M., Peirce, S. M., & Murfee, W. L. (2016). Macrophages: An Inflammatory Link Between Angiogenesis and Lymphangiogenesis. *Microcirculation*, 23(2), 95-121. doi:10.1111/micc.12259
- Costanza, B., Umelo, I. A., Bellier, J., Castronovo, V., & Turtoi, A. (2017). Stromal Modulators of TGF- β in Cancer. *Journal of Clinical Medicine*, 6(1), 7.
- Cox, T. R., Bird, D., Baker, A. M., Barker, H. E., Ho, M. W., Lang, G., & Erler, J. T. (2013). LOX-mediated collagen crosslinking is responsible for fibrosis-enhanced metastasis. *Cancer Res*, 73(6), 1721-1732. doi:10.1158/0008-5472.CAN-12-2233

- Darakhshan, S., Bidmeshkipour, A., Khazaei, M., Rabzia, A., & Ghanbari, A. (2013). Synergistic Effects of Tamoxifen and Tranilast on VEGF and MMP-9 Regulation in Cultured Human Breast Cancer Cells. *Asian Pacific Journal of Cancer Prevention*, 14(11), 6869-6874. doi:10.7314/apjcp.2013.14.11.6869
- Darakhshan, S., & Ghanbari, A. (2013). Tranilast enhances the anti-tumor effects of tamoxifen on human breast cancer cells in vitro. *Journal of Biomedical Science*, 20(1), 76. doi:10.1186/1423-0127-20-76
- Darakhshan, S., & Pour, A. B. (2015). Tranilast: A review of its therapeutic applications. *Pharmacological Research*, 91, 15-28. doi:https://doi.org/10.1016/j.phrs.2014.10.009
- De Francesco, E. M., Lappano, R., Santolla, M. F., Marsico, S., Caruso, A., & Maggiolini, M. (2013). HIF-1 α /GPER signaling mediates the expression of VEGF induced by hypoxia in breast cancer associated fibroblasts (CAFs). *Breast Cancer Research*, 15(4), R64. doi:10.1186/bcr3458
- Dudley, A. C. (2012). Tumor Endothelial Cells. *Cold Spring Harbor Perspectives in Medicine*, 2(3). doi:10.1101/cshperspect.a006536
- Dumont, N., Liu, B., DeFilippis, R. A., Chang, H., Rabban, J. T., Karnezis, A. N., . . . Tlsty, T. D. (2013). Breast Fibroblasts Modulate Early Dissemination, Tumorigenesis, and Metastasis through Alteration of Extracellular Matrix Characteristics. *Neoplasia*, 15(3), 249-IN247. doi:https://doi.org/10.1593/neo.121950
- Dunn, G. P., Old, L. J., & Schreiber, R. D. (2004). The Three Es of Cancer Immunoediting. *Annual Review of Immunology*, 22(1), 329-360. doi:10.1146/annurev.immunol.22.012703.104803
- Dvorak, H. F. (2015). Tumor Stroma, Tumor Blood Vessels, and Antiangiogenesis Therapy. *The Cancer Journal*, 21(4), 237-243. doi:10.1097/ppo.000000000000124

- Ehrbar, M., Sala, A., Lienemann, P., Ranga, A., Mosiewicz, K., Bittermann, A., . . . Lutolf, M. P. (2011). Elucidating the Role of Matrix Stiffness in 3D Cell Migration and Remodeling. *Biophysical Journal*, *100*(2), 284-293. doi:10.1016/j.bpj.2010.11.082
- Emilia Manole, A. E. B., Ionela D. Popescu, Carolina Constantin, Simona Mihai, Gisela F. Gaina, Elena Codrici and Monica T. Neagu. (2018). Immunoassay Techniques Highlighting Biomarkers in Immunogenetic Diseases. In: IntechOpen.
- Erdogan, B., Ao, M., White, L. M., Means, A. L., Brewer, B. M., Yang, L., . . . Webb, D. J. (2017). Cancer-associated fibroblasts promote directional cancer cell migration by aligning fibronectin. *The Journal of Cell Biology*, *216*(11), 3799-3816. doi:10.1083/jcb.201704053
- Fang, M., Yuan, J., Peng, C., & Li, Y. (2014). Collagen as a double-edged sword in tumor progression. *Tumour Biology*, *35*(4), 2871-2882. doi:10.1007/s13277-013-1511-7
- Farahmand, L., Esmaeili, R., Eini, L., & Majidzadeh-A, K. (2018). The effect of mesenchymal stem cell-conditioned medium on proliferation and apoptosis of breast cancer cell line. *Journal of Cancer Research and Therapeutics*, *14*(2), 341-344. doi:10.4103/0973-1482.177213
- Farmer, P., Bonnefoi, H., Anderle, P., Cameron, D., Wirapati, P., Becette, V., . . . Delorenzi, M. (2009). A stroma-related gene signature predicts resistance to neoadjuvant chemotherapy in breast cancer. *Nat Med*, *15*(1), 68-74. doi:10.1038/nm.1908
- Fedotov, S., & Iomin, A. (2007). Migration and Proliferation Dichotomy in Tumor-Cell Invasion. *Physical Review Letters*, *98*(11), 118101.
- Fiori, M. E., Di Franco, S., Villanova, L., Bianca, P., Stassi, G., & De Maria, R. (2019). Cancer-associated fibroblasts as abettors of tumor progression at the crossroads of EMT and therapy resistance. *Molecular Cancer*, *18*(1), 70. doi:10.1186/s12943-019-0994-2

- Gascard, P., & Tlsty, T. D. (2016). Carcinoma-associated fibroblasts: orchestrating the composition of malignancy. *Genes & Development*, *30*(9), 1002-1019. doi:10.1101/gad.279737.116
- Gevorkian, S. G., Allahverdyan, A. E., Gevorgyan, D. S., & Hu, C. K. (2011). Glassy state of native collagen fibril? *EPL (Europhysics Letters)*, *95*(2), 23001.
- Gilkes, D. M., Chaturvedi, P., Bajpai, S., Wong, C. C., Wei, H., Pitcairn, S., . . . Semenza, G. L. (2013). Collagen Prolyl Hydroxylases Are Essential for Breast Cancer Metastasis. *Cancer Research*, *73*(11), 3285-3296. doi:10.1158/0008-5472.Can-12-3963
- Gilkes, D. M., Semenza, G. L., & Wirtz, D. (2014). Hypoxia and the extracellular matrix: drivers of tumour metastasis. *Nature Reviews Cancer*, *14*, 430. doi:10.1038/nrc3726
- Giordano, S. H. (2003). Update on Locally Advanced Breast Cancer. *The Oncologist*, *8*(6), 521-530. doi:10.1634/theoncologist.8-6-521
- Gjorevski, N., Piotrowski, A. S., Varner, V. D., & Nelson, C. M. (2015). Dynamic tensile forces drive collective cell migration through three-dimensional extracellular matrices. *Sci Rep*, *5*, 11458. doi:10.1038/srep11458
- GM., C. (2000a). Cell-Cell Interactions. In *The Cell: A Molecular Approach*. (2nd edition ed.). Sunderland (MA): Sinauer Associates.
- GM., C. (2000b). Signaling Molecules and Their Receptors. In *The Cell: A Molecular Approach*. Sunderland (MA): Sinauer Associates.
- Gok Yavuz, B., Gunaydin, G., Gedik, M. E., Kosemehmetoglu, K., Karakoc, D., Ozgur, F., & Guc, D. (2019). Cancer associated fibroblasts sculpt tumour microenvironment by recruiting monocytes and inducing immunosuppressive PD-1(+) TAMs. *Sci Rep*, *9*(1), 3172. doi:10.1038/s41598-019-39553-z

- Grivennikov, S. I., Greten, F. R., & Karin, M. (2010). Immunity, Inflammation, and Cancer. *Cell*, *140*(6), 883-899. doi:<https://doi.org/10.1016/j.cell.2010.01.025>
- Han, W., Chen, S., Yuan, W., Fan, Q., Tian, J., Wang, X., . . . Liu, L. (2016). Oriented collagen fibers direct tumor cell intravasation. *Proc Natl Acad Sci U S A*, *113*(40), 11208-11213. doi:[10.1073/pnas.1610347113](https://doi.org/10.1073/pnas.1610347113)
- Hanahan, D., & Coussens, Lisa M. (2012). Accessories to the Crime: Functions of Cells Recruited to the Tumor Microenvironment. *Cancer Cell*, *21*(3), 309-322. doi:<https://doi.org/10.1016/j.ccr.2012.02.022>
- Hanahan, D., & Folkman, J. (1996). Patterns and Emerging Mechanisms of the Angiogenic Switch during Tumorigenesis. *Cell*, *86*(3), 353-364. doi:[https://doi.org/10.1016/S0092-8674\(00\)80108-7](https://doi.org/10.1016/S0092-8674(00)80108-7)
- Hanahan, D., & Weinberg, R. A. (2011). Hallmarks of cancer: the next generation. *Cell*, *144*(5), 646-674. doi:[10.1016/j.cell.2011.02.013](https://doi.org/10.1016/j.cell.2011.02.013)
- Hao, N.-B., Lü, M.-H., Fan, Y.-H., Cao, Y.-L., Zhang, Z.-R., & Yang, S.-M. (2012). Macrophages in Tumor Microenvironments and the Progression of Tumors. *Clinical and Developmental Immunology*, *2012*, 11. doi:[10.1155/2012/948098](https://doi.org/10.1155/2012/948098)
- Harigai, R., Sakai, S., Nobusue, H., Hirose, C., Sampetean, O., Minami, N., . . . Arima, Y. (2018). Tranilast inhibits the expression of genes related to epithelial-mesenchymal transition and angiogenesis in neurofibromin-deficient cells. *Sci Rep*, *8*(1), 6069. doi:[10.1038/s41598-018-24484-y](https://doi.org/10.1038/s41598-018-24484-y)
- Harlan, R., & Zhang, H. (2014). Targeted proteomics: a bridge between discovery and validation. *Expert Review of Proteomics*, *11*(6), 657-661. doi:[10.1586/14789450.2014.976558](https://doi.org/10.1586/14789450.2014.976558)
- Hatzikirou, H., Basanta, D., Simon, M., Schaller, K., & Deutsch, A. (2012). 'Go or Grow': the key to the emergence of invasion in tumour progression? *Mathematical*

- Medicine and Biology: A Journal of the IMA*, 29(1), 49-65.
doi:10.1093/imammb/dqq011
- Hecht, I., Natan, S., Zaritsky, A., Levine, H., Tsarfaty, I., & Ben-Jacob, E. (2015). The motility-proliferation-metabolism interplay during metastatic invasion. *Sci Rep*, 5, 13538. doi:10.1038/srep13538
- Hirata, E., Girotti, M. R., Viros, A., Hooper, S., Spencer-Dene, B., Matsuda, M., . . . Sahai, E. (2015). Intravital imaging reveals how BRAF inhibition generates drug-tolerant microenvironments with high integrin beta1/FAK signaling. *Cancer Cell*, 27(4), 574-588. doi:10.1016/j.ccell.2015.03.008
- Howlader N, N. A., Krapcho M, Miller D, Brest A, Yu M, Ruhl J, Tatalovich Z, Mariotto A, Lewis DR, Chen HS, Feuer EJ, Cronin KA (eds). (2019). SEER Cancer Statistics Review, 1975-2016,. Retrieved from https://seer.cancer.gov/csr/1975_2016/
- Hsieh, J. Y., Keating, M. T., Smith, T. D., Meli, V. S., Botvinick, E. L., & Liu, W. F. (2019). Matrix crosslinking enhances macrophage adhesion, migration, and inflammatory activation. *APL Bioengineering*, 3(1), 016103. doi:10.1063/1.5067301
- Huang, M., Li, Y., Zhang, H., & Nan, F. (2010). Breast cancer stromal fibroblasts promote the generation of CD44+CD24- cells through SDF-1/CXCR4 interaction. *Journal of Experimental & Clinical Cancer Research*, 29(1), 80. doi:10.1186/1756-9966-29-80
- Hutter, J. L., & Bechhoefer, J. (1993). Calibration of atomic-force microscope tips. *Review of Scientific Instruments*, 64(7), 1868-1873. doi:10.1063/1.1143970
- Hynds, R. E., Vladimirov, E., & Janes, S. M. (2018). The secret lives of cancer cell lines. *Disease Models & Mechanisms*, 11(11), dmm037366. doi:10.1242/dmm.037366

- Insua-Rodríguez, J., & Oskarsson, T. (2016). The extracellular matrix in breast cancer. *Advanced Drug Delivery Reviews*, 97, 41-55. doi:<https://doi.org/10.1016/j.addr.2015.12.017>
- Izumi, K., Mizokami, A., Li, Y. Q., Narimoto, K., Sugimoto, K., Kadono, Y., . . . Namiki, M. (2009). Tranilast inhibits hormone refractory prostate cancer cell proliferation and suppresses transforming growth factor beta1-associated osteoblastic changes. *Prostate*, 69(11), 1222-1234. doi:10.1002/pros.20975
- Jeong, S. Y., Lee, J. H., Shin, Y., Chung, S., & Kuh, H. J. (2016). Co-Culture of Tumor Spheroids and Fibroblasts in a Collagen Matrix-Incorporated Microfluidic Chip Mimics Reciprocal Activation in Solid Tumor Microenvironment. *PLOS ONE*, 11(7), e0159013. doi:10.1371/journal.pone.0159013
- Jones, D. P., Hanna, W., Cramer, G. M., & Celli, J. P. (2017). *In situ* measurement of ECM rheology and microheterogeneity in embedded and overlaid 3D pancreatic tumor stroma co-cultures via passive particle tracking. *Journal of Innovative Optical Health Sciences*, 10(06), 1742003. doi:10.1142/s1793545817420032
- Kalluri, R. (2016). The biology and function of fibroblasts in cancer. *Nat Rev Cancer*, 16(9), 582-598. doi:10.1038/nrc.2016.73
- Kalluri, R., & Weinberg, R. A. (2009). The basics of epithelial-mesenchymal transition. *J Clin Invest*, 119(6), 1420-1428. doi:10.1172/JCI39104
- Kalluri, R., & Zeisberg, M. (2006). Fibroblasts in cancer. *Nat Rev Cancer*, 6(5), 392-401. doi:10.1038/nrc1877
- Katt, M. E., Placone, A. L., Wong, A. D., Xu, Z. S., & Searson, P. C. (2016). In Vitro Tumor Models: Advantages, Disadvantages, Variables, and Selecting the Right Platform. *Frontiers in Bioengineering and Biotechnology*, 4, 12. doi:10.3389/fbioe.2016.00012

- Katt, M. E., Placone, A. L., Wong, A. D., Xu, Z. S., & Searson, P. C. (2016). In Vitro Tumor Models: Advantages, Disadvantages, Variables, and Selecting the Right Platform. *Front Bioeng Biotechnol*, 4, 12. doi:10.3389/fbioe.2016.00012
- Kenny, P. A., Lee, G. Y., Myers, C. A., Neve, R. M., Semeiks, J. R., Spellman, P. T., . . . Bissell, M. J. (2007). The morphologies of breast cancer cell lines in three-dimensional assays correlate with their profiles of gene expression. *Mol Oncol*, 1(1), 84-96. doi:10.1016/j.molonc.2007.02.004
- Kessenbrock, K., Plaks, V., & Werb, Z. (2010). Matrix Metalloproteinases: Regulators of the Tumor Microenvironment. *Cell*, 141(1), 52-67. doi:10.1016/j.cell.2010.03.015
- Klein, G. (2014). Evolutionary aspects of cancer resistance. *Seminars in Cancer Biology*, 25, 10-14. doi:https://doi.org/10.1016/j.semcancer.2014.01.001
- Kojima, Y., Acar, A., Eaton, E. N., Mellody, K. T., Scheel, C., Ben-Porath, I., . . . Orimo, A. (2010). Autocrine TGF-beta and stromal cell-derived factor-1 (SDF-1) signaling drives the evolution of tumor-promoting mammary stromal myofibroblasts. *Proc Natl Acad Sci U S A*, 107(46), 20009-20014. doi:10.1073/pnas.1013805107
- Kozono, S., Ohuchida, K., Eguchi, D., Ikenaga, N., Fujiwara, K., Cui, L., . . . Tanaka, M. (2013). Pirfenidone Inhibits Pancreatic Cancer Desmoplasia by Regulating Stellate Cells. *Cancer Research*, 73(7), 2345-2356. doi:10.1158/0008-5472.Can-12-3180
- Kraning-Rush, C. M., Carey, S. P., Lampi, M. C., & Reinhart-King, C. A. (2013). Microfabricated collagen tracks facilitate single cell metastatic invasion in 3D. *Integr Biol (Camb)*, 5(3), 606-616. doi:10.1039/c3ib20196a
- Labernadie, A., Kato, T., Brugués, A., Serra-Picamal, X., Derzsi, S., Arwert, E., . . . Trepats, X. (2017). A mechanically active heterotypic E-cadherin/N-cadherin adhesion enables fibroblasts to drive cancer cell invasion. *Nature Cell Biology*, 19, 224. doi:10.1038/ncb3478
- <https://www.nature.com/articles/ncb3478#supplementary-information>

- Lampi, M. C., & Reinhart-King, C. A. (2018). Targeting extracellular matrix stiffness to attenuate disease: From molecular mechanisms to clinical trials. *Science Translational Medicine*, *10*(422), eaao0475. doi:10.1126/scitranslmed.aao0475
- Lang, N. R., Skodzek, K., Hurst, S., Mainka, A., Steinwachs, J., Schneider, J., . . . Fabry, B. (2015). Biphasic response of cell invasion to matrix stiffness in 3-dimensional biopolymer networks. *Acta biomaterialia*, *13*, 61-67. doi:10.1016/j.actbio.2014.11.003
- Lawrence, Robert T., Perez, Elizabeth M., Hernández, D., Miller, Chris P., Haas, Kelsey M., Irie, Hanna Y., . . . Villén, J. (2015). The Proteomic Landscape of Triple-Negative Breast Cancer. *Cell Reports*, *11*(4), 630-644. doi:10.1016/j.celrep.2015.03.050
- Lee, H.-Y., & Hong, I.-S. (2017). Double-edged sword of mesenchymal stem cells: Cancer-promoting versus therapeutic potential. *Cancer Science*, *108*(10), 1939-1946. doi:10.1111/cas.13334
- Leng, S. X., McElhaney, J. E., Walston, J. D., Xie, D., Fedarko, N. S., & Kuchel, G. A. (2008). ELISA and Multiplex Technologies for Cytokine Measurement in Inflammation and Aging Research. *The Journals of Gerontology: Series A*, *63*(8), 879-884. doi:10.1093/gerona/63.8.879
- Lovitt, C. J., Shelper, T. B., & Avery, V. M. (2018). Doxorubicin resistance in breast cancer cells is mediated by extracellular matrix proteins. *BMC Cancer*, *18*(1), 41. doi:10.1186/s12885-017-3953-6
- Lu, P., Weaver, V. M., & Werb, Z. (2012). The extracellular matrix: a dynamic niche in cancer progression. *J Cell Biol*, *196*(4), 395-406. doi:10.1083/jcb.201102147
- Luo, H., Tu, G., Liu, Z., & Liu, M. (2015). Cancer-associated fibroblasts: A multifaceted driver of breast cancer progression. *Cancer Letters*, *361*(2), 155-163. doi:https://doi.org/10.1016/j.canlet.2015.02.018

- Maffey, A., Storini, C., Diceglie, C., Martelli, C., Sironi, L., Calzarossa, C., . . . Bianco, F. (2017). Mesenchymal stem cells from tumor microenvironment favour breast cancer stem cell proliferation, cancerogenic and metastatic potential, via ionotropic purinergic signalling. *Scientific Reports*, *7*(1), 13162. doi:10.1038/s41598-017-13460-7
- Mak, I. W. Y., Evaniew, N., & Ghert, M. (2014). Lost in translation: animal models and clinical trials in cancer treatment. *American Journal of Translational Research*, *6*(2), 114-118.
- Massagué, J. TGF β 2; in Cancer. *Cell*, *134*(2), 215-230. doi:10.1016/j.cell.2008.07.001
- Mediavilla-Varela, M., Boateng, K., Noyes, D., & Antonia, S. J. (2016). The anti-fibrotic agent pirfenidone synergizes with cisplatin in killing tumor cells and cancer-associated fibroblasts. *BMC Cancer*, *16*, 176. doi:10.1186/s12885-016-2162-z
- Menck, K., Behme, D., Pantke, M., Reiling, N., Binder, C., Pukrop, T., & Klemm, F. (2014). Isolation of human monocytes by double gradient centrifugation and their differentiation to macrophages in teflon-coated cell culture bags. *Journal of visualized experiments : JoVE*(91), e51554-e51554. doi:10.3791/51554
- Millioni, R., Tolin, S., Puricelli, L., Sbrignadello, S., Fadini, G. P., Tessari, P., & Arrigoni, G. (2011). High Abundance Proteins Depletion vs Low Abundance Proteins Enrichment: Comparison of Methods to Reduce the Plasma Proteome Complexity. *PLOS ONE*, *6*(5), e19603. doi:10.1371/journal.pone.0019603
- Mittal, D., Gubin, M. M., Schreiber, R. D., & Smyth, M. J. (2014). New insights into cancer immunoediting and its three component phases—elimination, equilibrium and escape. *Current Opinion in Immunology*, *27*, 16-25. doi:https://doi.org/10.1016/j.coi.2014.01.004
- Miyazaki, K., Oyanagi, J., Hoshino, D., Togo, S., Kumagai, H., & Miyagi, Y. (2019). Cancer cell migration on elongate protrusions of fibroblasts in collagen matrix. *Scientific Reports*, *9*(1), 292. doi:10.1038/s41598-018-36646-z

- Moulder, S. (2010). Intrinsic Resistance to Chemotherapy in Breast Cancer. *Women's Health*, 6(6), 821-830. doi:10.2217/whe.10.60
- Mueller, M. M., & Fusenig, N. E. (2004). Friends or foes - bipolar effects of the tumour stroma in cancer. *Nat Rev Cancer*, 4(11), 839-849. doi:10.1038/nrc1477
- Muñoz-Nájjar, U. M., Neurath, K. M., Vumbaca, F., & Claffey, K. P. (2006). Hypoxia stimulates breast carcinoma cell invasion through MT1-MMP and MMP-2 activation. *Oncogene*, 25(16), 2379-2392. doi:10.1038/sj.onc.1209273
- Muz, B., de la Puente, P., Azab, F., & Azab, A. K. (2015). The role of hypoxia in cancer progression, angiogenesis, metastasis, and resistance to therapy. *Hypoxia (Auckl)*, 3, 83-92. doi:10.2147/HP.S93413
- Nagaraju, S., Truong, D., Mouneimne, G., & Nikkhah, M. (2018). Microfluidic Tumor-Vascular Model to Study Breast Cancer Cell Invasion and Intravasation. *Adv Healthc Mater*. doi:10.1002/adhm.201701257
- Nagaraju, S., Truong, D., Mouneimne, G., & Nikkhah, M. (2018). Microfluidic Tumor-Vascular Model to Study Breast Cancer Cell Invasion and Intravasation. *Advanced Healthcare Materials*, 7(9), 1701257. doi:10.1002/adhm.201701257
- Nakagawa, S., Miki, Y., Miyashita, M., Hata, S., Takahashi, Y., Rai, Y., . . . Sasano, H. (2016). Tumor microenvironment in invasive lobular carcinoma: possible therapeutic targets. *Breast Cancer Res Treat*, 155(1), 65-75. doi:10.1007/s10549-015-3668-9
- Nawrocki Raby, B., Polette, M., Gilles, C., Clavel, C., Strumane, K., Matos, M., . . . Birembaut, P. (2001). Quantitative cell dispersion analysis: New test to measure tumor cell aggressiveness. *International Journal of Cancer*, 93(5), 644-652. doi:10.1002/ijc.1380

- Nelson, C. M., Inman, J. L., & Bissell, M. J. (2008). Three-dimensional lithographically defined organotypic tissue arrays for quantitative analysis of morphogenesis and neoplastic progression. *Nat. Protocols*, 3(4), 674-678.
- Netti, P. A., Berk, D. A., Swartz, M. A., Grodzinsky, A. J., & Jain, R. K. (2000). Role of Extracellular Matrix Assembly in Interstitial Transport in Solid Tumors. *Cancer Research*, 60(9), 2497-2503.
- Ng, M. R., Besser, A., Danuser, G., & Brugge, J. S. (2012). Substrate stiffness regulates cadherin-dependent collective migration through myosin-II contractility. *J Cell Biol*, 199(3), 545-563. doi:10.1083/jcb.201207148
- Nickel, A., Blücher, C., Kadri, O. A., Schwagarus, N., Müller, S., Schaab, M., . . . Stadler, S. C. (2018). Adipocytes induce distinct gene expression profiles in mammary tumor cells and enhance inflammatory signaling in invasive breast cancer cells. *Scientific Reports*, 8(1), 9482. doi:10.1038/s41598-018-27210-w
- Nikkhah, M., Strobl, J. S., & Agah, M. (2008). Attachment and response of human fibroblast and breast cancer cells to three dimensional silicon microstructures of different geometries. *Biomedical Microdevices*, 11(2), 429. doi:10.1007/s10544-008-9249-5
- Nikkhah, M., Strobl, J. S., Schmelz, E. M., Roberts, P. C., Zhou, H., & Agah, M. (2011). MCF10A and MDA-MB-231 human breast basal epithelial cell co-culture in silicon micro-arrays. *Biomaterials*, 32(30), 7625-7632. doi:https://doi.org/10.1016/j.biomaterials.2011.06.041
- Nishida, N., Yano, H., Nishida, T., Kamura, T., & Kojiro, M. (2006). Angiogenesis in cancer. *Vascular health and risk management*, 2(3), 213-219.
- Noy, R., & Pollard, J. W. (2014). Tumor-associated macrophages: from mechanisms to therapy. *Immunity*, 41(1), 49-61. doi:10.1016/j.immuni.2014.06.010

- Ohshio, Y., Hanaoka, J., Kontani, K., & Teramoto, K. (2014). Tranilast Inhibits the Function of Cancer-Associated Fibroblasts Responsible for the Induction of Immune Suppressor Cell Types. *Scandinavian Journal of Immunology*, *80*(6), 408-416. doi:10.1111/sji.12242
- Okamoto, T., Takagi, Y., Kawamoto, E., Park, E. J., Usuda, H., Wada, K., & Shimaoka, M. (2018). Reduced substrate stiffness promotes M2-like macrophage activation and enhances peroxisome proliferator-activated receptor γ expression. *Experimental Cell Research*, *367*(2), 264-273. doi:https://doi.org/10.1016/j.yexcr.2018.04.005
- Okazaki, M., Fushida, S., Harada, S., Tsukada, T., Kinoshita, J., Oyama, K., . . . Ohta, T. (2014). The angiotensin II type 1 receptor blocker candesartan suppresses proliferation and fibrosis in gastric cancer. *Cancer Lett*, *355*(1), 46-53. doi:10.1016/j.canlet.2014.09.019
- Olson, E. M., Lin, N. U., Krop, I. E., & Winer, E. P. (2011). The ethical use of mandatory research biopsies. *Nature Reviews Clinical Oncology*, *8*, 620. doi:10.1038/nrclinonc.2011.114
- Onoue, S., Kojo, Y., Aoki, Y., Kawabata, Y., Yamauchi, Y., & Yamada, S. (2012). Physicochemical and Pharmacokinetic Characterization of Amorphous Solid Dispersion of Tranilast with Enhanced Solubility in Gastric Fluid and Improved Oral Bioavailability. *Drug Metabolism and Pharmacokinetics*, *27*(4), 379-387. doi:10.2133/dmpk.DMPK-11-RG-101
- Orimo, A., Gupta, P. B., Sgroi, D. C., Arenzana-Seisdedos, F., Delaunay, T., Naeem, R., . . . Weinberg, R. A. (2005). Stromal fibroblasts present in invasive human breast carcinomas promote tumor growth and angiogenesis through elevated SDF-1/CXCL12 secretion. *Cell*, *121*(3), 335-348. doi:10.1016/j.cell.2005.02.034
- Oskarsson, T. (2013). Extracellular matrix components in breast cancer progression and metastasis. *Breast*, *22 Suppl 2*, S66-72. doi:10.1016/j.breast.2013.07.012

- Papageorgis, P., Polydorou, C., Mpekris, F., Voutouri, C., Agathokleous, E., Kapnissi-Christodoulou, C. P., & Stylianopoulos, T. (2017). Tranilast-induced stress alleviation in solid tumors improves the efficacy of chemo- and nanotherapeutics in a size-independent manner. *Sci Rep*, *7*, 46140. doi:10.1038/srep46140
- Patel, S. A., Meyer, J. R., Greco, S. J., Corcoran, K. E., Bryan, M., & Rameshwar, P. (2010). Mesenchymal stem cells protect breast cancer cells through regulatory T cells: role of mesenchymal stem cell-derived TGF-beta. *J Immunol*, *184*(10), 5885-5894. doi:10.4049/jimmunol.0903143
- Peela, N., Barrientos, E. S., Truong, D., Mouneimne, G., & Nikkhah, M. (2017). Effect of suberoylanilide hydroxamic acid (SAHA) on breast cancer cells within a tumor-stroma microfluidic model. *Integrative Biology*, *9*(12), 988-999. doi:10.1039/C7IB00180K
- Peela, N., Sam, F. S., Christenson, W., Truong, D., Watson, A. W., Mouneimne, G., . . . Nikkhah, M. (2016). A three dimensional micropatterned tumor model for breast cancer cell migration studies. *Biomaterials*, *81*, 72-83. doi:10.1016/j.biomaterials.2015.11.039
- Peela, N., Truong, D., Saini, H., Chu, H., Mashaghi, S., Ham, S. L., . . . Nikkhah, M. (2017). Advanced biomaterials and microengineering technologies to recapitulate the stepwise process of cancer metastasis. *Biomaterials*, *133*, 176-207. doi:https://doi.org/10.1016/j.biomaterials.2017.04.017
- Pickup, M. W., Mouw, J. K., & Weaver, V. M. (2014). The extracellular matrix modulates the hallmarks of cancer. *EMBO Reports*, *15*(12), 1243-1253. doi:10.15252/embr.201439246
- Pilco-Ferreto, N., & Calaf, G. M. (2016). Influence of doxorubicin on apoptosis and oxidative stress in breast cancer cell lines. *Int J Oncol*, *49*(2), 753-762. doi:10.3892/ijo.2016.3558

- Place, A. E., Jin Huh, S., & Polyak, K. (2011). The microenvironment in breast cancer progression: biology and implications for treatment. *Breast Cancer Research*, 13(6), 227. doi:10.1186/bcr2912
- Plodinec, M., Loparic, M., Monnier, C. A., Obermann, E. C., Zanetti-Dallenbach, R., Oertle, P., . . . Schoenenberger, C. A. (2012). The nanomechanical signature of breast cancer. *Nat Nanotechnol*, 7(11), 757-765. doi:10.1038/nnano.2012.167
- Previtera, M. L., & Sengupta, A. (2016). Substrate Stiffness Regulates Proinflammatory Mediator Production through TLR4 Activity in Macrophages. *PLOS ONE*, 10(12), e0145813. doi:10.1371/journal.pone.0145813
- Rahman, N. A., Yazan, L. S., Wibowo, A., Ahmat, N., Foo, J. B., Tor, Y. S., . . . Fakurazi, S. (2016). Induction of apoptosis and G2/M arrest by ampelopsin E from *Dryobalanops* towards triple negative breast cancer cells, MDA-MB-231. *BMC Complement Altern Med*, 16, 354. doi:10.1186/s12906-016-1328-1
- Redig, A. J., & McAllister, S. S. (2013a). Breast cancer as a systemic disease: a view of metastasis. *Journal of internal medicine*, 274(2), 113-126. doi:10.1111/joim.12084
- Redig, A. J., & McAllister, S. S. (2013b). Breast cancer as a systemic disease: a view of metastasis. *J Intern Med*, 274(2), 113-126. doi:10.1111/joim.12084
- Rother, J., Nöding, H., Mey, I., & Janshoff, A. (2014). Atomic force microscopy-based microrheology reveals significant differences in the viscoelastic response between malign and benign cell lines. *Open Biology*, 4(5), 140046. doi:10.1098/rsob.140046
- Rozenchan, P. B., Carraro, D. M., Brentani, H., de Carvalho Mota, L. D., Bastos, E. P., e Ferreira, E. N., . . . Brentani, M. M. (2009). Reciprocal changes in gene expression profiles of cocultured breast epithelial cells and primary fibroblasts. *Int J Cancer*, 125(12), 2767-2777. doi:10.1002/ijc.24646

- Rudnick, J. A., Arendt, L. M., Klebba, I., Hinds, J. W., Iyer, V., Gupta, P. B., . . . Kuperwasser, C. (2011). Functional Heterogeneity of Breast Fibroblasts Is Defined by a Prostaglandin Secretory Phenotype that Promotes Expansion of Cancer-Stem Like Cells. *PLOS ONE*, *6*(9), e24605. doi:10.1371/journal.pone.0024605
- Saini, H., Rahmani Eliato, K., Silva, C., Allam, M., Mouneimne, G., Ros, R., & Nikkhah, M. (2018). The Role of Desmoplasia and Stromal Fibroblasts on Anti-cancer Drug Resistance in a Microengineered Tumor Model. *Cellular and Molecular Bioengineering*, *11*(5), 419-433. doi:10.1007/s12195-018-0544-9
- Saito, H., Fushida, S., Harada, S., Miyashita, T., Oyama, K., Yamaguchi, T., . . . Ohta, T. (2018). Importance of human peritoneal mesothelial cells in the progression, fibrosis, and control of gastric cancer: inhibition of growth and fibrosis by tranilast. *Gastric Cancer*, *21*(1), 55-67. doi:10.1007/s10120-017-0726-5
- Sakai, S., Iwata, C., Tanaka, H. Y., Cabral, H., Morishita, Y., Miyazono, K., & Kano, M. R. (2016). Increased fibrosis and impaired intratumoral accumulation of macromolecules in a murine model of pancreatic cancer co-administered with FGF-2. *J Control Release*, *230*, 109-115. doi:10.1016/j.jconrel.2016.04.007
- Samani, A., Zubovits, J., & Plewes, D. (2007). Elastic moduli of normal and pathological human breast tissues: an inversion-technique-based investigation of 169 samples. *Physics in Medicine and Biology*, *52*(6), 1565-1576. doi:10.1088/0031-9155/52/6/002
- Santi, A., Kugeratski, F. G., & Zanivan, S. (2018). Cancer Associated Fibroblasts: The Architects of Stroma Remodeling. *Proteomics*, *18*(5-6), e1700167. doi:10.1002/pmic.201700167
- Sato, S., Takahashi, S., Asamoto, M., Naiki, T., Naiki-Ito, A., Asai, K., & Shirai, T. (2010). Tranilast suppresses prostate cancer growth and osteoclast differentiation in vivo and in vitro. *Prostate*, *70*(3), 229-238. doi:10.1002/pros.21056

- Schedin, P., & Keely, P. J. (2011). Mammary gland ECM remodeling, stiffness, and mechanosignaling in normal development and tumor progression. *Cold Spring Harb Perspect Biol*, 3(1), a003228. doi:10.1101/cshperspect.a003228
- Schrader, J., Gordon-Walker, T. T., Aucott, R. L., van Deemter, M., Quaas, A., Walsh, S., . . . Iredale, J. P. (2011). Matrix stiffness modulates proliferation, chemotherapeutic response, and dormancy in hepatocellular carcinoma cells. *Hepatology*, 53(4), 1192-1205. doi:10.1002/hep.24108
- Segovia-Mendoza, M., & Morales-Montor, J. (2019). Immune Tumor Microenvironment in Breast Cancer and the Participation of Estrogens and Its Receptors Into Cancer Physiopathology. *Frontiers in Immunology*, 10(348). doi:10.3389/fimmu.2019.00348
- Seniutkin, O., Furuya, S., Luo, Y. S., Cichocki, J. A., Fukushima, H., Kato, Y., . . . Rusyn, I. (2018). Effects of pirfenidone in acute and sub-chronic liver fibrosis, and an initiation-promotion cancer model in the mouse. *Toxicol Appl Pharmacol*, 339, 1-9. doi:10.1016/j.taap.2017.11.024
- Senthebane, D. A., Rowe, A., Thomford, N. E., Shipanga, H., Munro, D., Mazeedi, M., . . . Dzobo, K. (2017). The Role of Tumor Microenvironment in Chemoresistance: To Survive, Keep Your Enemies Closer. *Int J Mol Sci*, 18(7). doi:10.3390/ijms18071586
- Sever, R., & Brugge, J. S. (2015). Signal Transduction in Cancer. *Cold Spring Harbor Perspectives in Medicine*, 5(4). doi:10.1101/cshperspect.a006098
- Sewell-Loftin, M. K., Bayer, S. V. H., Crist, E., Hughes, T., Joison, S. M., Longmore, G. D., & George, S. C. (2017). Cancer-associated fibroblasts support vascular growth through mechanical force. *Scientific Reports*, 7(1), 12574. doi:10.1038/s41598-017-13006-x
- Shao, Z.-M., Nguyen, M., & Barsky, S. H. (2000). Human breast carcinoma desmoplasia is PDGF initiated. *Oncogene*, 19(38), 4337-4345. doi:10.1038/sj.onc.1203785

- Shen, K., Luk, S., Hicks, D. F., Elman, J. S., Bohr, S., Iwamoto, Y., . . . Parekkadan, B. (2014). Resolving cancer-stroma interfacial signalling and interventions with micropatterned tumour-stromal assays. *Nat Commun*, *5*, 5662. doi:10.1038/ncomms6662
- Shevchenko, A., Tomas, H., Havli, J., Olsen, J. V., & Mann, M. (2006). In-gel digestion for mass spectrometric characterization of proteins and proteomes. *Nature Protocols*, *1*(6), 2856-2860. doi:10.1038/nprot.2006.468
- Shimoda, M., Mellody, K. T., & Orimo, A. (2010). Carcinoma-associated fibroblasts are a rate-limiting determinant for tumour progression. *Seminars in Cell & Developmental Biology*, *21*(1), 19-25. doi:https://doi.org/10.1016/j.semcdb.2009.10.002
- Sica, A., Schioppa, T., Mantovani, A., & Allavena, P. (2006). Tumour-associated macrophages are a distinct M2 polarised population promoting tumour progression: potential targets of anti-cancer therapy. *Eur J Cancer*, *42*(6), 717-727. doi:10.1016/j.ejca.2006.01.003
- Siegel, R. L., Miller, K. D., & Jemal, A. (2017). Cancer Statistics, 2017. *CA Cancer J Clin*, *67*(1), 7-30. doi:10.3322/caac.21387
- Smith, L., Watson, M. B., O'Kane, S. L., Drew, P. J., Lind, M. J., & Cawkwell, L. (2006). The analysis of doxorubicin resistance in human breast cancer cells using antibody microarrays. *Mol Cancer Ther*, *5*(8), 2115-2120. doi:10.1158/1535-7163.MCT-06-0190
- Smith, M. P. W., Wood, S. L., Zougman, A., Ho, J. T. C., Peng, J., Jackson, D., . . . Banks, R. E. (2011). A systematic analysis of the effects of increasing degrees of serum immunodepletion in terms of depth of coverage and other key aspects in top-down and bottom-up proteomic analyses. *Proteomics*, *11*(11), 2222-2235. doi:10.1002/pmic.201100005
- Sollich, P. (1998). Rheological constitutive equation for a model of soft glassy materials. *Physical Review E*, *58*(1), 738-759.

- Solon, J., Levental, I., Sengupta, K., Georges, P. C., & Janmey, P. A. (2007). Fibroblast adaptation and stiffness matching to soft elastic substrates. *Biophys J*, *93*(12), 4453-4461. doi:10.1529/biophysj.106.101386
- Soon, P. S., Kim, E., Pon, C. K., Gill, A. J., Moore, K., Spillane, A. J., . . . Baxter, R. C. (2013). Breast cancer-associated fibroblasts induce epithelial-to-mesenchymal transition in breast cancer cells. *Endocr Relat Cancer*, *20*(1), 1-12. doi:10.1530/ERC-12-0227
- Speicher, K. D., Kolbas, O., Harper, S., & Speicher, D. W. (2000). Systematic analysis of peptide recoveries from in-gel digestions for protein identifications in proteome studies. *J Biomol Tech*, *11*(2), 74-86.
- Srinivas, P. R., Verma, M., Zhao, Y., & Srivastava, S. (2002). Proteomics for Cancer Biomarker Discovery. *Clinical Chemistry*, *48*(8), 1160-1169.
- Stanisavljevic, J., Loubat-Casanovas, J., Herrera, M., Luque, T., Pena, R., Lluch, A., . . . Baulida, J. (2015). Snail1-expressing fibroblasts in the tumor microenvironment display mechanical properties that support metastasis. *Cancer Res*, *75*(2), 284-295. doi:10.1158/0008-5472.CAN-14-1903
- Staunton, J. R., Doss, B. L., Lindsay, S., & Ros, R. (2016). Correlating confocal microscopy and atomic force indentation reveals metastatic cancer cells stiffen during invasion into collagen I matrices. *Sci Rep*, *6*, 19686. doi:10.1038/srep19686
- Strobl, J. S., Nikkhah, M., & Agah, M. (2010). Actions of the anti-cancer drug suberoylanilide hydroxamic acid (SAHA) on human breast cancer cytoarchitecture in silicon microstructures. *Biomaterials*, *31*(27), 7043-7050. doi:https://doi.org/10.1016/j.biomaterials.2010.05.023
- Stroncek JD, R. W. (2008). Overview of Wound Healing in Different Tissue Types. In R. WM (Ed.), *Indwelling Neural Implants: Strategies for Contending with the In Vivo Environment*. Boca Raton (FL): CRC Press/Taylor & Francis; 2008.

- Subramaniam, V., Ace, O., Prud'homme, G. J., & Jothy, S. (2011). Tranilast treatment decreases cell growth, migration and inhibits colony formation of human breast cancer cells. *Exp Mol Pathol*, *90*(1), 116-122. doi:10.1016/j.yexmp.2010.10.012
- Subramaniam, V., Chakrabarti, R., Prud'homme, G. J., & Jothy, S. (2010). Tranilast inhibits cell proliferation and migration and promotes apoptosis in murine breast cancer. *Anticancer Drugs*, *21*(4), 351-361. doi:10.1097/CAD.0b013e328334992c
- Suklabaidya, S., Das, B., Ali, S. A., Jain, S., Swaminathan, S., Mohanty, A. K., . . . Senapati, S. (2016). Characterization and use of HapT1-derived homologous tumors as a preclinical model to evaluate therapeutic efficacy of drugs against pancreatic tumor desmoplasia. *Oncotarget*, *7*(27), 41825-41842. doi:10.18632/oncotarget.9729
- Sundaram, G. M., Quah, S., & Sampath, P. (2018). Cancer: the dark side of wound healing. *FEBS J*, *285*(24), 4516-4534. doi:10.1111/febs.14586
- Sung, K. E., Su, X., Berthier, E., Pehlke, C., Friedl, A., & Beebe, D. J. (2013). Understanding the Impact of 2D and 3D Fibroblast Cultures on In Vitro Breast Cancer Models. *PLOS ONE*, *8*(10), e76373. doi:10.1371/journal.pone.0076373
- SUROWIAK, P., MURAWA, D., MATERNA, V., MACIEJCZYK, A., PUDELKO, M., CIESLA, S., . . . LAGE, H. (2007). Occurrence of Stromal Myofibroblasts in the Invasive Ductal Breast Cancer Tissue is an Unfavourable Prognostic Factor. *Anticancer Research*, *27*(4C), 2917-2924.
- Suzawa, H., Kikuchi, S., Arai, N., & Koda, A. (1992). The Mechanism Involved in the Inhibitory Action of Tranilast on Collagen Biosynthesis of Keloid Fibroblasts. *The Japanese Journal of Pharmacology*, *60*(2), 91-96. doi:10.1254/jjp.60.91
- Takai, K., Drain, A. P., Lawson, D. A., Littlepage, L. E., Karpuj, M., Kessenbrock, K., . . . Werb, Z. (2018). Discoidin domain receptor 1 (DDR1) ablation promotes tissue fibrosis and hypoxia to induce aggressive basal-like breast cancers. *Genes Dev*, *32*(3-4), 244-257. doi:10.1101/gad.301366.117

- Takai, K., Le, A., Weaver, V. M., & Werb, Z. (2016). Targeting the cancer-associated fibroblasts as a treatment in triple-negative breast cancer. *Oncotarget*, 7(50), 82889-82901. doi:10.18632/oncotarget.12658
- Tassone, P., Tagliaferri, P., Perricelli, A., Blotta, S., Quaresima, B., Martelli, M. L., . . . Venuta, S. (2003). BRCA1 expression modulates chemosensitivity of BRCA1-defective HCC1937 human breast cancer cells. *Br J Cancer*, 88(8), 1285-1291. doi:10.1038/sj.bjc.6600859
- Têtu, B., Brisson, J., Wang, C. S., Lapointe, H., Beaudry, G., Blanchette, C., & Trudel, D. (2006). The influence of MMP-14, TIMP-2 and MMP-2 expression on breast cancer prognosis. *Breast Cancer Research*, 8(3), R28-R28. doi:10.1186/bcr1503
- Tredan, O., Galmarini, C. M., Patel, K., & Tannock, I. F. (2007). Drug resistance and the solid tumor microenvironment. *J Natl Cancer Inst*, 99(19), 1441-1454. doi:10.1093/jnci/djm135
- Tripathi, M., Billet, S., & Bhowmick, N. A. (2012). Understanding the role of stromal fibroblasts in cancer progression. *Cell Adhesion & Migration*, 6(3), 231-235. doi:10.4161/cam.20419
- Truong, D., Fiorelli, R., Barrientos, E. S., Melendez, E. L., Sanai, N., Mehta, S., & Nikkhah, M. (2019). A three-dimensional (3D) organotypic microfluidic model for glioma stem cells – Vascular interactions. *Biomaterials*, 198, 63-77. doi:https://doi.org/10.1016/j.biomaterials.2018.07.048
- Truong, D., Puleo, J., Llave, A., Mouneimne, G., Kamm, R. D., & Nikkhah, M. (2016). Breast Cancer Cell Invasion into a Three Dimensional Tumor-Stroma Microenvironment. *Sci Rep*, 6, 34094. doi:10.1038/srep34094
- Truong, D. D., Kratz, A., Park, J. G., Barrientos, E. S., Saini, H., Nguyen, T., . . . Nikkhah, M. (2019). A human organotypic microfluidic tumor model permits investigation of the interplay between patient-derived fibroblasts and breast cancer cells. *Cancer Res*. doi:10.1158/0008-5472.CAN-18-2293

- Tsuyada, A., Chow, A., Wu, J., Somlo, G., Chu, P., Loera, S., . . . Wang, S. E. (2012). CCL2 Mediates Cross-talk between Cancer Cells and Stromal Fibroblasts That Regulates Breast Cancer Stem Cells. *Cancer Research*, *72*(11), 2768-2779. doi:10.1158/0008-5472.Can-11-3567
- Tyan, S.-W., Kuo, W.-H., Huang, C.-K., Pan, C.-C., Shew, J.-Y., Chang, K.-J., . . . Lee, W.-H. (2011). Breast Cancer Cells Induce Cancer-Associated Fibroblasts to Secrete Hepatocyte Growth Factor to Enhance Breast Tumorigenesis. *PLOS ONE*, *6*(1), e15313. doi:10.1371/journal.pone.0015313
- Wang, W., Li, Q., Yamada, T., Matsumoto, K., Matsumoto, I., Oda, M., . . . Yano, S. (2009). Crosstalk to stromal fibroblasts induces resistance of lung cancer to epidermal growth factor receptor tyrosine kinase inhibitors. *Clin Cancer Res*, *15*(21), 6630-6638. doi:10.1158/1078-0432.CCR-09-1001
- Wang, Y. Y., Attané, C., Milhas, D., Dirat, B., Dauvillier, S., Guerard, A., . . . Muller, C. (2017). Mammary adipocytes stimulate breast cancer invasion through metabolic remodeling of tumor cells. *JCI Insight*, *2*(4). doi:10.1172/jci.insight.87489
- Watnick, R. S. (2012). The Role of the Tumor Microenvironment in Regulating Angiogenesis. *Cold Spring Harbor Perspectives in Medicine*, *2*(12). doi:10.1101/cshperspect.a006676
- Weigel, K. J., Jakimenko, A., Conti, B. A., Chapman, S. E., Kaliney, W. J., Leevy, W. M., . . . Schafer, Z. T. (2014). CAF-secreted IGFs regulate breast cancer cell anoikis. *Mol Cancer Res*, *12*(6), 855-866. doi:10.1158/1541-7786.MCR-14-0090
- Williams, C. B., Yeh, E. S., & Soloff, A. C. (2016). Tumor-associated macrophages: unwitting accomplices in breast cancer malignancy. *NPJ Breast Cancer*, *2*. doi:10.1038/npjbcancer.2015.25
- Witsch, E., Sela, M., & Yarden, Y. (2010). Roles for Growth Factors in Cancer Progression. *Physiology*, *25*(2), 85-101. doi:10.1152/physiol.00045.2009

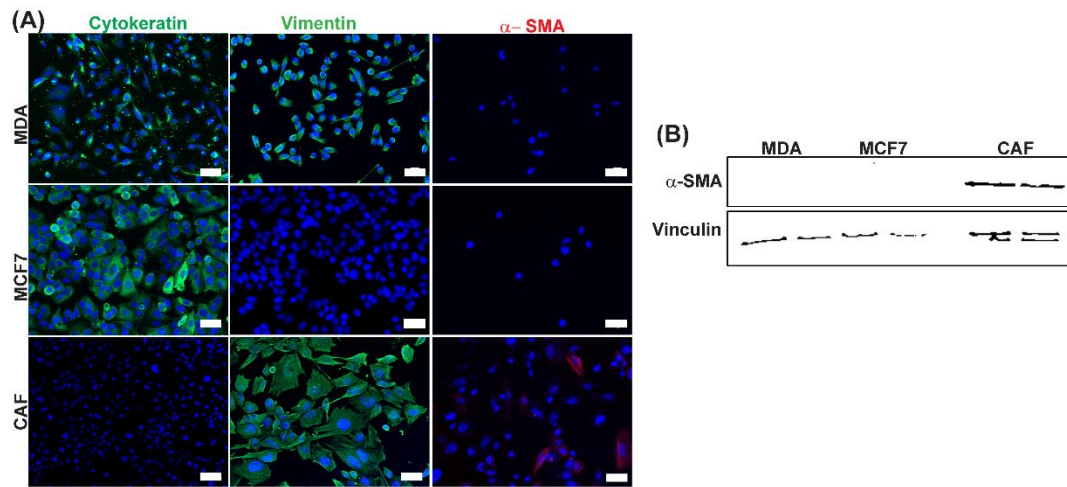
- Wong, C. C.-L., Gilkes, D. M., Zhang, H., Chen, J., Wei, H., Chaturvedi, P., . . . Semenza, G. L. (2011). Hypoxia-inducible factor 1 is a master regulator of breast cancer metastatic niche formation. *Proceedings of the National Academy of Sciences*, *108*(39), 16369-16374. doi:10.1073/pnas.1113483108
- Wu, A., Louterback, K., Lambert, G., Estevez-Salmeron, L., Tlsty, T. D., Austin, R. H., & Sturm, J. C. (2013). Cell motility and drug gradients in the emergence of resistance to chemotherapy. *Proc Natl Acad Sci U S A*, *110*(40), 16103-16108. doi:10.1073/pnas.1314385110
- Xiong, G.-F., & Xu, R. (2016). Function of cancer cell-derived extracellular matrix in tumor progression. *Journal of Cancer Metastasis and Treatment*, *2*(9), 357. doi:10.20517/2394-4722.2016.08
- Yang, H., Sun, L., Liu, M., & Mao, Y. (2018). Patient-derived organoids: a promising model for personalized cancer treatment. *Gastroenterology report*, *6*(4), 243-245. doi:10.1093/gastro/goy040
- Yang, X., Li, Y., Zou, L., & Zhu, Z. (2019). Role of Exosomes in Crosstalk Between Cancer-Associated Fibroblasts and Cancer Cells. *Frontiers in Oncology*, *9*(356). doi:10.3389/fonc.2019.00356
- Yanovich, G., Agmon, H., Harel, M., Sonnenblick, A., Peretz, T., & Geiger, T. (2018). Clinical Proteomics of Breast Cancer Reveals a Novel Layer of Breast Cancer Classification. *Cancer Research*, *78*(20), 6001-6010. doi:10.1158/0008-5472.Can-18-1079
- Ying, H.-Z., Chen, Q., Zhang, W.-Y., Zhang, H.-H., Ma, Y., Zhang, S.-Z., . . . Yu, C.-H. (2017). PDGF signaling pathway in hepatic fibrosis pathogenesis and therapeutics (Review). *Molecular medicine reports*, *16*(6), 7879-7889. doi:10.3892/mmr.2017.7641
- Yu, Y., Xiao, C. H., Tan, L. D., Wang, Q. S., Li, X. Q., & Feng, Y. M. (2014). Cancer-associated fibroblasts induce epithelial-mesenchymal transition of breast cancer

cells through paracrine TGF-beta signalling. *Br J Cancer*, 110(3), 724-732.
doi:10.1038/bjc.2013.768

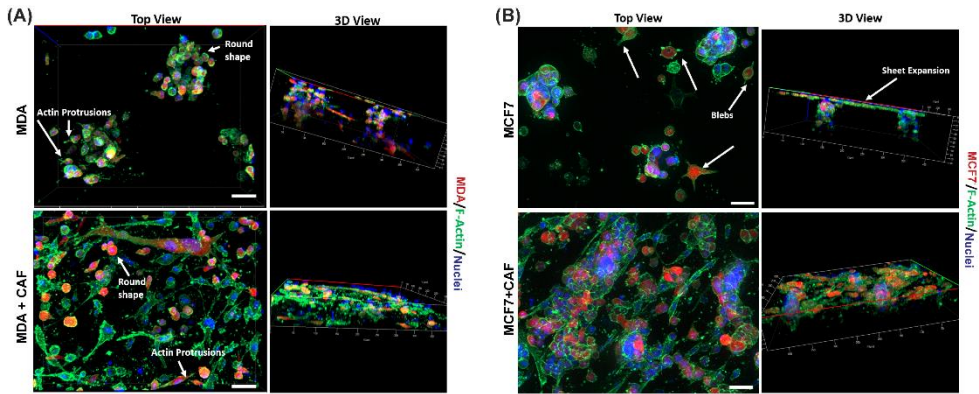
Zaman, M. H., Trapani, L. M., Sieminski, A. L., MacKellar, D., Gong, H., Kamm, R. D., . . . Matsudaira, P. (2006). Migration of tumor cells in 3D matrices is governed by matrix stiffness along with cell-matrix adhesion and proteolysis. *Proceedings of the National Academy of Sciences*, 103(29), 10889-10894.
doi:10.1073/pnas.0604460103

Zhang, B., Jiang, T., Shen, S., She, X., Tuo, Y., Hu, Y., . . . Jiang, X. (2016). Cyclopamine disrupts tumor extracellular matrix and improves the distribution and efficacy of nanotherapeutics in pancreatic cancer. *Biomaterials*, 103, 12-21.
doi:10.1016/j.biomaterials.2016.06.048

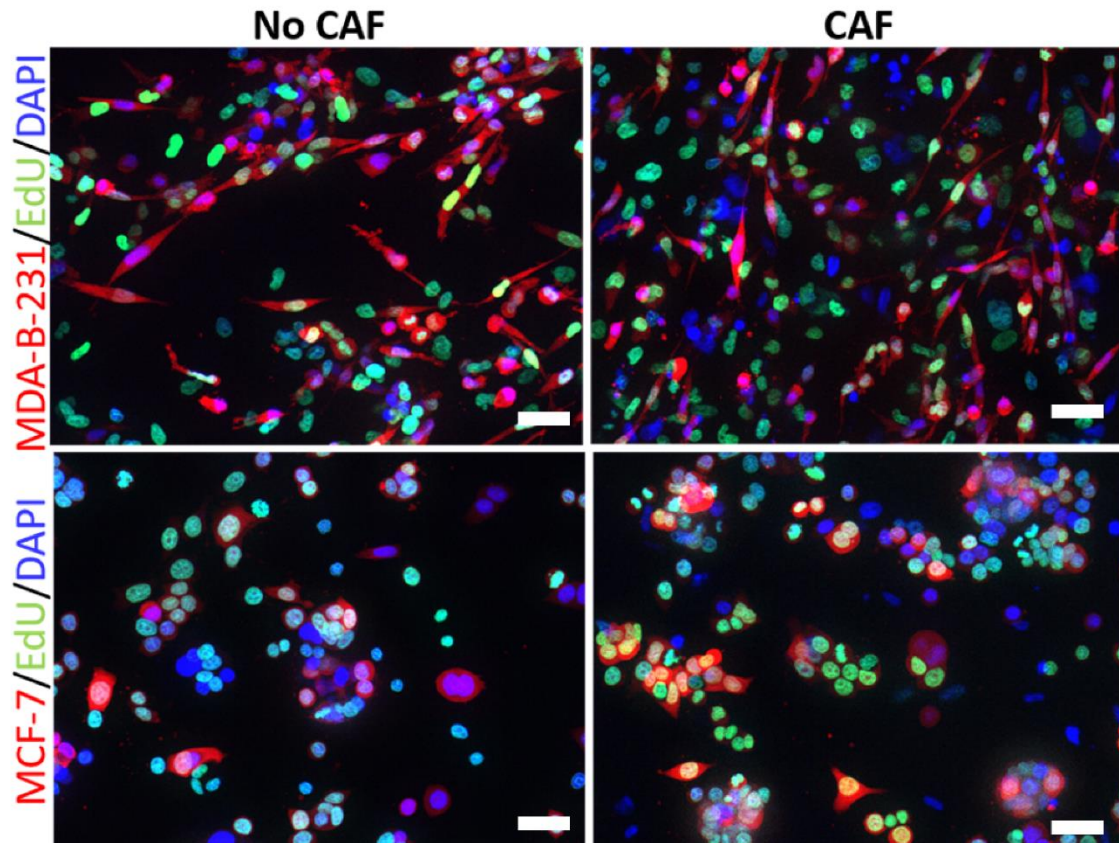
APPENDIX A
SUPPLEMENTARY FIGURES FOR CHAPTER 2



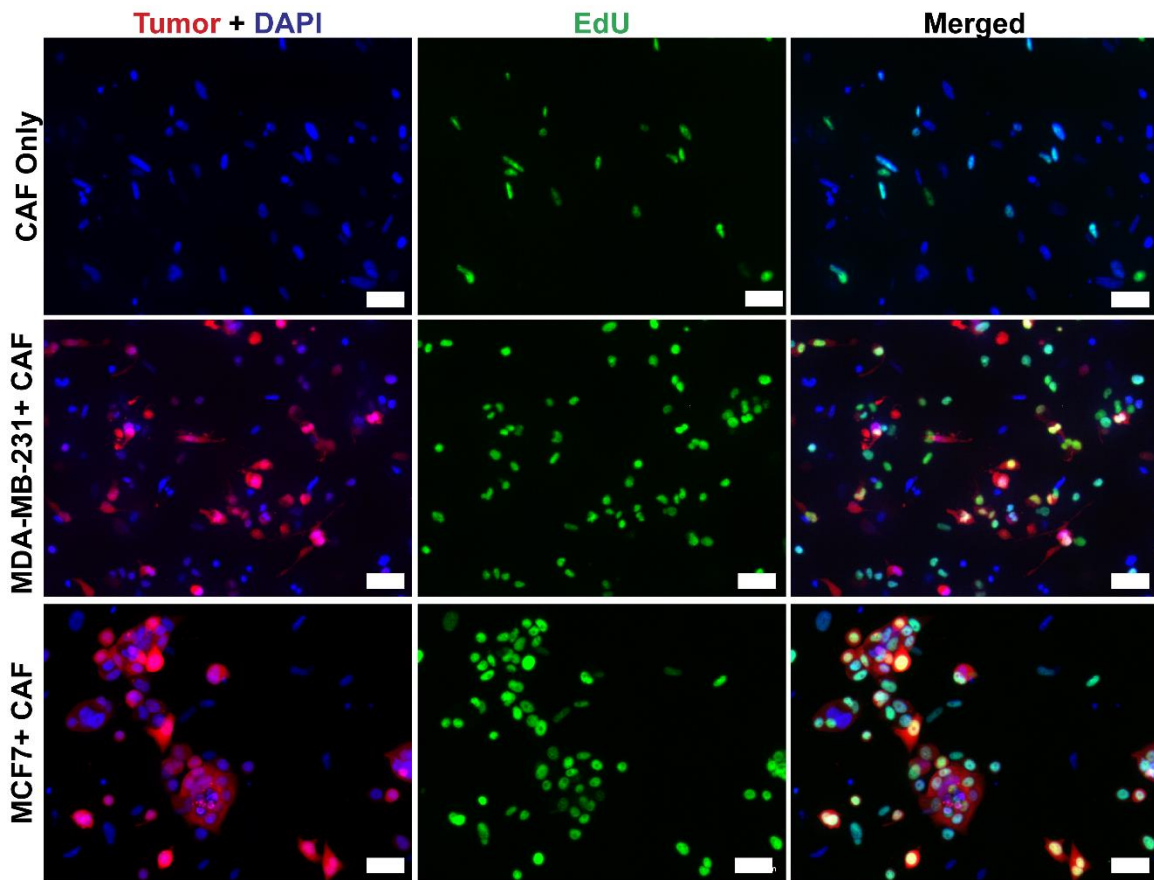
Supplementary Figure 1: Characterization of breast tumor and stromal cells. (A) Representative 2D immunostained images of MDA-MB-231, MCF7 and CAFs for pan cytokeratin, vimentin and α -SMA. (B) Representative western blot for α -SMA expression across all the cells. All scale bar represents 20 μ m.



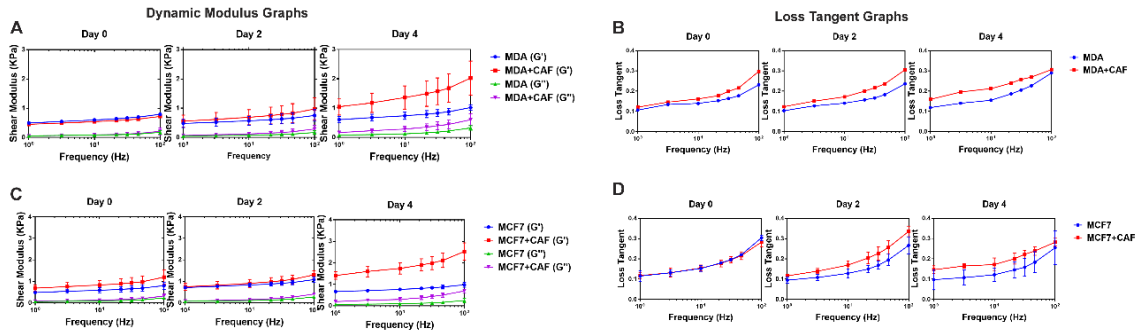
Supplementary Figure 2: Actin images within 3D tumor model. (A) Representative top and 3D view of actin images across monoculture and coculture condition of MDA group. (B) Actin images of MCF7 cells in monoculture and coculture group.



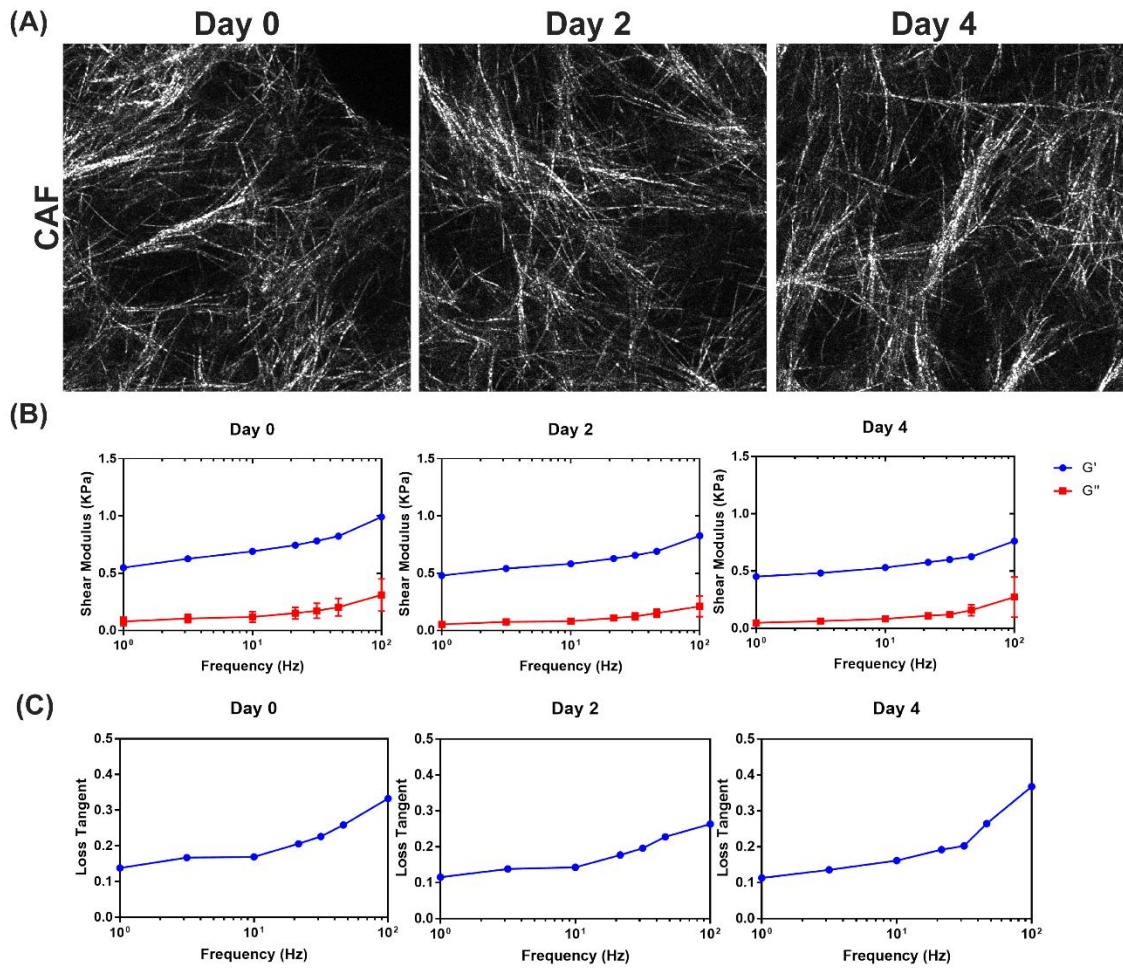
Supplementary Figure 3: Representative fluorescent images showing cancer cell (MDA-MB-231, MCF7) proliferation across all monoculture and coculture conditions. All scale bars represent 20 μm .



Supplementary Figure 4: Representative fluorescent images showing CAF proliferation across all monoculture and coculture condition with MDA-MB-231 and MCF7 cells. All scale bars represent 20 μm .

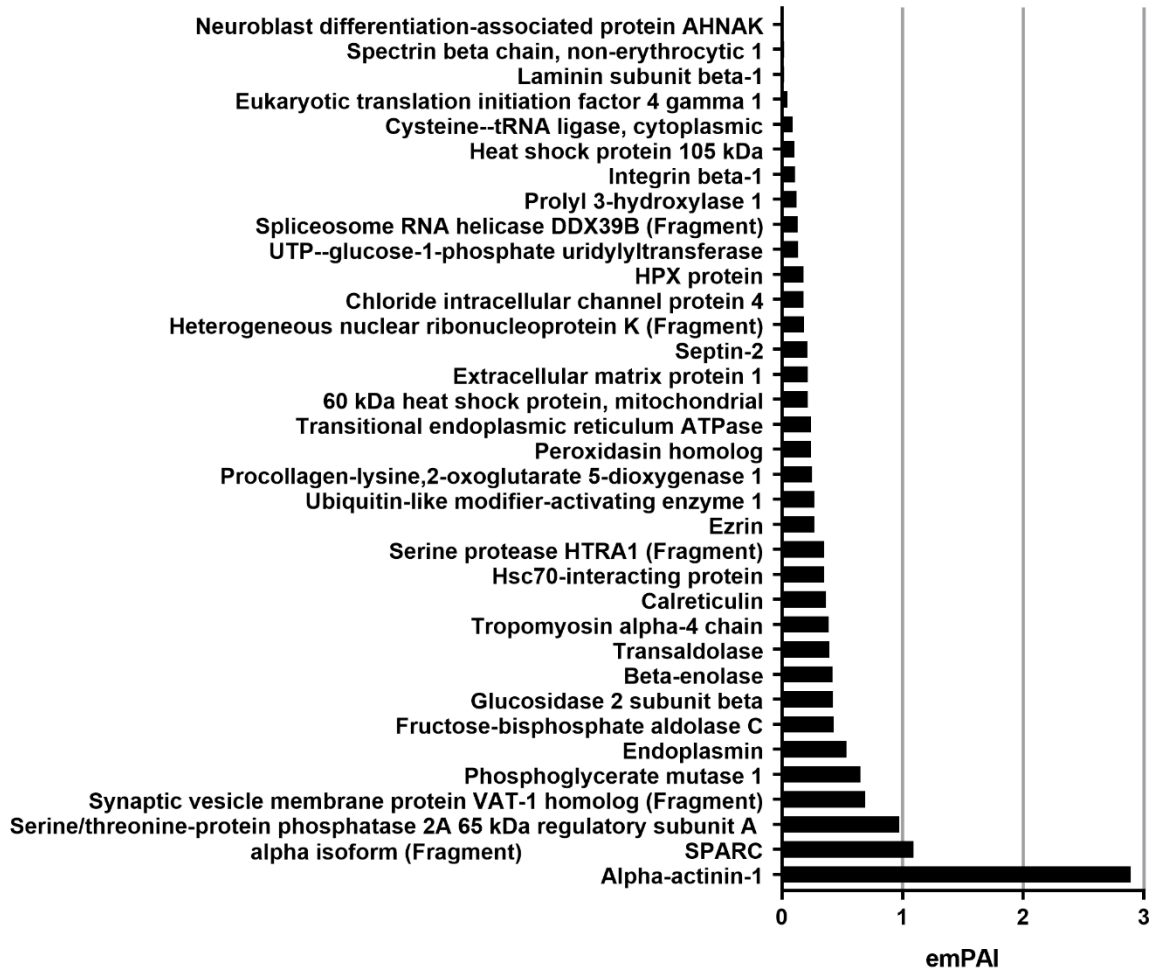


Supplementary Figure 5: (A), (C) Dynamic modulus plots for MDA-MB-231 and MCF7 cells across monoculture and coculture condition depicting G' and G'' across the culture period. (B), (D) Loss tangent graphs for MDA-MB-231 and MCF7 group across all conditions. (E) Dynamic modulus plots for CAF only depicting G' and G'' across the culture period. (F) Loss tangent graphs for CAF only group.



Supplementary Figure 6: (A) Representative Confocal Reflectance Images showing collagen deposition in CAF only groups across the culture period. (B) Dynamic modulus plots for CAF only depicting G' and G'' across the culture period. (C) Loss tangent graphs for CAF only group.

APPENDIX B
SUPPLEMENTARY FIGURES FOR CHAPTER 3



Supplementary Figure 1: List of 35 unique proteins detected in coculture group of MCF7 cells with CAFs sorted by their protein abundance.

Term	Count	%	PValue	Fold Enrichment	Bonferroni
GO:0006457~protein folding	5	14.70588	4.10E-04	13.71895425	0.160564988
GO:0006898~receptor-mediated endocytosis	5	14.70588	4.64E-04	13.27640734	0.179737778
GO:0051621~canonical glycolysis	3	8.823529	0.001182	56.98642534	0.396452467
GO:0098609~cell-cell adhesion	5	14.70588	0.001878	9.112220534	0.551925511
GO:0006096~glycolytic process	3	8.823529	0.00202	43.57785467	0.57828689
GO:0006094~gluconeogenesis	3	8.823529	0.003365	33.67379679	0.762882281
GO:0030198~extracellular matrix organization	4	11.76471	0.006604	10.07923169	0.940945701
GO:0051208~sequestering of calcium ion	2	5.882353	0.007838	246.9411765	0.965271736
GO:1903753~negative regulation of p38MAPK cascade	2	5.882353	0.007838	246.9411765	0.965271736
GO:0035088~establishment or maintenance of apical/basal cell polarity	2	5.882353	0.009789	197.5529412	0.985010075
GO:0002576~platelet degranulation	3	8.823529	0.017385	14.3849229	0.999440566
GO:0001960~negative regulation of cytokine-mediated signaling pathway	2	5.882353	0.017553	109.751634	0.999479947
GO:0036500~ATF6-mediated unfolded protein response	2	5.882353	0.017553	109.751634	0.999479947
GO:0051085~chaperone mediated protein folding requiring cofactor	2	5.882353	0.019485	98.77647059	0.999775583
GO:0016032~viral process	4	11.76471	0.020562	6.607121778	0.999859677
GO:0034975~protein folding in endoplasmic reticulum	2	5.882353	0.025258	75.98190045	0.999981972
GO:0030970~retrograde protein transport, ER to cytosol	2	5.882353	0.027175	70.55462185	0.999992222
GO:0050821~protein stabilization	3	8.823529	0.029187	10.89446367	0.999996787
GO:0001666~response to hypoxia	3	8.823529	0.044763	8.614227086	0.999999997
GO:0007159~leukocyte cell-cell adhesion	2	5.882353	0.048023	39.51058824	0.999999999
GO:0055007~cardiac muscle cell differentiation	2	5.882353	0.051766	36.583878	1
GO:0051017~actin filament bundle assembly	2	5.882353	0.057355	32.9254902	1
GO:0090004~positive regulation of establishment of protein localization to plasma membrane	2	5.882353	0.057355	32.9254902	1
GO:0042981~regulation of apoptotic process	3	8.823529	0.065412	6.956089478	1
GO:0051077~chaperone-mediated protein folding	2	5.882353	0.070272	26.6963434	1
GO:0006986~response to unfolded protein	2	5.882353	0.079393	23.51820728	1
GO:0060348~bone development	2	5.882353	0.079393	23.51820728	1
GO:0031623~receptor internalization	2	5.882353	0.081206	22.97127223	1

Supplementary Table 1: List of Biological Process in which identified unique proteins in MCF7+CAF group participate along with the p-value and fold enrichment values.

Term	Count	%	PValue	Fold Enrichment	Bonferroni
GO:0005515~protein binding	26	76.47059	0.004546	1.46943654	0.461884862
GO:0044822~poly(A) RNA binding	9	26.47059	0.001203	3.957927369	0.151059237
GO:0098641~cadherin binding involved in cell-cell adhesion	7	20.58824	1.83E-05	11.98448276	0.002485133
GO:0005509~calcium ion binding	6	17.64706	0.012058	4.154811715	0.807916635
GO:0051082~unfolded protein binding	4	11.76471	0.001274	18.05454545	0.159171476
GO:0032403~protein complex binding	4	11.76471	0.007463	9.640776699	0.638977743
GO:0003723~RNA binding	4	11.76471	0.090246	3.63071298	0.999997408
GO:0051087~chaperone binding	3	8.823529	0.010904	18.38888889	0.774872264
GO:0005178~integrin binding	3	8.823529	0.017848	14.18571429	0.913643249
GO:0051015~actin filament binding	3	8.823529	0.027355	11.28409091	0.976996616
GO:0005506~iron ion binding	3	8.823529	0.03587	9.735294118	0.993042639
GO:0019904~protein domain specific binding	3	8.823529	0.062167	7.161057692	0.999838177
GO:0044548~S100 protein binding	2	5.882353	0.025126	76.38461538	0.968595604
GO:0031418~L-ascorbic acid binding	2	5.882353	0.040283	47.28571429	0.996271921
GO:0043236~laminin binding	2	5.882353	0.047775	39.72	0.998715993

Supplementary Table 2: List of Molecular Functions performed by unique proteins

detected in MCF7+CAF group along with the p-value and fold enrichment values.

Term	Count	%	PValue	Fold Enrichment	Bonferroni
GO:0070062~extracellular exosome	30	88.23529	5.35E-20	5.720384205	8.78E-18
GO:0005829~cytosol	22	64.70588	9.96E-09	3.557164404	1.63E-06
GO:0005737~cytoplasm	21	61.76471	1.28E-04	2.155495979	0.020850064
GO:0016020~membrane	12	35.29412	0.001183	2.923636364	0.176409747
GO:0005615~extracellular space	11	32.35294	9.02E-05	4.377134373	0.01467709
GO:0005576~extracellular region	9	26.47059	0.00682	2.996273292	0.674486764
GO:0031012~extracellular matrix	8	23.52941	8.26E-07	14.48648649	1.36E-04
GO:0005925~focal adhesion	8	23.52941	5.23E-06	10.96675192	8.58E-04
GO:0048471~perinuclear region of cytoplasm	8	23.52941	1.02E-04	6.904991948	0.016546872
GO:0005913~cell-cell adherens junction	7	20.58824	2.19E-05	11.61609907	0.003583415
GO:0005783~endoplasmic reticulum	7	20.58824	0.003341	4.531400966	0.42236404
GO:0005739~mitochondrion	6	17.64706	0.089232	2.4162284	0.99999978
GO:0071682~endocytic vesicle lumen	5	14.70588	1.60E-08	167.5	2.62E-06
GO:0043209~myelin sheath	5	14.70588	1.58E-04	17.63157895	0.02552889
GO:0005578~proteinaceous extracellular matrix	5	14.70588	0.001338	10	0.197109958
GO:0009986~cell surface	5	14.70588	0.015993	4.944649446	0.928921598
GO:0005788~endoplasmic reticulum lumen	4	11.76471	0.004978	11.16666667	0.558891287
GO:0015629~actin cytoskeleton	4	11.76471	0.007072	9.834862385	0.687725276
GO:0005884~actin filament	3	8.823529	0.006159	24.73846154	0.636946793
GO:0042995~cell projection	3	8.823529	0.008125	21.44	0.737611094
GO:0001726~ruffle	3	8.823529	0.01153	17.86666667	0.850714193
GO:0030496~midbody	3	8.823529	0.02275	12.46511628	0.977043158
GO:0045121~membrane raft	3	8.823529	0.053397	7.805825243	0.999876547
GO:0030867~rough endoplasmic reticulum membrane	2	5.882353	0.014398	134	0.907299283
GO:0030863~cortical cytoskeleton	2	5.882353	0.039111	48.72727273	0.998559924
GO:0002102~podosome	2	5.882353	0.042592	44.66666667	0.999205879
GO:0019013~viral nucleocapsid	2	5.882353	0.049518	38.28571429	0.999758563
GO:0030315~T-tubule	2	5.882353	0.06662	28.21052632	0.999987709
GO:0005844~polysome	2	5.882353	0.06662	28.21052632	0.999987709
GO:0032154~cleavage furrow	2	5.882353	0.081756	22.80851064	0.999999158
GO:0001725~stress fiber	2	5.882353	0.093364	19.85185185	0.999999896
GO:0031093~platelet alpha granule lumen	2	5.882353	0.095011	19.49090909	0.999999922
GO:0005902~microvillus	2	5.882353	0.098295	18.80701754	0.999999957

Supplementary Table 3: Identification of Cellular location of the unique proteins

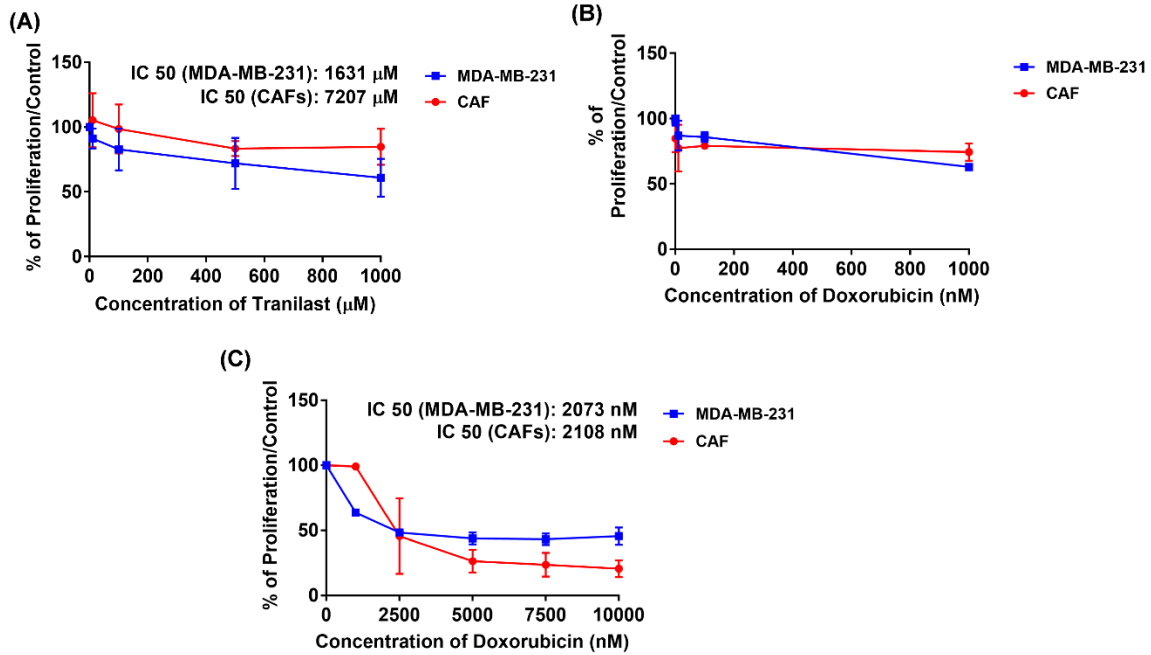
detected in MCF7+CAF group along with the p-value and fold enrichment values.

KEGG Pathway	observed gene count	false discovery rate	matching proteins in your network (labels)
Protein processing in endoplasmic reticulum	5	0.00066	CALR,HSP90B1,HSPH1,PRKCSH,VCP
Biosynthesis of amino acids	4	0.00066	ALDOC,ENO3,PGAM1,TALDO1
Carbon metabolism	4	0.0013	ALDOC,ENO3,PGAM1,TALDO1
Tight junction	4	0.004	ACTN1,EZR,ITGB1,PPP2R1A
PI3K-Akt signaling pathway	4	0.0291	HSP90B1,ITGB1,LAMB1,PPP2R1A
Glycolysis / Gluconeogenesis	3	0.004	ALDOC,ENO3,PGAM1
Leukocyte transendothelial migration	3	0.0129	ACTN1,EZR,ITGB1
Focal adhesion	3	0.0341	ACTN1,ITGB1,LAMB1
Regulation of actin cytoskeleton	3	0.0346	ACTN1,EZR,ITGB1
Pentose phosphate pathway	2	0.015	ALDOC,TALDO1
Pathogenic Escherichia coli infection	2	0.0341	EZR,ITGB1
Legionellosis	2	0.0341	HSPD1,VCP
Bacterial invasion of epithelial cells	2	0.0421	ITGB1,SEPT2
RNA degradation	2	0.0443	ENO3,HSPD1
ECM-receptor interaction	2	0.0455	ITGB1,LAMB1

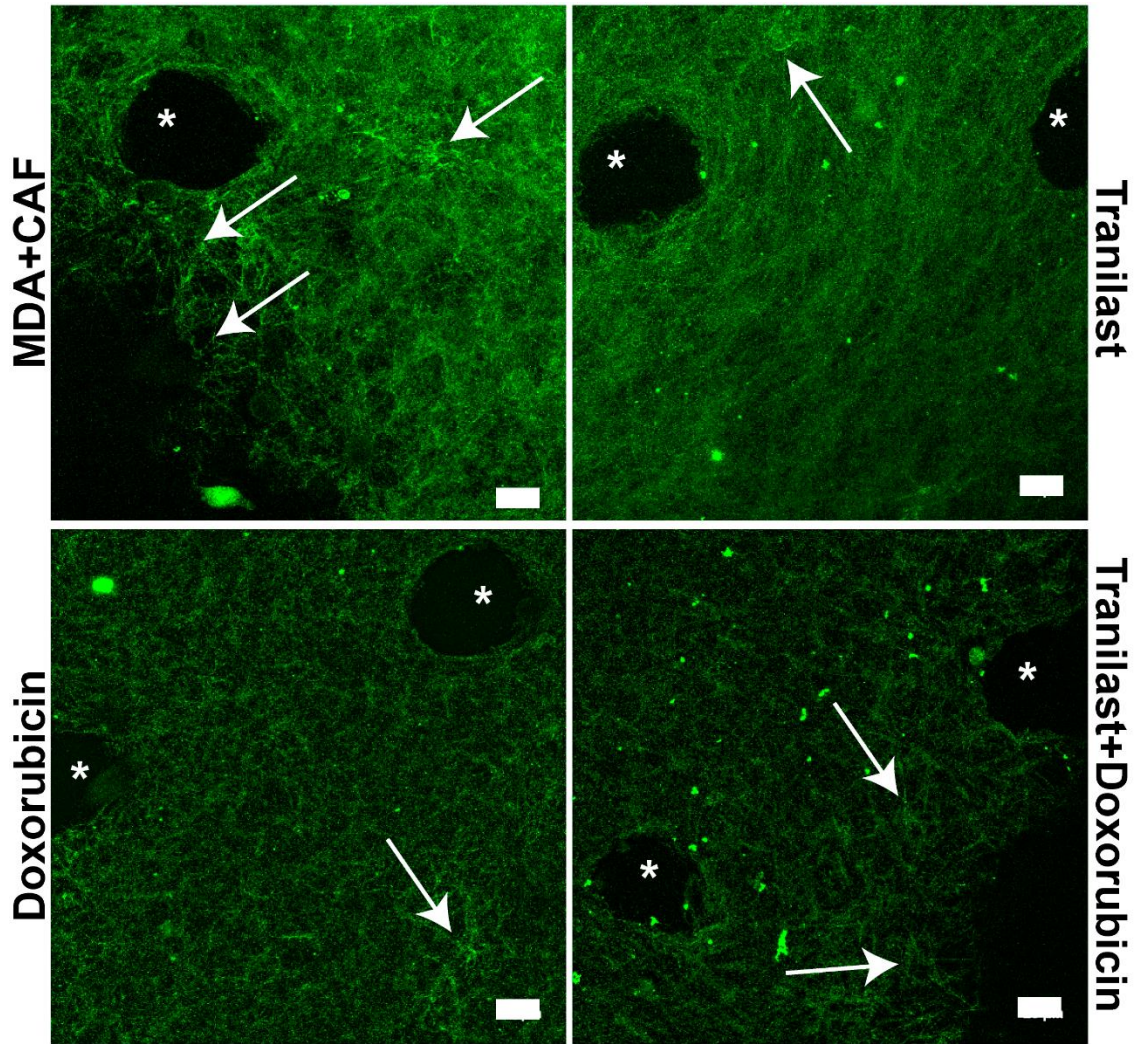
Supplementary Table 4: KEGG pathway analysis on unique proteins detected in

MCF7+CAF group along with their false discovery rate and participating gene list.

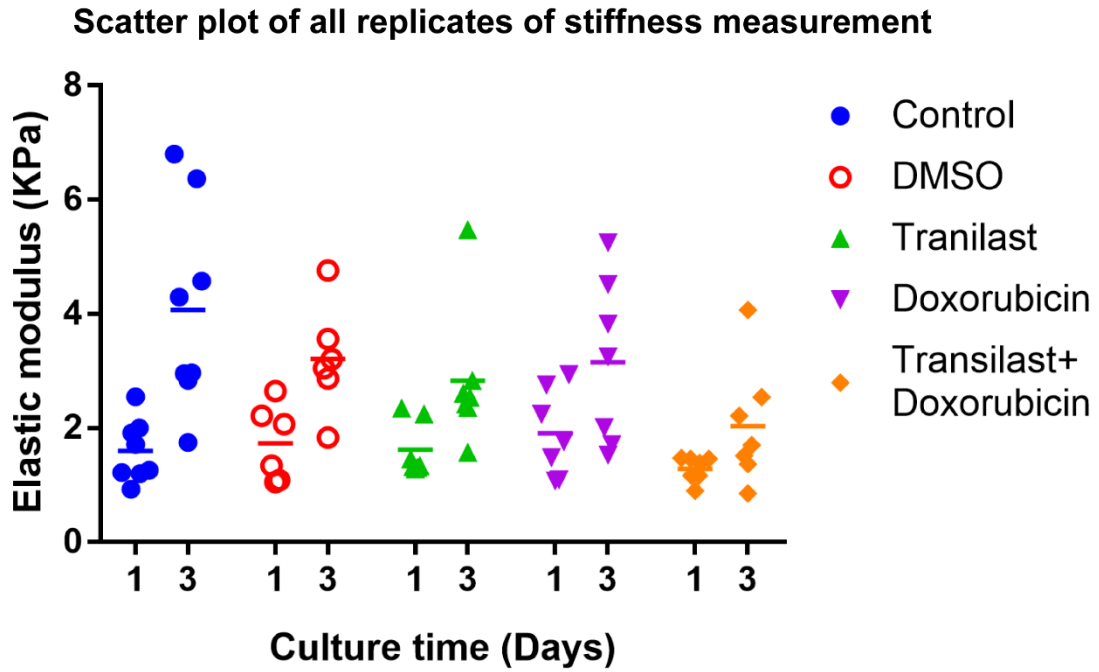
APPENDIX C
SUPPLEMENTARY FIGURES FOR CHAPTER 4



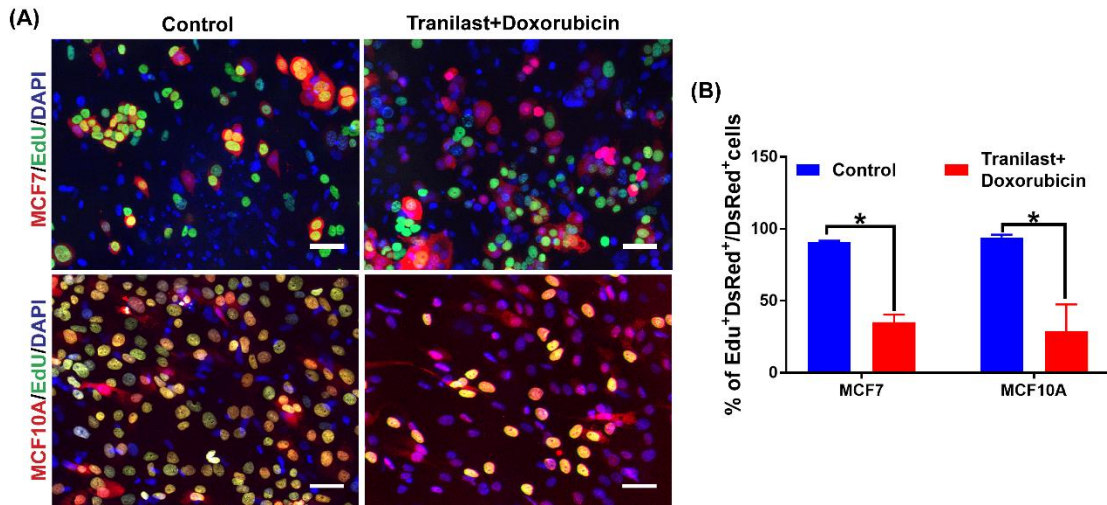
Supplementary Figure 1: IC 50 values in 3D assay for MDA-MB-231 and CAFs in response to different concentrations of **(A)** Tranilast and **(B)** Doxorubicin in 3D assay. **(C)** IC 50 values of MDA-MB-231 and CAFs at higher concentration of doxorubicin.



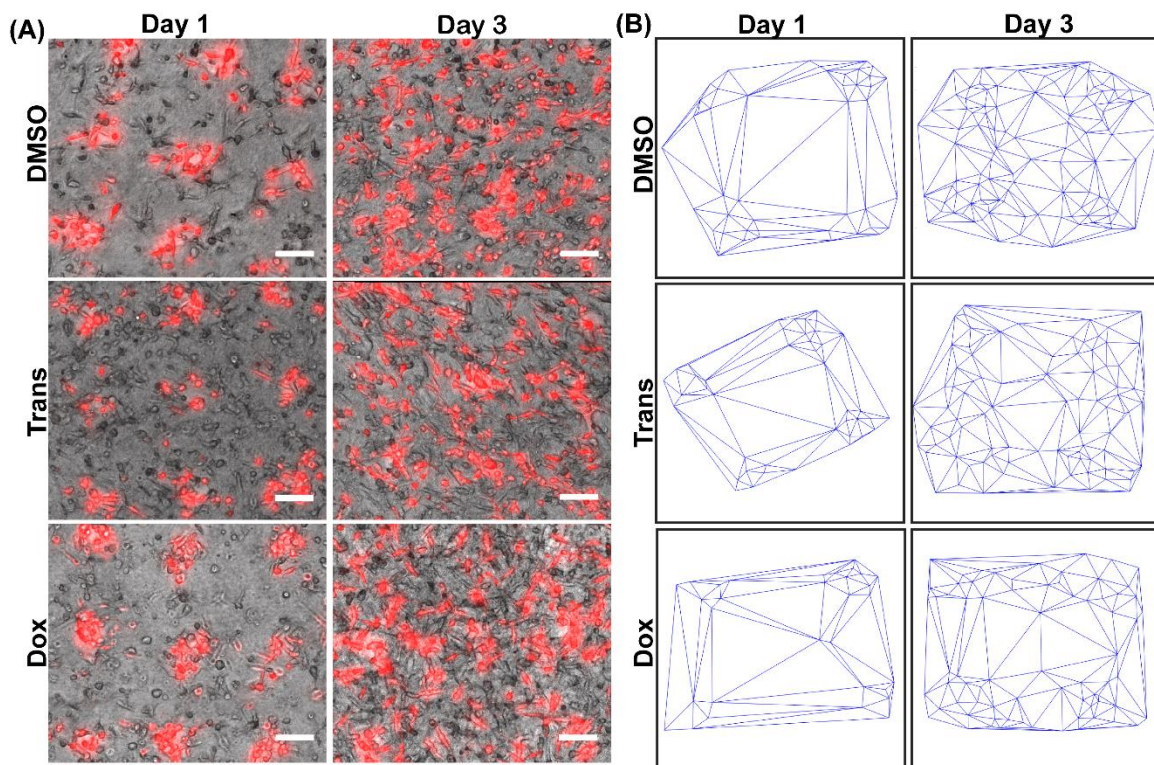
Supplementary Figure 2: Representative immunofluorescent images demonstrating fibronectin deposition and assembly within 3D matrix across experimental groups. Arrows representing the fibronectin fibers. * represent the microwells molded in collagen. Scale bar represent 20 μm .



Supplementary Figure 3: Scatter dot plot of data replicates for elastic modulus measurement showing variation of stiffness across all groups on day 1 and day 3 of the culture.



Supplementary Figure 4: (A) Representative immunofluorescent images of EdU assay depicting proliferation of MCF7 and MCF10A in control and Tranilast+Doxorubicin treated group. (B) Quantification of proliferation of MCF7 and MCF10A cells across culture conditions. Scale bar represents 50 μ m. (* represents p value < 0.05).



Supplementary Figure 5: (A) Representative phase contrast and fluorescent images of tumor cell dispersion in DMSO, tranilast and doxorubicin conditions on day 1 and day 3.

(B) Representative triangulation graphs depicting tumor cell invasion into the stroma

within DMSO, tranilast and doxorubicin group. (C) Quantification of area disorder of MDA-MB-231 cells across all the groups. Scale bar represent 100 μm . (* represents p value < 0.05).

APPENDIX D

LIST OF SUPPLEMENTARY VIDEOS

Supplementary Movie 1: Representative movie showing real time migration of MDA-MB-231 cells in monoculture condition for 18 hours with time interval of 45 minutes.


Supplementary Movie 2: Representative movie showing real time migration of MDA-MB-231 cells in coculture condition with CAFs for 18 hours with time interval of 45 minutes.


Supplementary Movie 1: Representative movie showing real time migration of MCF7 cells in monoculture condition for 18 hours with time interval of 45 minutes.


Supplementary Movie 1: Representative movie showing real time migration of MCF7 cells in coculture condition with CAFs for 18 hours with time interval of 45 minutes.


APPENDIX E
COPYRIGHTS AND PERMISSIONS

Permission for Chapter 1, Figure 1:

 **Copyright Clearance Center**

 **RightsLink®**

[Home](#) [Create Account](#) [Help](#) 



Title: Advanced biomaterials and microengineering technologies to recapitulate the stepwise process of cancer metastasis

Author: Nitish Peela, Danh Truong, Harpinder Saini, Hunghao Chu, Samaneh Mashaghi, Stephanie L. Ham, Sunil Singh, Hossein Taviana, Bobak Mosadegh, Mehdi Nikkhah

Publication: Biomaterials

Publisher: Elsevier

Date: July 2017

© 2017 Elsevier Ltd. All rights reserved.

LOGIN

If you're a [copyright.com](#) user, you can login to RightsLink using your [copyright.com](#) credentials.

Already a [RightsLink](#) user or want to [learn more?](#)

Please note that, as the author of this Elsevier article, you retain the right to include it in a thesis or dissertation, provided it is not published commercially. Permission is not required, but please ensure that you reference the journal as the original source. For more information on this and on your other retained rights, please visit: <https://www.elsevier.com/about/our-business/policies/copyright#Author-rights>

[BACK](#) [CLOSE WINDOW](#)

Copyright © 2019 [Copyright Clearance Center, Inc.](#) All Rights Reserved. [Privacy statement](#). [Terms and Conditions](#). Comments? We would like to hear from you. E-mail us at customercare@copyright.com

Permission for Chapter 1, Figure 2:

6/13/2019

RightsLink Printable License

**ELSEVIER LICENSE
TERMS AND CONDITIONS**

Jun 13, 2019

This Agreement between Harpinder Saini ("You") and Elsevier ("Elsevier") consists of your license details and the terms and conditions provided by Elsevier and Copyright Clearance Center.

License Number	4607251248885
License date	Jun 13, 2019
Licensed Content Publisher	Elsevier
Licensed Content Publication	Advanced Drug Delivery Reviews
Licensed Content Title	The extracellular matrix in breast cancer
Licensed Content Author	Jacob Insua-Rodríguez,Thordur Oskarsson
Licensed Content Date	Feb 1, 2016
Licensed Content Volume	97
Licensed Content Issue	n/a
Licensed Content Pages	15
Start Page	41
End Page	55
Type of Use	reuse in a thesis/dissertation
Intended publisher of new work	other
Portion	figures/tables/illustrations
Number of figures/tables/illustrations	1
Format	both print and electronic
Are you the author of this Elsevier article?	No
Will you be translating?	No
Original figure numbers	Figure 1
Title of your thesis/dissertation	A High-Density 3D Microengineered Platform to Study the Role of Tumor-Stroma Interactions on Desmoplasia and Breast Cancer Progression
Expected completion date	Aug 2019
Estimated size (number of pages)	200
Requestor Location	Harpinder Saini 1440 E Broadway Road Apt 2147 TEMPE, AZ 85282 United States Attn: Harpinder Saini
Publisher Tax ID	98-0397604
Total	0.00 USD

<https://s100.copyright.com/AppDispatchServlet>

1/6

Permission for Chapter 1, Figure 3A:

6/13/2019

RightsLink Printable License

**OXFORD UNIVERSITY PRESS LICENSE
TERMS AND CONDITIONS**

Jun 13, 2019

This Agreement between Harpinder Saini ("You") and Oxford University Press ("Oxford University Press") consists of your license details and the terms and conditions provided by Oxford University Press and Copyright Clearance Center.

License Number	4607231431779
License date	Jun 13, 2019
Licensed content publisher	Oxford University Press
Licensed content publication	Integrative Biology
Licensed content title	Human breast cancer invasion and aggression correlates with ECM stiffening and immune cell infiltration
Licensed content author	Acerbi, I.; Cassereau, L.
Licensed content date	May 11, 2015
Type of Use	Thesis/Dissertation
Institution name	
Title of your work	A High-Density 3D Microengineered Platform to Study the Role of Tumor-Stroma Interactions on Desmoplasia and Breast Cancer Progression
Publisher of your work	n/a
Expected publication date	Aug 2019
Permissions cost	0.00 USD
Value added tax	0.00 USD
Total	0.00 USD
Title	A High-Density 3D Microengineered Platform to Study the Role of Tumor-Stroma Interactions on Desmoplasia and Breast Cancer Progression
Institution name	n/a
Expected presentation date	Aug 2019
Portions	Figure 2A
Requestor Location	Harpinder Saini 1440 E Broadway Road Apt 2147 TEMPE, AZ 85282 United States Attn: Harpinder Saini
Publisher Tax ID	GB125506730
Total	0.00 USD

Terms and Conditions

**STANDARD TERMS AND CONDITIONS FOR REPRODUCTION OF MATERIAL
FROM AN OXFORD UNIVERSITY PRESS JOURNAL**

1. Use of the material is restricted to the type of use specified in your order details.

<https://s100.copyright.com/AppDispatchServlet>

1/3

Permission for Chapter 1, Figure 3B:

6/13/2019

RightsLink Printable License

**SPRINGER NATURE LICENSE
TERMS AND CONDITIONS**

Jun 13, 2019

This Agreement between Harpinder Saini ("You") and Springer Nature ("Springer Nature") consists of your license details and the terms and conditions provided by Springer Nature and Copyright Clearance Center.

License Number	4607240358895
License date	Jun 13, 2019
Licensed Content Publisher	Springer Nature
Licensed Content Publication	Nature Nanotechnology
Licensed Content Title	The nanomechanical signature of breast cancer
Licensed Content Author	Marija Plodinec, Marko Loparic, Christophe A. Monnier, Ellen C. Obermann, Rosanna Zanetti-Dallenbach et al.
Licensed Content Date	Oct 21, 2012
Licensed Content Volume	7
Licensed Content Issue	11
Type of Use	Thesis/Dissertation
Requestor type	academic/university or research institute
Format	print and electronic
Portion	figures/tables/illustrations
Number of figures/tables/illustrations	1
High-res required	no
Will you be translating?	no
Circulation/distribution	<501
Author of this Springer Nature content	no
Title	A High-Density 3D Microengineered Platform to Study the Role of Tumor-Stroma Interactions on Desmoplasia and Breast Cancer Progression
Institution name	n/a
Expected presentation date	Aug 2019
Portions	Figure 1B
Requestor Location	Harpinder Saini 1440 E Broadway Road Apt 2147 TEMPE, AZ 85282 United States Attn: Harpinder Saini
Total	0.00 USD
Terms and Conditions	

Springer Nature Terms and Conditions for RightsLink Permissions

<https://s100.copyright.com/AppDispatchServlet>

1/3

Permission for Chapter 1, Figure 3C:

The figure is from article published in year 2018 and as per journal policies it is now available as open access and under Creative Commons License – Non commercial 4.0

International License.

Permissions

1. Articles not designated as Open Access are distributed exclusively by Cold Spring Harbor Laboratory Press for the first six months after the full-issue publication date (see **Terms** for complete details). After six months, they are available under a Creative Commons License (**Attribution–NonCommercial 4.0 International License**).

Authors of these non-Open Access articles retain copyright in the articles but grant Cold Spring Harbor Laboratory Press exclusive publishing rights for six months following full-issue publication. This grant of rights includes the rights to publish, reproduce, distribute, display, and store the article in all formats; to translate the article into other languages; to create adaptations, summaries, extracts, or derivations of the article; and to license others to do any or all of the above.

2. Articles that carry the Open Access designation are immediately distributed under one of two Creative Commons Licenses: (i) **Creative Commons Attribution–NonCommercial 4.0 International License (CC–BY–NC)** or (ii) **Creative Commons Attribution 4.0 International License (CC–BY)**. The CC–BY license permits commercial use, including reproduction, adaptation, and distribution of the article provided the original author and source are credited. *Please note specific licensing information within article of interest.*

3. To request permission to reproduce/adapt artwork from *Genes & Development* elsewhere (e.g., in other publications) during the first six months after full-issue publication, **click here**.

4. Please contact **Copyright Clearance Center** to request permission to photocopy articles or for use in a coursepack during the first six months after full-issue publication.

5. To request permission for any other use, including for commercial purposes, **click here**.

Permission for Chapter 1, Figure 3D:

This figure was adopted from article titled ‘Targeting the cancer associated fibroblasts as a treatment in triple negative breast cancer’ which is published by open access journal Oncotarget that distribute its content using CC BY 3.0

II. EDITORIAL POLICIES

COPYRIGHT AND LICENSE POLICIES

**Open-Access License
No Permission Required**



Oncotarget applies the **Creative Commons Attribution 3.0 License** (CC BY 3.0) to all works we publish (read the **human-readable summary** or the **full license legal code**). Under the CC BY, authors retain ownership of the copyright for their article, but authors allow anyone to download, reuse, reprint, modify, distribute, and/or copy articles in *Oncotarget*, so long as the original authors and source are cited.

No permission is required from the authors or the publishers.

In most cases, appropriate attribution can be provided by simply citing the original article. If the item you plan to reuse is not part of a published article (e.g., a featured issue image), then please indicate the originator of the work, and the volume, issue, and date of the journal in which the item appeared. For any reuse or redistribution of a work, you must also make clear the license terms under which the work was published. This broad license was developed to facilitate open access to, and free use of, original works of all types. Applying this standard license to your own work will ensure your right to make your work freely and openly available.

For queries about the license, please contact us at forms@oncotarget.com

Permission for Chapter 1, Figure 3E:

6/13/2019

Copyright Clearance Center



Note: Copyright.com supplies permissions but not the copyrighted content itself.

1
PAYMENT

2
REVIEW

3
CONFIRMATION

Step 3: Order Confirmation

Thank you for your order! A confirmation for your order will be sent to your account email address. If you have questions about your order, you can call us 24 hrs/day, M-F at +1.855.239.3415 Toll Free, or write to us at info@copyright.com. This is not an invoice.

Confirmation Number: 11823596
Order Date: 06/13/2019

If you paid by credit card, your order will be finalized and your card will be charged within 24 hours. If you choose to be invoiced, you can change or cancel your order until the invoice is generated.

Payment Information

Harpinder Saini
hsaini2@asu.edu
+1 (573) 466-6646
Payment Method: n/a

Order Details

Journal of biological chemistry

Order detail ID: 71923067
Order License Id: 4607250393990
ISSN: 1083-351X
Publication Type: e-Journal
Volume:
Issue:
Start page:
Publisher: AMERICAN SOCIETY FOR
BIOCHEMISTRY AND MOLECULAR BI
AMERICAN SOCIETY FOR
BIOCHEMISTRY & MOLECULAR BIOL
Author/Editor:

Permission Status: **Granted**

Permission type: Republish or display content
Type of use: Thesis/Dissertation

Requestor type: Academic institution

Format: Print, Electronic

Portion: chart/graph/table/figure

Number of charts/graphs/tables/figures: 1

The requesting person/organization: Harpinder Saini

Title or numeric reference of the portion(s): Figure 4

Title of the article or chapter the portion is from: PRL increases invasiveness in stiff matrices.

Editor of portion(s)

<https://www.copyright.com/printCoIConfirmPurchase.do?operation=defaultOperation&confirmNum=11823596&showTCCitation=TRUE>

1/7

Permission for Chapter 1, Figure 3F:

6/13/2019

RightsLink Printable License

**SPRINGER NATURE LICENSE
TERMS AND CONDITIONS**

Jun 13, 2019

This Agreement between Harpinder Saini ("You") and Springer Nature ("Springer Nature") consists of your license details and the terms and conditions provided by Springer Nature and Copyright Clearance Center.

License Number	4607250728108
License date	Jun 13, 2019
Licensed Content Publisher	Springer Nature
Licensed Content Publication	Nature Materials
Licensed Content Title	Extracellular matrix stiffness and composition jointly regulate the induction of malignant phenotypes in mammary epithelium
Licensed Content Author	Ovijit Chaudhuri, Sandeep T. Koshy, Cristiana Branco da Cunha, Jae-Won Shin, Catia S. Verbeke et al.
Licensed Content Date	Jun 15, 2014
Licensed Content Volume	13
Licensed Content Issue	10
Type of Use	Thesis/Dissertation
Requestor type	academic/university or research institute
Format	print and electronic
Portion	figures/tables/illustrations
Number of figures/tables/illustrations	1
High-res required	no
Will you be translating?	no
Circulation/distribution	<501
Author of this Springer Nature content	no
Title	A High-Density 3D Microengineered Platform to Study the Role of Tumor-Stroma Interactions on Desmoplasia and Breast Cancer Progression
Institution name	n/a
Expected presentation date	Aug 2019
Portions	Supplementary Figure S6
Requestor Location	Harpinder Saini 1440 E Broadway Road Apt 2147 TEMPE, AZ 85282 United States Attn: Harpinder Saini
Total	0.00 USD
Terms and Conditions	

Springer Nature Terms and Conditions for RightsLink Permissions

<https://s100.copyright.com/AppDispatchServlet>

1/3

Permission for Chapter 4:

6/13/2019

RightsLink Printable License

SPRINGER NATURE LICENSE TERMS AND CONDITIONS

Jun 13, 2019

This Agreement between Harpinder Saini ("You") and Springer Nature ("Springer Nature") consists of your license details and the terms and conditions provided by Springer Nature and Copyright Clearance Center.

License Number	4607250963661
License date	Jun 13, 2019
Licensed Content Publisher	Springer Nature
Licensed Content Publication	Cellular and Molecular Bioengineering
Licensed Content Title	The Role of Desmoplasia and Stromal Fibroblasts on Anti-cancer Drug Resistance in a Microengineered Tumor Model
Licensed Content Author	Harpinder Saini, Kiarash Rahmani Eliato, Casey Silva et al
Licensed Content Date	Jan 1, 2018
Licensed Content Volume	11
Licensed Content Issue	5
Type of Use	Thesis/Dissertation
Requestor type	academic/university or research institute
Format	print and electronic
Portion	full article/chapter
Will you be translating?	no
Circulation/distribution	<501
Author of this Springer Nature content	yes
Title	A High-Density 3D Microengineered Platform to Study the Role of Tumor-Stroma Interactions on Desmoplasia and Breast Cancer Progression
Institution name	n/a
Expected presentation date	Aug 2019
Requestor Location	Harpinder Saini 1440 E Broadway Road Apt 2147 TEMPE, AZ 85282 United States Attn: Harpinder Saini
Total	0.00 USD

Terms and Conditions

Springer Nature Terms and Conditions for RightsLink Permissions
Springer Nature Customer Service Centre GmbH (the Licensor) hereby grants you a non-exclusive, world-wide licence to reproduce the material and for the purpose and requirements specified in the attached copy of your order form, and for no other use, subject to the conditions below:

<https://s100.copyright.com/AppDispatchServlet>

1/3